Appendix A.14:

Wattle Dr – CPT 90678

Table 1: Site Description for Wattle Dr (CPT 90678 – CC LIQ 3).

Attribute	Yes/No			Description/Date	Symbol in Figure 1
	10-m Buffer	20-m Buffer	50-m Buffer		
Near a body of surface water or other free face features?	No	No	No	The center of the site is 240 meters away from a pond (~2.0 m high, N-S free face) near Anzac Drive Reserve and 480 meters away from the Avon River (~1.5 m high, NW-SE free face).	NA
Lateral spreading observed during the CES?	No	No	No	Absence of ground cracks indicates no lateral spreading, as observed by the mapping team.[1]	NA
Nearby buildings or structures?	Yes	Yes	Yes	Building coverage of the 10-m, 20-m, and 50-m buffers is 16%, 24%, and 27%, respectively.	White Fill + Brown Outline
Sloping land?	No	No	No	Flat land, residential area.	NA
Step changes in the ground surface?	Yes	Yes	Yes	Approximately 0.5-m change in ground surface elevation with a higher elevation in the E portion of the buffers.	NA
Retaining walls?	Yes	Yes	Yes	Retaining wall is positioned roughly N-S, offset from the center of the site to the W by 8 meters.	Thin Black Line
Vegetation?	Yes	Yes	Yes	Trees and bushes cover 51% of the 10-m buffer, 40% of the 20-m buffer and 22% of the 50-m buffer. They are in the N half of the 10-m buffer and throughout all quadrants of the 20-m and 50-m buffers.	White Fill + Green Outline
Anthropogenic changes to the site between the LiDAR surveys?	No	Yes	Yes	First building within the 50-m buffer was removed between Mar 2013 and Aug 2013. Second building within the 20-m and 50-m buffers was removed between Mar 2014 and Aug 2014. Two more buildings (one within the 20-m and 50-m buffers and the other within the 50-m buffer) were demolished between Aug 2014 and Sep 2014. Last building was removed between July 2015 and Sep 2015.	Orange Crossline
Other important factors?	No	No	Yes	Low-motor-vehicle-volume, two-way roadway occupies 5% of the 50-m buffer and stretches throughout the NE and SE quadrants. Trampoline is in the NW quadrant of the 50-m buffer.	Road: White Fill + Gray Outline; Trampoline: White Fill + Blue Outline

Note: Buffer is the area within a circle of a specified radius with CPT investigations done at its center (172.706167°, -43.497325°).

[1] Canterbury Geotechnical Database. (2012). "Observed Ground Crack Locations", Map Layer CGD0400 - 23 July 2012, retrieved July 09, 2018 from https://canterburygeotechnicaldatabase.projectorbit.com/

Figure 1: Site plan with areas where LiDAR survey data is considered.

Note 1: Eight patches (outlined in red) in free field were initially selected for settlement assessment as areas free of vegetation and structures. Further analyses such as proximity of a patch to a CPT, proximity of a patch to a property subjected to addition and/or demolition of a structure, front yard/backyard alterations (e.g., ploughing, rubble, scrap), and density of LiDAR points for 2003 resulted in Patches A, B, and C being selected for detailed settlement assessment and other patches being discarded in detailed settlement assessment. In addition, since significant amounts of ejecta were observed on roads in the CES, the entire road and the driveway were considered for settlement assessment. Roads as hard, relatively flat surfaces provide many ground-classified points. Therefore, it is very useful to compare settlement estimates on roads with settlement estimates for the unpaved patches.

Table 2: LiDAR flight error adjustments, global adjustments for the difference between average LiDAR point elevations and benchmark survey elevations, and vertical tectonic movement adjustments.

	Adjustments (mm)		
Earthquake Event(s)	LiDAR Flight Error	Global Offset[2]	Tectonic Vertical Movement
Sep-10	-50	-3	0
Feb-11	50	16	-30
Jun-11	0	38	-45
Dec-11	0	-65	0
CES	0	-14	-75
Post Sep 2010 LiDAR survey affected by ejecta?			No

Note: The negative sign indicates the subtraction from the ground surface subsidence, while the positive sign indicates the addition to the ground surface subsidence.

Table 3a: LiDAR Measurement Error for Patch A.

Surveys	Buffer	Area Averaged Difference Indicating Repeat Measurement Error (mm)	$\sigma^*_{\text{individual LiDAR points}}$ (mm)	%Reduction in σ due to Area Averaging of LiDAR Points
Post Feb 2011: Mar 2011 and May 2011	10-m	54	59	[92,92]
	20-m	54		
	50-m	54		
Post Dec 2011: Feb 2012 and Oct 2015	10-m	34	70	[49,49]
	20-m	34		
	50-m	34		

*Standard deviation.

[2] Russell, J., & van Ballegooy, S. (2015). *Canterbury Earthquake Sequence: Increased liquefaction vulnerability assessment methodology*. New Zealand: Tonkin & Taylor Ltd.

Table 3b: LiDAR Measurement Error for Patch B.

Surveys	Buffer	Area Averaged Difference Indicating Repeat Measurement Error (mm)	$\sigma^*_{individual\ LiDAR\ points}$ (mm)	%Reduction in σ due to Area Averaging of LiDAR Points
Post Feb 2011: Mar 2011 and May 2011	10-m	NA	59	[97,97]
	20-m	NA		
	50-m	57		
Post Dec 2011: Feb 2012 and Oct 2015	10-m	NA	70	[33,33]
	20-m	NA		
	50-m	23		

*Standard deviation.

Table 3c: LiDAR Measurement Error for Patch C.

Surveys	Buffer	Area Averaged Difference Indicating Repeat Measurement Error (mm)	$\sigma^*_{individual\ LiDAR\ points}$ (mm)	%Reduction in σ due to Area Averaging of LiDAR Points
Post Feb 2011: Mar 2011 and May 2011	10-m	NA	59	[78,78]
	20-m	NA		
	50-m	46		
Post Dec 2011: Feb 2012 and Oct 2015	10-m	NA	70	[70,70]
	20-m	NA		
	50-m	49		

*Standard deviation.

Table 3d: LiDAR Measurement Error for Road.

Surveys	Buffer	Area Averaged Difference Indicating Repeat Measurement Error (mm)	$\sigma^*_{\text{individual LiDAR points}}$ (mm)	%Reduction in σ due to Area Averaging of LiDAR Points
Post Feb 2011: Mar 2011 and May 2011	10-m	NA	59	[76,76]
	20-m	NA		
	50-m	45		
Post Dec 2011: Feb 2012 and Oct 2015	10-m	NA	70	[66,66]
	20-m	NA		
	50-m	46		

*Standard deviation.

Table 4a: Ground surface subsidence adjustments due to LiDAR measurement error for Patch A.

Earthquake Event(s)	$\sigma_{\text{pre-EQ LiDAR survey}}$ (mm)	$\sigma_{\text{post-EQ LiDAR survey}}$ (mm)	σ_{total} (mm)	Area Average Adjusted σ (mm) **
Sep-10	158	56	134	±123
Feb-11	56	59	59	±54
Jun-11	59	61	62	±57
Dec-11	61	70	87	±79
CES	158	70	124	±114

**Based on the highest %Reduction in Table 3a.

Table 4b: Ground surface subsidence adjustments due to LiDAR measurement error for Patch B.

Earthquake Event(s)	$\sigma_{\text{pre-EQ LiDAR survey}}$ (mm)	$\sigma_{\text{post-EQ LiDAR survey}}$ (mm)	σ_{total} (mm)	Area Average Adjusted σ (mm) **
Sep-10	158	56	134	±130
Feb-11	56	59	59	±57
Jun-11	59	61	62	±60
Dec-11	61	70	87	±84
CES	158	70	124	±120

**Based on the highest %Reduction in Table 3b.

Table 4c: Ground surface subsidence adjustments due to LiDAR measurement error for Patch C.

Earthquake Event(s)	$\sigma_{\text{pre-EQ LiDAR survey}}$ (mm)	$\sigma_{\text{post-EQ LiDAR survey}}$ (mm)	σ_{total} (mm)	Area Average Adjusted σ (mm)**
Sep-10	158	56	134	±105
Feb-11	56	59	59	±46
Jun-11	59	61	62	±48
Dec-11	61	70	87	±68
CES	158	70	124	±97

**Based on the highest %Reduction in Table 3c.

Table 4d: Ground surface subsidence adjustments due to LiDAR measurement error for Road.

Earthquake Event(s)	$\sigma_{\text{pre-EQ LiDAR survey}}$ (mm)	$\sigma_{\text{post-EQ LiDAR survey}}$ (mm)	σ_{total} (mm)	Area Average Adjusted σ (mm) **
Sep-10	158	56	134	±102
Feb-11	56	59	59	±45
Jun-11	59	61	62	±47
Dec-11	61	70	87	±66
CES	158	70	124	±95

**Based on the highest %Reduction in Table 3c.

Table 5a: Raw liquefaction-related ground surface subsidence using original LiDAR points for Patch A.

	Average Ground Surface Subsidence (mm)		
Earthquake Event(s)	10-m Buffer	20-m Buffer	50-m Buffer
Sep-10	86	86	86
Feb-11	247	247	247
Jun-11	168	168	168
Dec-11	66	66	66
CES	567	567	567

Table 5b: Raw liquefaction-related ground surface subsidence using original LiDAR points for Patch B.

	Average Ground Surface Subsidence (mm)		
Earthquake Event(s)	10-m Buffer	20-m Buffer	50-m Buffer
Sep-10	NA	NA	114
Feb-11	NA	NA	263
Jun-11	NA	NA	140
Dec-11	NA	NA	94
CES	NA	NA	610

Table 5c: Raw liquefaction-related ground surface subsidence using original LiDAR points for Patch C.

	Average Ground Surface Subsidence (mm)		
Earthquake Event(s)	10-m Buffer	20-m Buffer	50-m Buffer
Sep-10	NA	NA	79
Feb-11	NA	NA	238
Jun-11	NA	NA	100
Dec-11	NA	NA	59
CES	NA	NA	476

Table 5d: Raw liquefaction-related ground surface subsidence using original LiDAR points for Road.

	Average Ground Surface Subsidence (mm)		
Earthquake Event(s)	10-m Buffer	20-m Buffer	50-m Buffer
Sep-10	NA	NA	29
Feb-11	NA	NA	168
Jun-11	NA	NA	143
Dec-11	NA	NA	50
CES	NA	NA	389

Table 6a: Corrected liquefaction-related ground surface subsidence using original LiDAR points for Patch A with the calculated adjustments in Table 2.

	Average Calculated Ground Surface Subsidence (mm)		
Earthquake Event(s)	10-m Buffer	20-m Buffer	50-m Buffer
Sep-10	33±125	33±125	33±125
Feb-11	283±50	283±50	283±50
Jun-11	161±50	161±50	161±50
Dec-11	1±75	1±75	1±75
CES	478±125	478±125	478±125

Notes: Plus/minus values are same as those in Table 4a, but rounded to the nearest 25; Positive overall values indicate ground surface subsidence, while negative overall values indicate ground surface uplift.

Table 6b: Corrected liquefaction-related ground surface subsidence using original LiDAR points for Patch B with the calculated adjustments in Table 2.

	Average Calculated Ground Surface Subsidence (mm)		
Earthquake Event(s)	10-m Buffer	20-m Buffer	50-m Buffer
Sep-10	NA	NA	61±125
Feb-11	NA	NA	299±50
Jun-11	NA	NA	133±50
Dec-11	NA	NA	29±75
CES	NA	NA	521±125

Notes: Plus/minus values are same as those in Table 4b, but rounded to the nearest 25; Positive overall values indicate ground surface subsidence, while negative overall values indicate ground surface uplift.

Table 6c: Corrected liquefaction-related ground surface subsidence using original LiDAR points for Patch C with the calculated adjustments in Table 2.

	Average Calculated Ground Surface Subsidence (mm)		
Earthquake Event(s)	10-m Buffer	20-m Buffer	50-m Buffer
Sep-10	NA	NA	26±100
Feb-11	NA	NA	274±50
Jun-11	NA	NA	93±50
Dec-11	NA	NA	-7±75
CES	NA	NA	387±100

Notes: Plus/minus values are same as those in Table 4c, but rounded to the nearest 25; Positive overall values indicate ground surface subsidence, while negative overall values indicate ground surface uplift.

Table 6d: Corrected liquefaction-related ground surface subsidence using original LiDAR points for Road with the calculated adjustments in Table 2.

	Average Calculated Ground Surface Subsidence (mm)		
Earthquake Event(s)	10-m Buffer	20-m Buffer	50-m Buffer
Sep-10	NA	NA	-24±100
Feb-11	NA	NA	204±50
Jun-11	NA	NA	136±50
Dec-11	NA	NA	-15±75
CES	NA	NA	300±100

Notes: Plus/minus values are same as those in Table 4c, but rounded to the nearest 25; Positive overall values indicate ground surface subsidence, while negative overall values indicate ground surface uplift.

Table 7a: Corrected liquefaction-related ground surface subsidence for Patch A using LiDAR DEMs.

	Estimated Ground Surface Subsidence (mm)								
	10-m Buffer			20-m Buffer			50-m Buffer		
Earthquake Event(s)	16th %ile	50th %ile	84th %ile	16th %ile	50th %ile	84th %ile	16th %ile	50th %ile	84th %ile
Sep-10	<50	<50	50	<50	<50	50	<50	<50	50
Feb-11	300	300	300	300	300	300	300	300	300
Jun-11	100	150	150	100	150	150	100	150	150
Dec-11	150	150	150	150	150	150	150	150	150
CES	750	750	750	750	750	750	750	750	750

Note: These percentiles are not the exact statistical measures; they indicate the spatial variability of ground surface subsidence.

Table 7b: Corrected liquefaction-related ground surface subsidence for Patch B using LiDAR DEMs.

	Estimated Ground Surface Subsidence (mm)								
	10-m Buffer			20-m Buffer			50-m Buffer		
Earthquake Event(s)	16th %ile	50th %ile	84th %ile	16th %ile	50th %ile	84th %ile	16th %ile	50th %ile	84th %ile
Sep-10	NA	NA	NA	NA	NA	NA	<50	<50	50
Feb-11	NA	NA	NA	NA	NA	NA	300	300	300
Jun-11	NA	NA	NA	NA	NA	NA	50	50	100
Dec-11	NA	NA	NA	NA	NA	NA	150	150	150
CES	NA	NA	NA	NA	NA	NA	450	450	450

Note: These percentiles are not the exact statistical measures; they indicate the spatial variability of ground surface subsidence.

Table 7c: Corrected liquefaction-related ground surface subsidence for Patch C using LiDAR DEMs.

	Estimated Ground Surface Subsidence (mm)								
	10-m Buffer			20-m Buffer			50-m Buffer		
Earthquake Event(s)	16th %ile	50th %ile	84th %ile	16th %ile	50th %ile	84th %ile	16th %ile	50th %ile	84th %ile
Sep-10	NA	NA	NA	NA	NA	NA	<50	<50	<50
Feb-11	NA	NA	NA	NA	NA	NA	200	250	300
Jun-11	NA	NA	NA	NA	NA	NA	50	50	50
Dec-11	NA	NA	NA	NA	NA	NA	50	50	50
CES	NA	NA	NA	NA	NA	NA	350	350	350

Note: These percentiles are not the exact statistical measures; they indicate the spatial variability of ground surface subsidence.

Table 7d: Corrected liquefaction-related ground surface subsidence for Road using LiDAR DEMs.

	Estimated Ground Surface Subsidence (mm)								
	10-m Buffer			20-m Buffer			50-m Buffer		
Earthquake Event(s)	16th %ile	50th %ile	84th %ile	16th %ile	50th %ile	84th %ile	16th %ile	50th %ile	84th %ile
Sep-10	NA	NA	NA	NA	NA	NA	<50	<50	50
Feb-11	NA	NA	NA	NA	NA	NA	200	200	250
Jun-11	NA	NA	NA	NA	NA	NA	50	50	50
Dec-11	NA	NA	NA	NA	NA	NA	50	50	150
CES	NA	NA	NA	NA	NA	NA	350	350	450

Note: These percentiles are not the exact statistical measures; they indicate the spatial variability of ground surface subsidence.

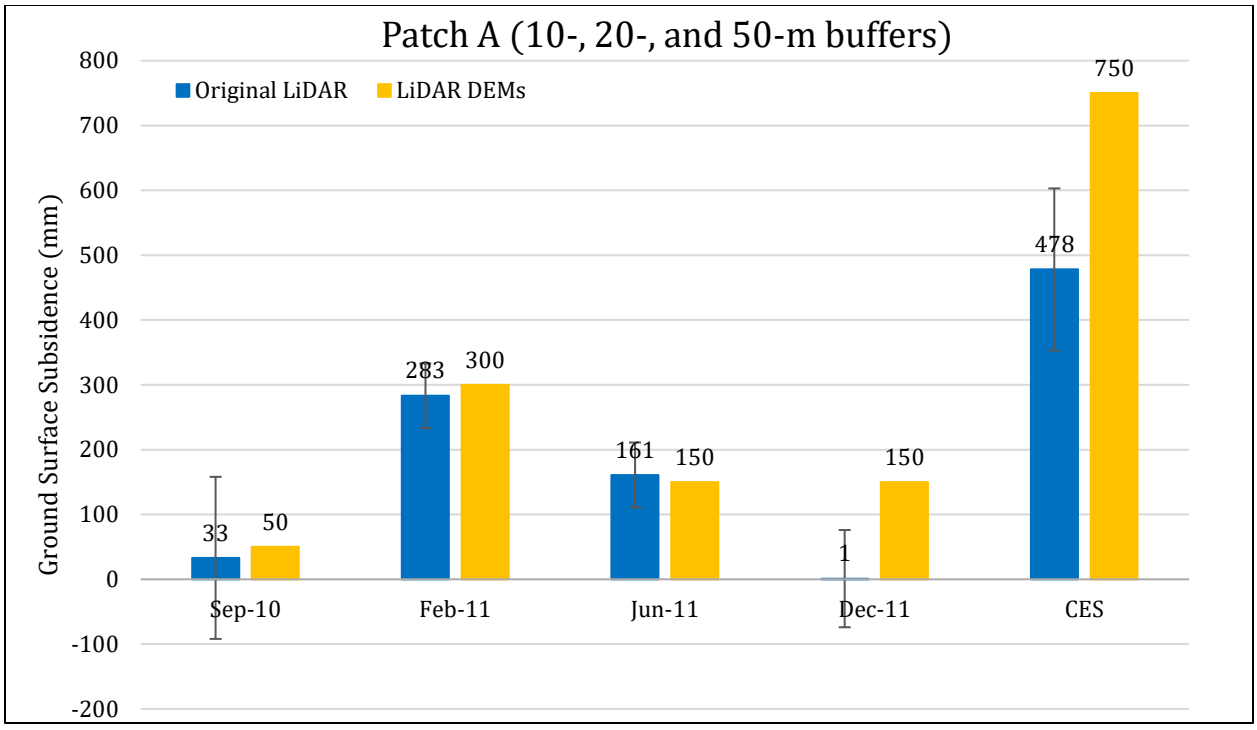

Figure 2: Comparison between ground surface subsidence determined from original LiDAR survey points and ground surface subsidence (50th %ile) estimated using LiDAR DEMs for Patch A.

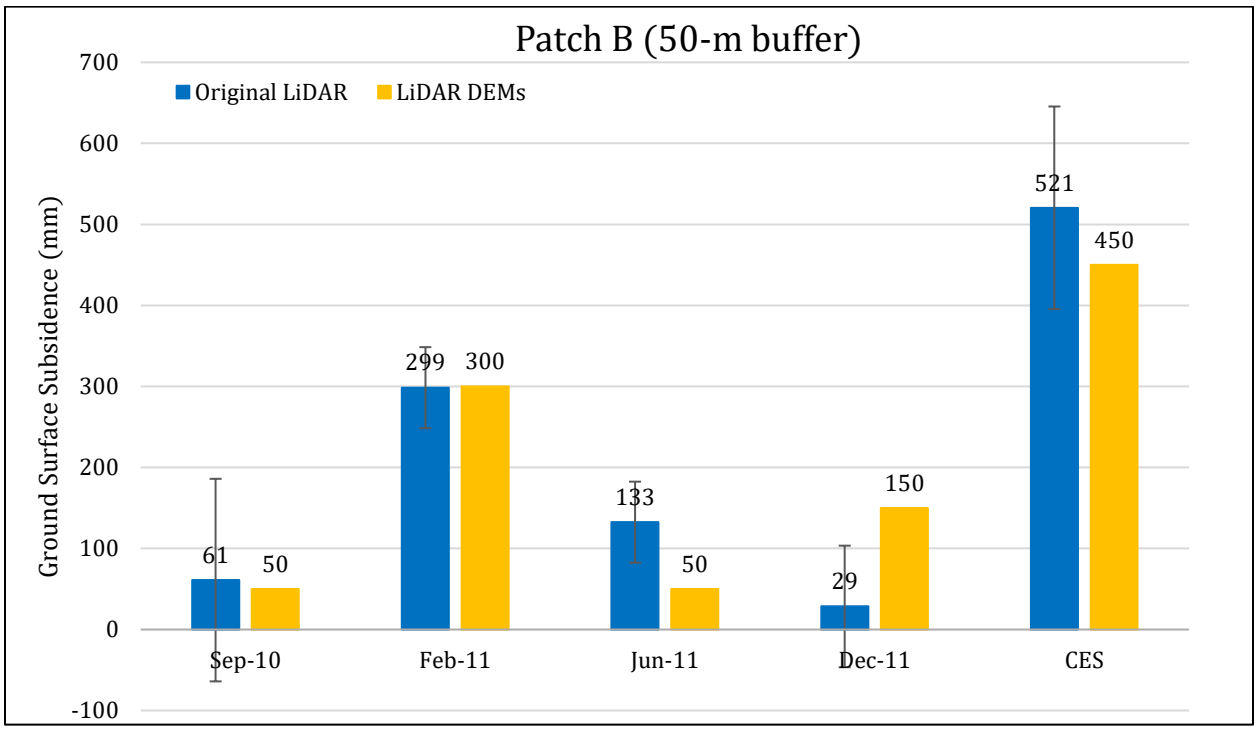

Figure 3: Comparison between ground surface subsidence determined from original LiDAR survey points and ground surface subsidence (50th %ile) estimated using LiDAR DEMs for Patch B.

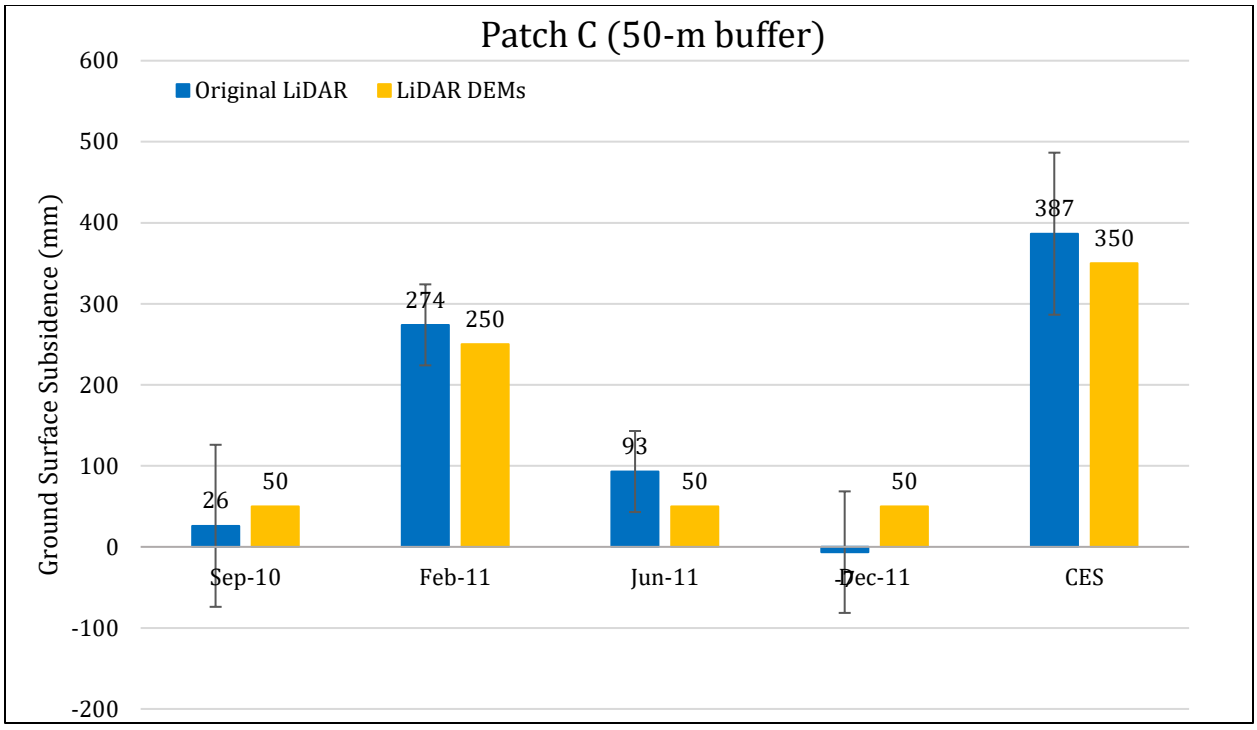

Figure 4: Comparison between ground surface subsidence determined from original LiDAR survey points and ground surface subsidence (50th %ile) estimated using LiDAR DEMs for Patch C.

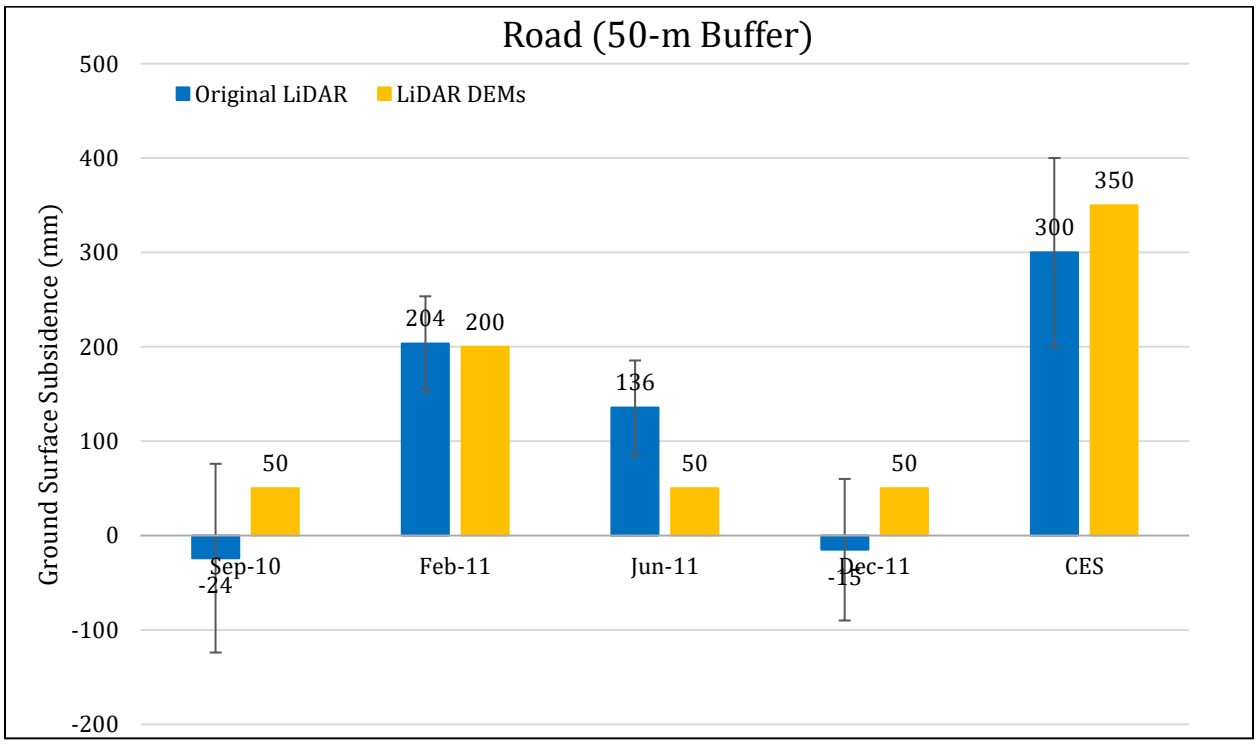

Figure 5: Comparison between ground surface subsidence determined from original LiDAR survey points and ground surface subsidence (50th %ile) estimated using LiDAR DEMs for Road.

Note 2: The ground surface subsidence values determined from original LiDAR survey points are similar to the ground surface subsidence values estimated using LiDAR DEMs for all earthquake events.

Table 8a: Ejecta-Induced settlement for the top 20 m of the soil profile for Patch A for the 50th %ile PGA, P_L=50%, and C_{FC}=0.13 using BI-2014, ZRB-2002, and I_C cutoff of 2.6.

Earthquake Event(s)	M_W	PGA (g)	Depth to Groundwater (m)	S_T (mm)	S_{V1D} (mm)	$S_{E,L}$ (mm)
Sep-10	7.1	0.17	1.5	33±125	12±20	21±127
Feb-11	6.2	0.38	1.2	283±50	98±50	185±71
Jun-11	6.2	0.24	2.2	161±50	18±25	143±56
Dec-11	6.1	0.33	1.2	1±75	67±50	-66±90

Notes: S_T = Total settlement (Table 6); S_{V1D} = Average vertical settlement due to volumetric compression using Boulanger and Idriss (2014) (BI-2014), Zhang et al. (2002) (ZRB-2002) procedures and de Greef and Lengkeek (2018) thin-layer correction; $S_{E,L}$ = Ejecta-induced settlement as the difference between the LiDAR-based S_T and S_{V1D}.

Table 8b: Ejecta-Induced settlement for the top 20 m of the soil profile for Patch B for the 50th %ile PGA, P_L=50%, and C_{FC}=0.13 using BI-2014, ZRB-2002, and I_C cutoff of 2.6.

Earthquake Event(s)	M_W	PGA (g)	Depth to Groundwater (m)	S_T (mm)	S_{V1D} (mm)	$S_{E,L}$ (mm)
Sep-10	7.1	0.17	1.5	61±125	10±20	51±127
Feb-11	6.2	0.38	1.2	299±50	81±50	218±71
Jun-11	6.2	0.24	2.2	133±50	17±25	116±56
Dec-11	6.1	0.33	1.2	29±75	60±50	-31±90

Notes: S_T = Total settlement (Table 6); S_{V1D} = Average vertical settlement due to volumetric compression using Boulanger and Idriss (2014) (BI-2014), Zhang et al. (2002) (ZRB-2002) procedures and de Greef and Lengkeek (2018) thin-layer correction; $S_{E,L}$ = Ejecta-induced settlement as the difference between the LiDAR-based S_T and S_{V1D}.

Table 8c: Ejecta-Induced settlement for the top 20 m of the soil profile for Patch C for the 50th %ile PGA, P_L=50%, and C_{FC}=0.13 using BI-2014, ZRB-2002, and I_C cutoff of 2.6.

Earthquake Event(s)	M_W	PGA (g)	Depth to Groundwater (m)	S_T (mm)	S_{V1D} (mm)	$S_{E,L}$ (mm)
Sep-10	7.1	0.17	1.5	26±100	57±20	-31±102
Feb-11	6.2	0.38	1.2	274±50	188±50	86±71
Jun-11	6.2	0.24	2.2	93±50	86±25	7±56
Dec-11	6.1	0.33	1.2	-7±75	165±50	-172±90

Notes: S_T = Total settlement (Table 6); S_{V1D} = Average vertical settlement due to volumetric compression using Boulanger and Idriss (2014) (BI-2014), Zhang et al. (2002) (ZRB-2002) procedures and de Greef and Lengkeek (2018) thin-layer correction; $S_{E,L}$ = Ejecta-induced settlement as the difference between the LiDAR-based S_T and S_{V1D}.

Table 8d: Ejecta-Induced settlement for the top 20 m of the soil profile for Road for the 50th %ile PGA, P_L=50%, and C_{FC}=0.13 using BI-2014, ZRB-2002, and I_C cutoff of 2.6.

Earthquake Event(s)	M_W	PGA (g)	Depth to Groundwater (m)	S_T (mm)	S_{V1D} (mm)	$S_{E,L}$ (mm)
Sep-10	7.1	0.17	1.5	-24±100	25±20	-49±102
Feb-11	6.2	0.38	1.2	204±50	112±50	92±71
Jun-11	6.2	0.24	2.2	136±50	39±25	97±56
Dec-11	6.1	0.33	1.2	-15±75	92±50	-107±90

Notes: S_T = Total settlement (Table 6); S_{V1D} = Average vertical settlement due to volumetric compression using Boulanger and Idriss (2014) (BI-2014), Zhang et al. (2002) (ZRB-2002) procedures and de Greef and Lengkeek (2018) thin-layer correction; $S_{E,L}$ = Ejecta-induced settlement as the difference between the LiDAR-based S_T and S_{V1D}.

Note 3: The uncertainty for volumetric settlement was derived based on the sensitivity of volumetric settlement to PGA, C_{FC}, and P_L for each earthquake event for VsVp 57203 *Shirley Intermediate School* and CC LIQ 1 – CPT 5586 – *Vivian St* sites. Taking the 50th percentile as the baseline case, the minimum and maximum values corresponding to the difference between the 25th percentile and the 50th percentile and the 75th percentile and the 50th percentile were determined. The arithmetic mean of the range of the minimum and maximum difference was evaluated for each patch at the two sites. The maximum arithmetic mean for each earthquake event was rounded to the nearest five and used as the uncertainty value. Accordingly, the 1-D volumetric settlement uncertainties of ±20, ±50, ±25, and ±50 mm for the Sep-10, Feb-11, Jun-11, and Dec-11 earthquake events, respectively, were used for all sites in this study.

Table 9a: Coverage area and height of ejecta estimates for Patch A using photographs.

EQ Event	$H_{E,thin1}$ (mm)	$A_{E,thin1}$ (m^2)	$H_{E,thin2}$ (mm)	$A_{E,thin2}$ (m^2)	$H_{E,thick1}$ (mm)	$A_{E,thick1}$ (m^2)	$H_{E,thick2}$ (mm)	$A_{E,thick2}$ (m^2)	A_T (m^2)
Sep-10	0	0	0	0	0	0	0	0	89.5
Feb-11	30-50	12.3	50-100	21.5	80-160	31.2	100-200	13.2	89.5
Jun-11	0	0	40-100*	67.3	0	0	0	0	89.5
Dec-11	5-10	6.9	0	0	50-80	11.4	60-100	61.8	89.5

Notes: $A_{E,thick/thin}$ = Coverage area of thick/thin ejecta layers; $H_{E,thick/thin}$ = Lower-upper estimate of height of thick/thin ejecta layers; A_T= Total assessment area of a buffer being considered; Thin and thick layers correspond to light gray and dark gray colors of ejecta observed in aerial photographs; NA = Not available due to the lack of lack of physical evidence; * indicates uncertainty in the estimate due to the presence of shadows in the aerial photographs.

Table 9b: Coverage area and height of ejecta estimates for Patch B using photographs.

Earthquake Event	$A_{E,thick}$ (m^2)	$H_{E,thick}$ (m)	$A_{E,thin}$ (m^2)	$H_{E,thin}$ (m)	A_T (m^2)
Sep-10	0	0	0	0	23.8
Feb-11	0	0	0	0	23.8
Jun-11	0	0	0	0	23.8
Dec-11	0	0	0	0	23.8

Notes: $A_{E,thick/thin}$ =Coverage area of thick/thin ejecta layers; $H_{E,thick/thin}$ = Lower-upper estimate of height of thick/thin ejecta layers; A_T= Total assessment area of a buffer being considered; Thin and thick layers correspond to light gray and dark gray colors of ejecta observed in aerial photographs.

Table 9c: Coverage area and height of ejecta estimates for Patch C using photographs.

Earthquake Event	$A_{E,thick}$ (m^2)	$H_{E,thick}$ (m)	$A_{E,thin}$ (m^2)	$H_{E,thin}$ (m)	A_T (m^2)
Sep-10	0	0	0	0	29.3
Feb-11	0	0	0	0	29.3
Jun-11	0	0	0	0	29.3
Dec-11	0	0	0	0	29.3

Notes: $A_{E,thick/thin}$ =Coverage area of thick/thin ejecta layers; $H_{E,thick/thin}$ = Lower-upper estimate of height of thick/thin ejecta layers; A_T= Total assessment area of a buffer being considered; Thin and thick layers correspond to light gray and dark gray colors of ejecta observed in aerial photographs.

Table 9d: Coverage area and height of ejecta estimates for Road within the 50-m buffer using photographs.

Earthquake Event	Sep-10	Feb-11	Jun-11	Dec-11
$H_{E,thin1}$ (mm)	0	3-6	3-6	0
$A_{E,thin1}$ (m^2)	0	37.8	210	0
$H_{E,thin2}$ (mm)	0	5-10	0	5-10
$A_{E,thin2}$ (m^2)	0	214	0	49.9
$H_{E,thick1}$ (mm)	0	10-20	0	0
$A_{E,thick1}$ (m^2)	0	55.2	0	0
$H_{E,thick2}$ (mm)	0	60-80	0	0
$A_{E,thick2}$ (m^2)	0	44.7	0	0
$H_{E,prism+pyr}$ (mm)	0	14-82	9-210	7-75
$V_{E,prism+pyr}$ (m^3)	0	0.164-0.327	3.87-6.74	0.350-0.700
$H_{E,cc}$ (mm)	0	300-549	0	0
$V_{E,cc}$ (m^3)	0	8.00	0	0
$H_{E,t.prism1}$ (mm)	0	0	20-40	0
$H_{E,prism2}$ (mm)	0	0	120-160	0
$V_{E,t.prism}$ (m^3)	0	0	3.89-5.69	0
A_T (m^2)	381	361	380	394

Notes: $A_{E,thick/thin}$ = Coverage area of thick/thin ejecta layers; $H_{E,thick/thin}$ = Lower-upper estimate of height of thick/thin ejecta layers; $H_{E,prism+pyr}$ = Lower-upper estimate of ejecta height near the curb based on 2-4% cross slope of normal crown; $V_{E,prism}$ = Lower-upper estimate of total volume of prismatic-shape ejecta; $V_{E,pyr}$ = Lower-upper estimate of total volume of pyramidal-shape ejecta; $V_{E,cc}$ = Volume of conically shaped ejecta pile components; $H_{E,cc}$ = Lower-upper estimate of height of conically shaped ejecta pile components (based on the repose angle of 30°); $H_{E,t.prism1/2}$ = Lower-upper estimate of height of sides of ejecta layers shaped as a trapezoidal prism; $V_{E,t.prism}$ = Volume of ejecta layers shaped as a trapezoidal prism; A_T= Total assessment area of a buffer being considered.

Note 4: The values in Table 9 correspond to the coverage area of ejecta outlined in aerial photographs (Figures 78-82) and the lower and upper estimates of ejecta height based on geometry, ground photographs (Figures 83 and 84), and EQC LDAT property inspection notes (Figure 85 and 87) and reports (up to 500 mm in height of ejecta at 26 Atlantis St, a property near Patch A). The ejecta-induced settlement using photographs and engineering judgment, $S_{E,P}$, is estimated as

$$S_{E,P} = \frac{\sum_{i=1}^{a} A_{E,thick,i} * H_{E,thick,i} + \sum_{j=1}^{b} A_{E,thin,j} * H_{E,thin,j} + \frac{1}{3}\sum_{k=1}^{c} A_{E,pile,k} * R_{E,pile,k} * tan30°}{A_T} + \frac{\frac{1}{2}\sum_{n=1}^{f} W_{E,prism,n} * H_{E,prism,n} * L_{E,prism,n}}{A_T} + \frac{\frac{1}{2}\sum_{p=1}^{g} W_{E,t.prism,p} * L_{E,t.prism,p} * \left(H_{E,t.prism1,p} + H_{E,t.prism2,p}\right)}{A_T} = \frac{\sum_{i=1}^{a} V_{E,thick,i} + \sum_{j=1}^{b} V_{E,thin,j} + \sum_{k=1}^{c} V_{E,conical\ component,k} + \sum_{n=1}^{f} V_{E,prism,n} + \sum_{p=1}^{g} V_{E,t.prism,p}}{A_T}$$

where

- $A_{E,thick,i}$ and $H_{E,thick,i}$ are the area and the height of a thick ejecta layer, respectively;
- $A_{E,thin,j}$ and $H_{E,thin,j}$ are the area and the height of a thin ejecta layer, respectively;
- $A_{E,pile,k}$ and $R_{E,pile,k}$ are the area and the radius of an ejecta pile component, respectively, shaped as a cone with the repose angle of 30°;
- $W_{E,prism,n}$ and $L_{E,prism,n}$ are the width and the length of the coverage area of a prismatically shaped ejecta layer, respectively, and $H_{E,prism,n}$ is the height of a prism-like ejecta layer;
- $W_{E,t.prism,p}$ and $L_{E,t.prism,p}$ are the width and the length, respectively, of the coverage area of an ejecta layer shaped as a trapesoidal prism, and $H_{E,t.prism,p}$ is the height of a trapesoidal prism ejecta layer;
- A_T is the total assessment area for a buffer being considered (Figure 1).

Table 10a: Ejecta-induced settlement estimates for Patches A, B, and C based on photographs.

Earthquake Event	Patch A		Patch B		Patch C	
	$S_{E,P,lower}$ (mm)	$S_{E,P,upper}$ (mm)	$S_{E,P,lower}$ (mm)	$S_{E,P,upper}$ (mm)	$S_{E,P,lower}$ (mm)	$S_{E,P,upper}$ (mm)
Sep-10	0	0	0	0	0	0
Feb-11	59	116	0	0	0	0
Jun-11	30*	75*	0	0	0	0
Dec-11	48	80	0	0	0	0

Note: $S_{E,P,lower}$ and $S_{E,P,upper}$ correspond to lower and upper estimates of $S_{E,P}$, respectively; NA = Not available due to the lack of physical evidence; * indicates uncertainty in the estimate due to the presence of shadows on the aerial photographs.

Table 10b: Ejecta-induced settlement estimates for Road based on photographs.

Earthquake Event	Road (50-m buffer)	
	$S_{E,P,lower}$ (mm)	$S_{E,P,upper}$ (mm)
Sep-10	0	0
Feb-11	35	43
Jun-11	22	36
Dec-11	2	3

Note: $S_{E,P,lower}$ and $S_{E,P,upper}$ correspond to lower and upper estimates of $S_{E,P}$, respectively.

Table 11a: Best final estimates of ejecta-induced settlement for Patches A, B, and C.

EQ Event	Patch A			Patch B			Patch C		
	$S_{E,L}$ (mm)	$S_{E,P}$ (mm)	$S_{E,final}$ (mm)	$S_{E,L}$ (mm)	$S_{E,P}$ (mm)	$S_{E,final}$ (mm)	$S_{E,L}$ (mm)	$S_{E,P}$ (mm)	$S_{E,final}$ (mm)
Sep-10	21±127	0	0	51±127	0	0	-31±102	0	0
Feb-11	185±71	88±28	120±30	218±71	0	0	86±71	0	0
Jun-11	143±56	*53±22	*85±25	116±56	0	0	7±56	0	0
Dec-11	-66±90	64±16	65±15	-31±90	0	0	-172±90	0	0

Notes: $S_{E,L}$ = Ejecta-induced settlement based on LiDAR data reported in Table 8; $S_{E,P}$ = Median ejecta-induced settlement for the range of values reported in Table 10; $S_{E,final}$ = Best final estimate of ejecta-induced settlement rounded to the nearest 5; Final plus/minus values are also rounded to the nearest 5; * indicates uncertainty in the estimate due to the presence of shadows in the aerial photographs.

Table 11b: Best final estimates of ejecta-induced settlement for Road.

EQ Event	Road (50-m buffer)		
	$S_{E,L}$ (mm)	$S_{E,P}$ (mm)	$S_{E,final}$ (mm)
Sep-10	-49±102	0	0
Feb-11	92±71	39±4	50±20
Jun-11	97±56	29±7	45±15
Dec-11	-107±90	2.5±0.5	5±5

Notes: $S_{E,L}$ = Ejecta-induced settlement based on LiDAR data reported in Table 8; $S_{E,P}$ = Median ejecta-induced settlement for the range of values reported in Table 10; $S_{E,final}$ = Best final estimate of ejecta-induced settlement rounded to the nearest 5; Final plus/minus values are also rounded to the nearest 5.

Note 5:

- For Patch A, $S_{E,final}$ for the Sep-10 and Dec-11 EQs is based on $S_{E,P}$ only. $S_{E,final}$ for the Feb-11 EQ and Jun-11 EQs is the weighted average of $S_{E,L}$ and $S_{E,P}$ with respective weight coefficients of 1/3 and 2/3.
- $S_{E,final}$ for Patches B and C is based solely on $S_{E,P}$ for all earthquake events.

- For Road, $S_{E,final}$ for the Sep-10 and Dec-11 EQs is based on $S_{E,P}$ only. For the Feb-11 and Jun-11 EQs, $S_{E,final}$ is a weighted average of $S_{E,L}$ and $S_{E,P}$ with weights coefficients of 0.25 and 0.75, respectively.
- The $S_{E,final}$ uncertainties are also a weighted average of uncertainties associated with $S_{E,L}$ and $S_{E,P}$ with the same weights used for the median $S_{E,L}$ and $S_{E,P}$ estimates.
- The weights are based on the LiDAR error bands, density of LiDAR points, LPI prediction error (Maurer et al. 2014[3]), presence of ejecta at the time of LiDAR surveys, and completeness of visual evidence (i.e., ground and aerial photographs and EQC LDAT property inspection reports for the site). The Wattle Dr site is in the apparent zone of higher ground surface subsidence for the Sep-10 EQ and the apparent zone of lower ground surface subsidence for the Feb-11 EQ (i.e., the underestimate of the ground surface elevation by the Sep-10 LiDAR survey). The site is in the zone of accurate LPI prediction of liquefaction severity for the Sep-10 EQ, but in the zone of accurate to slight LPI underprediction of liquefaction severity for the Feb-11 EQ. The LDAT property inspection reports are available for Patches A, B, and C; however, the ejecta within Patch A had already been removed at the time of the inspection. There are no ground photographs of the road.

Note 6: The inspection team did not observe lateral spreading and the retaining wall at the property with Patch A was not damaged as a result of the Feb-11 or Jun-11 earthquake (Figure 86).

Summary 1:

- **The best estimate of the ejecta-induced free-field ground settlement at the Wattle Dr site for the SEP 2010, FEB 011, JUN 2011, and DEC 2011 earthquake is 0 mm, 120±30 mm, 85±25 mm, and 65±15 mm, respectively.**
- **The eastern portion of the site, as divided by the retaining wall, exhibited less ejecta during the FEB 2011, JUN 2011, and DEC 2011 earthquakes than the western portion of the site. All houses in the western portion were at a lower elevation by ~0.5-1 m relative to the eastern portion of the site and had to be demolished; however, no house was damaged beyond economic repair in the eastern portion. The nearest CPT that could characterize the western portion of the site is 115 m away from the center of the site toward the SW, CPT 1402; its measurements are similar to the measurements of CPT 3966, which is in the NE quadrant.**
- **The best estimate of the ejecta-induced settlement of the road at the Wattle Dr site for the SEP 2010, FEB 2011, JUN 2011, and DEC 2011 earthquake is 0 mm, 50±20 mm, 45±15 mm, and <5 mm, respectively.**

Note 7: CC LIQ 3 was later renamed as CPT 90678.

[3] Maurer, B. W., Green, R. A., Cubrinovski, M., & Bradley, B. A. (2014). Evaluation of the Liquefaction Potential Index for Assessing Liquefaction Hazard in Christchurch, New Zealand. *Journal of Geotechnical and Geoenvironmental Engineering*, 140(7), 04014032-1-11. doi:10.1061/(asce)gt.1943-5606.0001117

Figure 6: Location of the site.

Figure 7: Position of the site relative to nearby buildings, vegetation, and free-face features.

Figure 8: Street view of the site showing flat land.

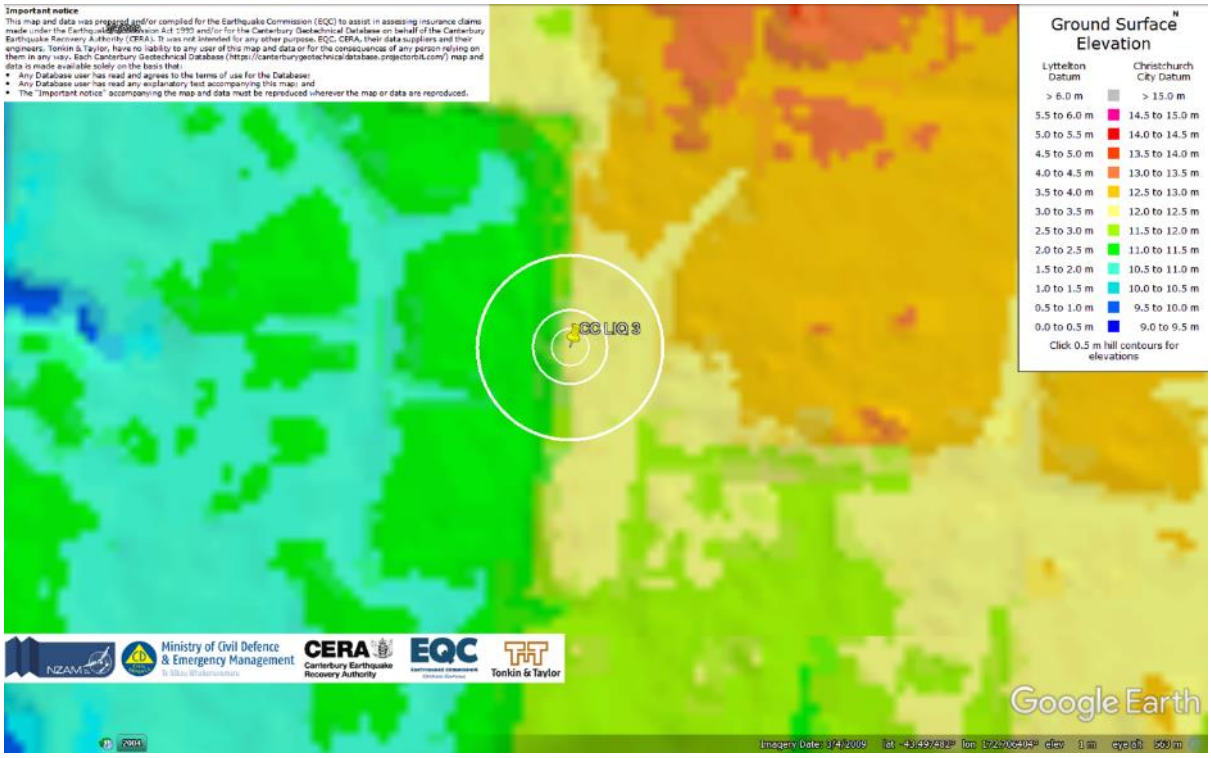

Figure 9: Ground surface elevation for Mar 2011 showing step changes in the ground surface.

Figure 10: Step change in ground surface elevation supported by retaining wall.

Figure 11: Satellite image of the site taken in Dec 2004.

Figure 12: Satellite image of the site taken in Mar 2009.

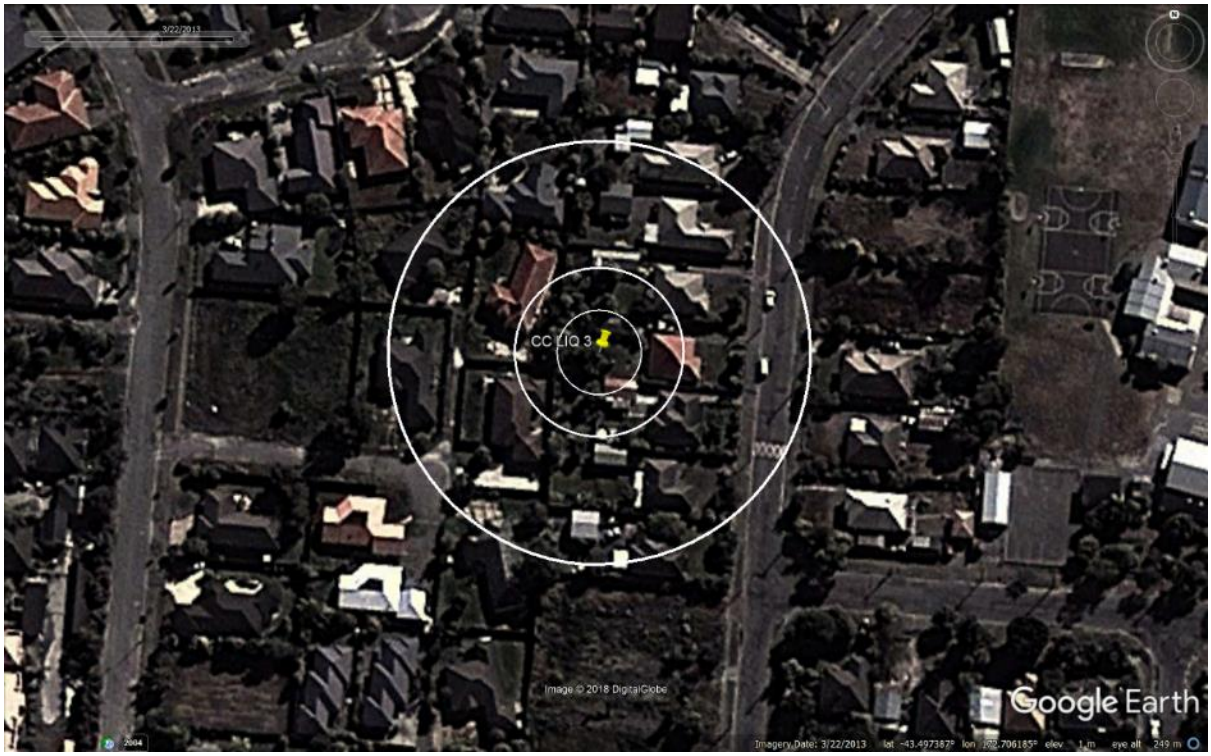

Figure 13: Satellite image of the site taken in Mar 2013.

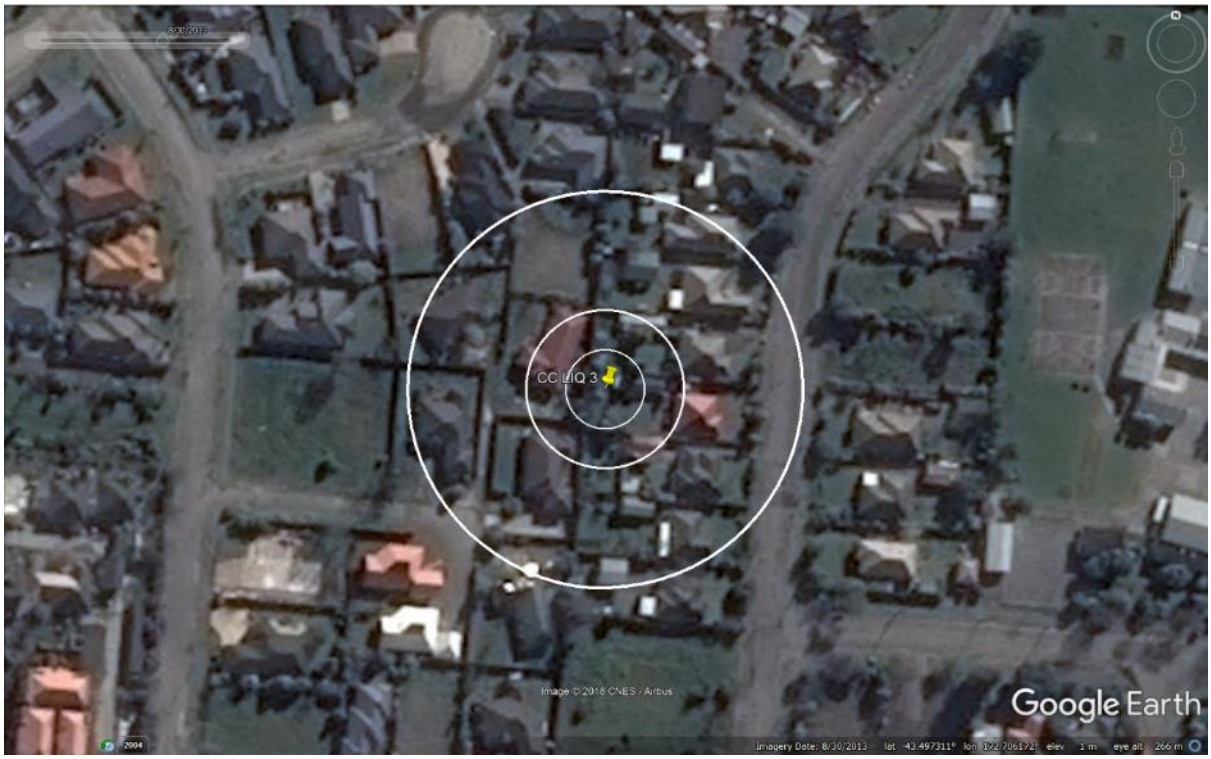

Figure 14: Satellite image of the site taken in Aug 2013.

Figure 15: Satellite image of the site taken in Mar 2014.

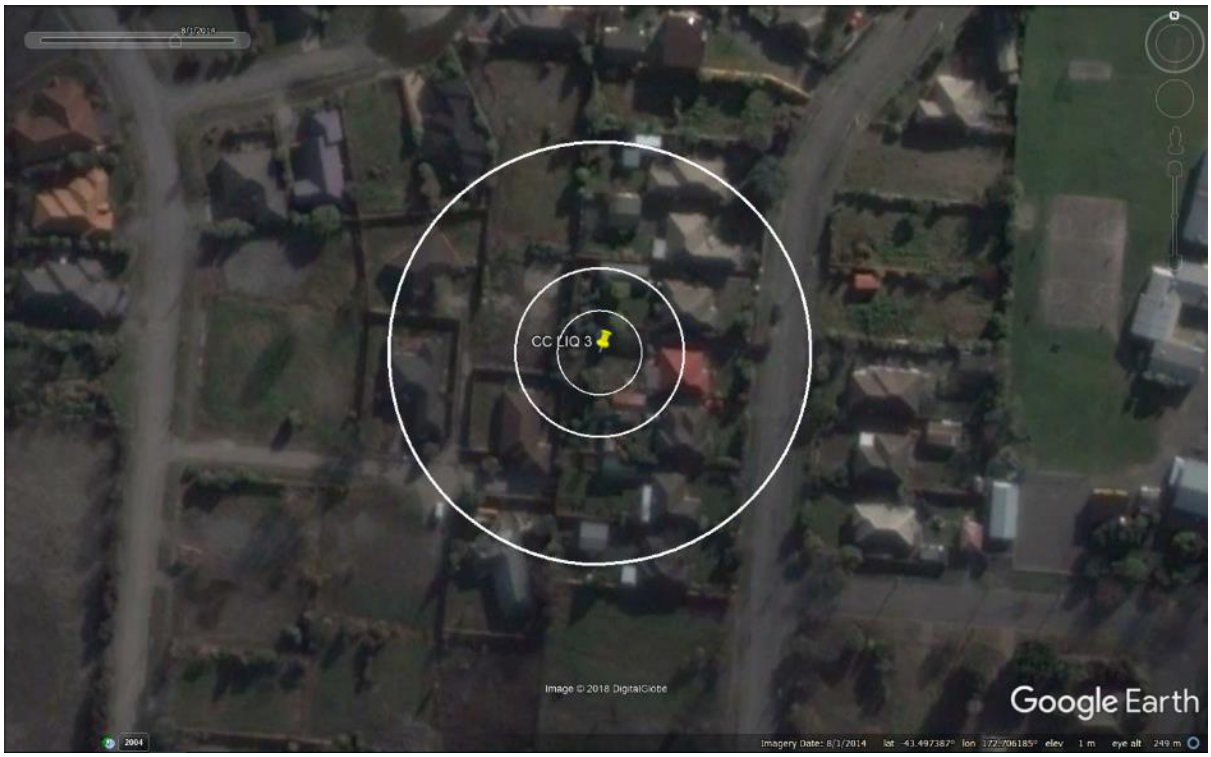

Figure 16: Satellite image of the site taken in Aug 2014.

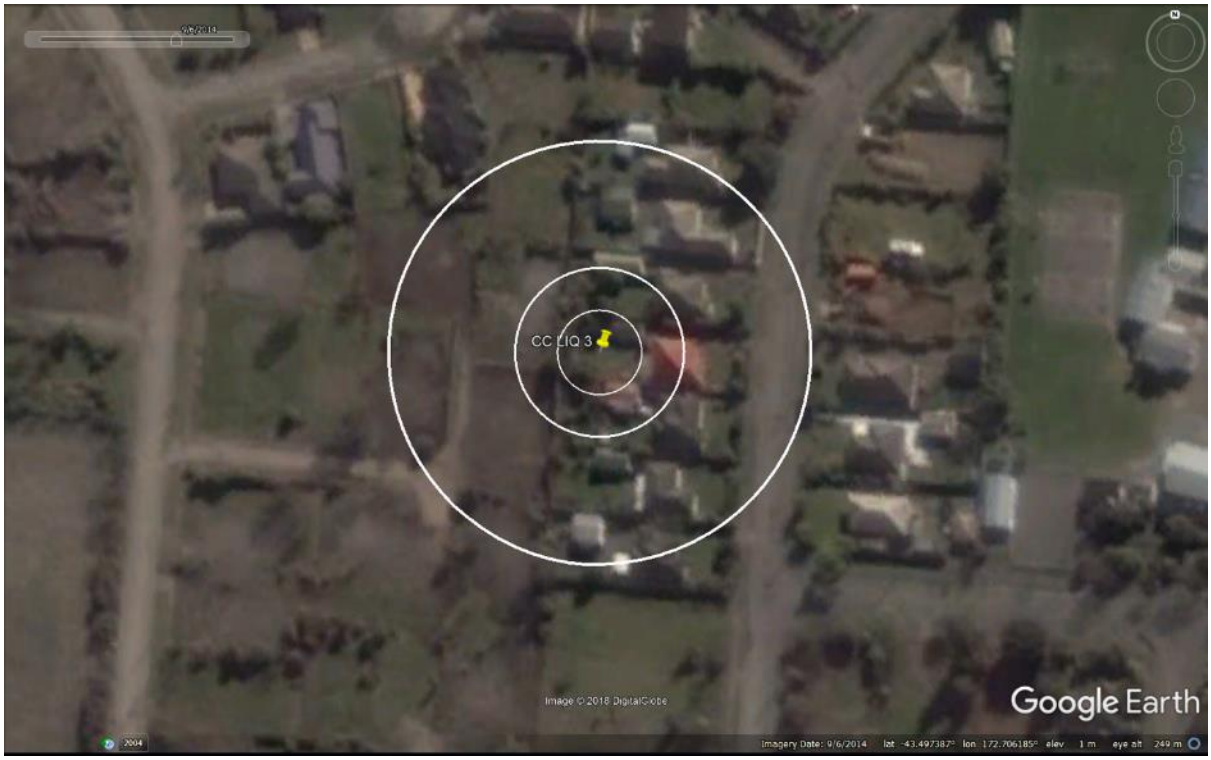

Figure 17: Satellite image of the site taken in Sep 2014.

Figure 18: Satellite image of the site taken in Jul 2015.

Figure 19: Satellite image of the site taken in Sep 2015.

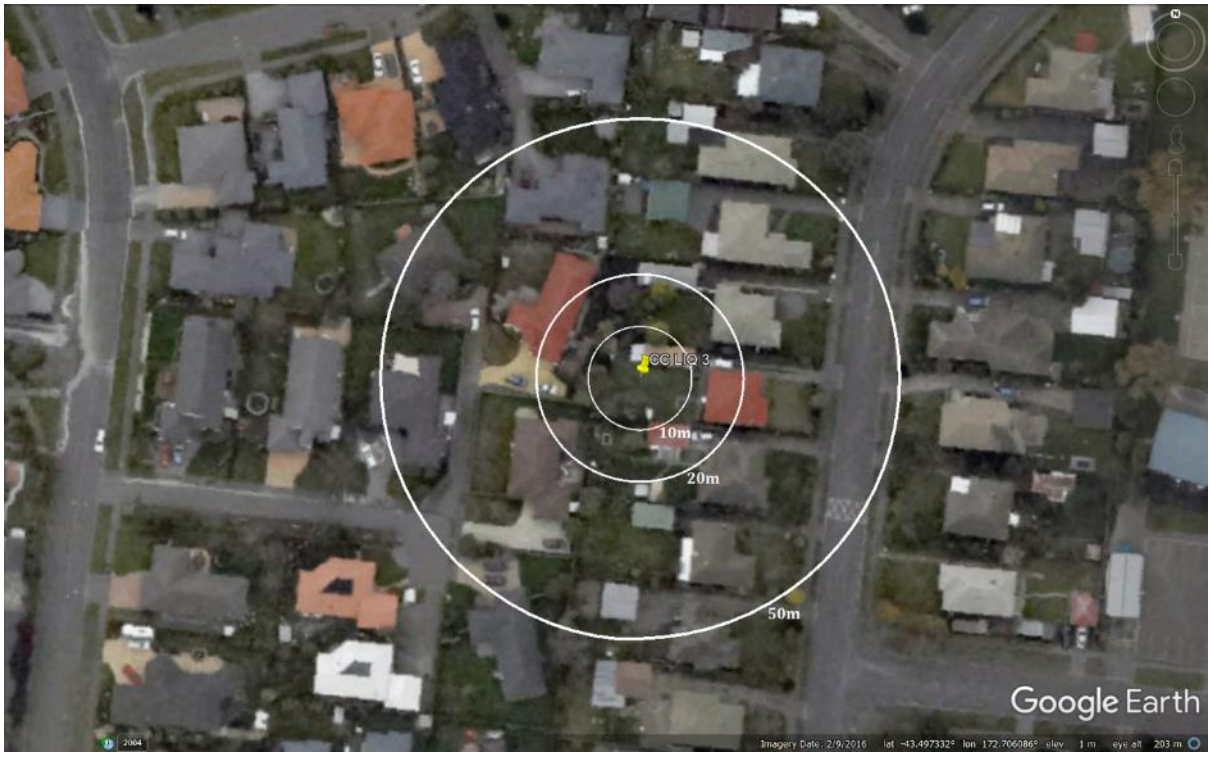

Figure 20: Aerial photograph of the site taken on Sep 4, 2010.

Figure 21: Aerial photograph of the site taken on Feb 24, 2011.

Figure 22: Aerial photograph of the site taken on June 14-15, 2011.

Figure 23: Aerial photograph of the site taken on Dec 24, 2011.

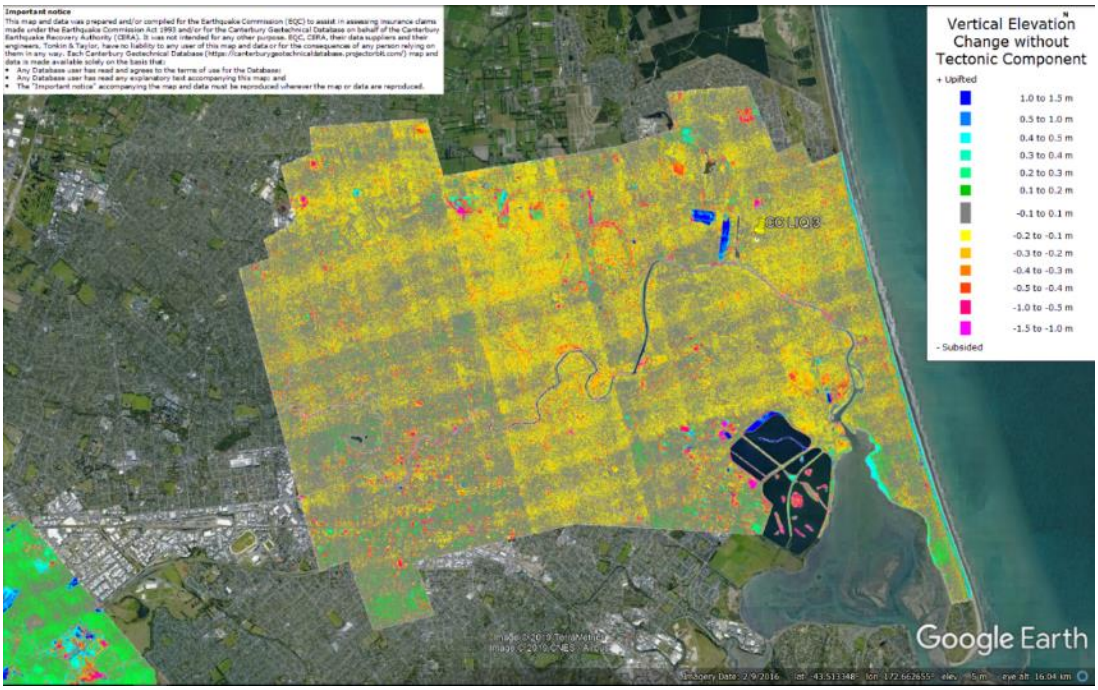

Figure 24: Vertical Ground Movements (Surface – Tectonic) for Sep 2010 Earthquake – the site is in the apparent zone of overestimated ground surface subsidence (i.e., Sep 2010 flight band error).

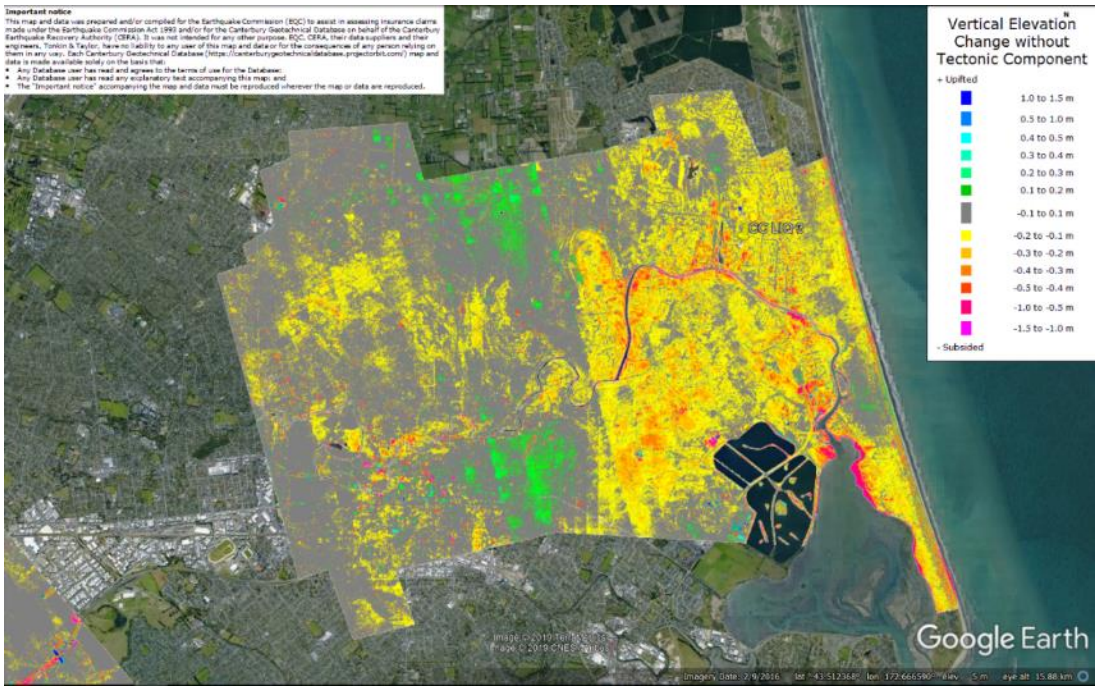

Figure 25: Vertical Ground Movements (Surface – Tectonic) for Feb 2011 Earthquake – the site is in the apparent zone of underestimated ground surface subsidence (i.e., Sep 2010 flight band error).

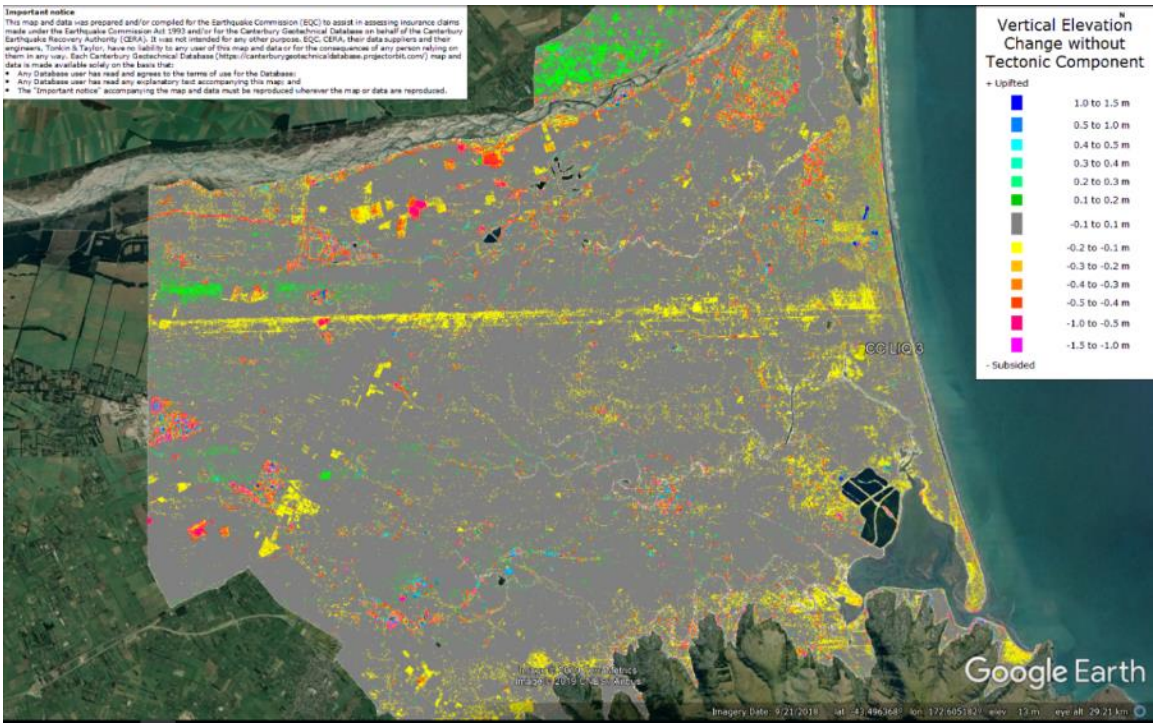

Figure 26: Vertical Ground Movements (Surface – Tectonic) for June 2011 Earthquake – the site is not in the apparent zone of overestimated or underestimated ground surface subsidence.

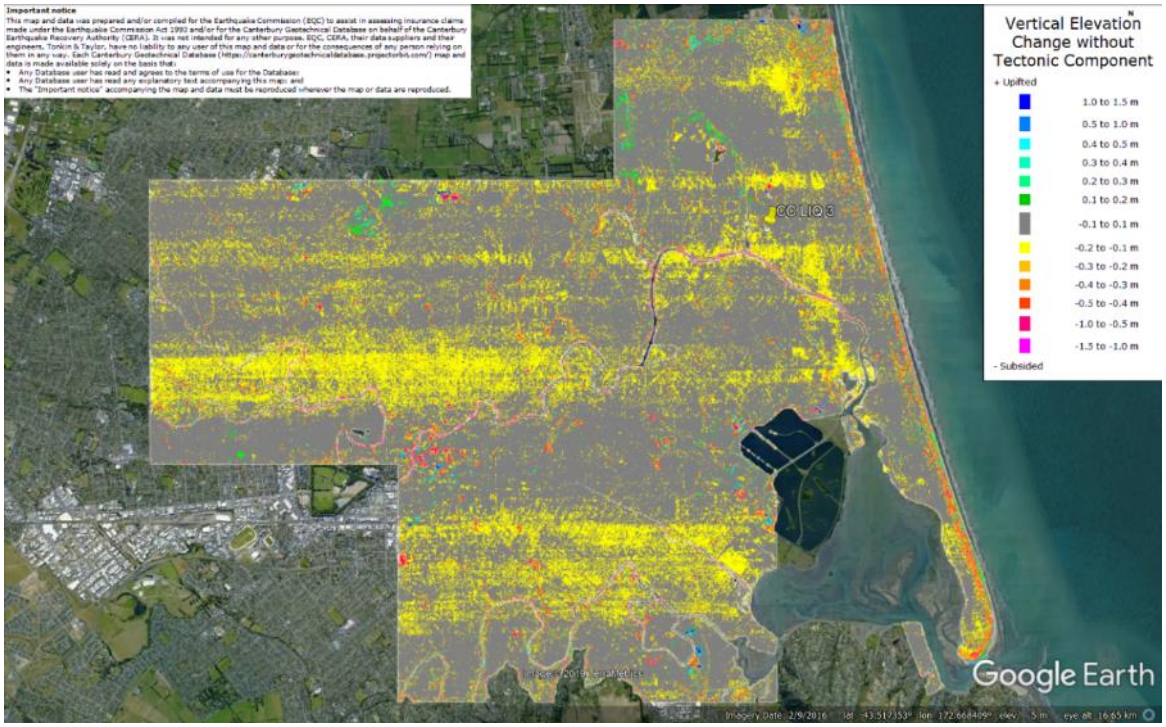

Figure 27: Vertical Ground Movements (Surface – Tectonic) for Dec 2011 Earthquake – the site is not in the apparent zone of overestimated or underestimated ground surface subsidence.

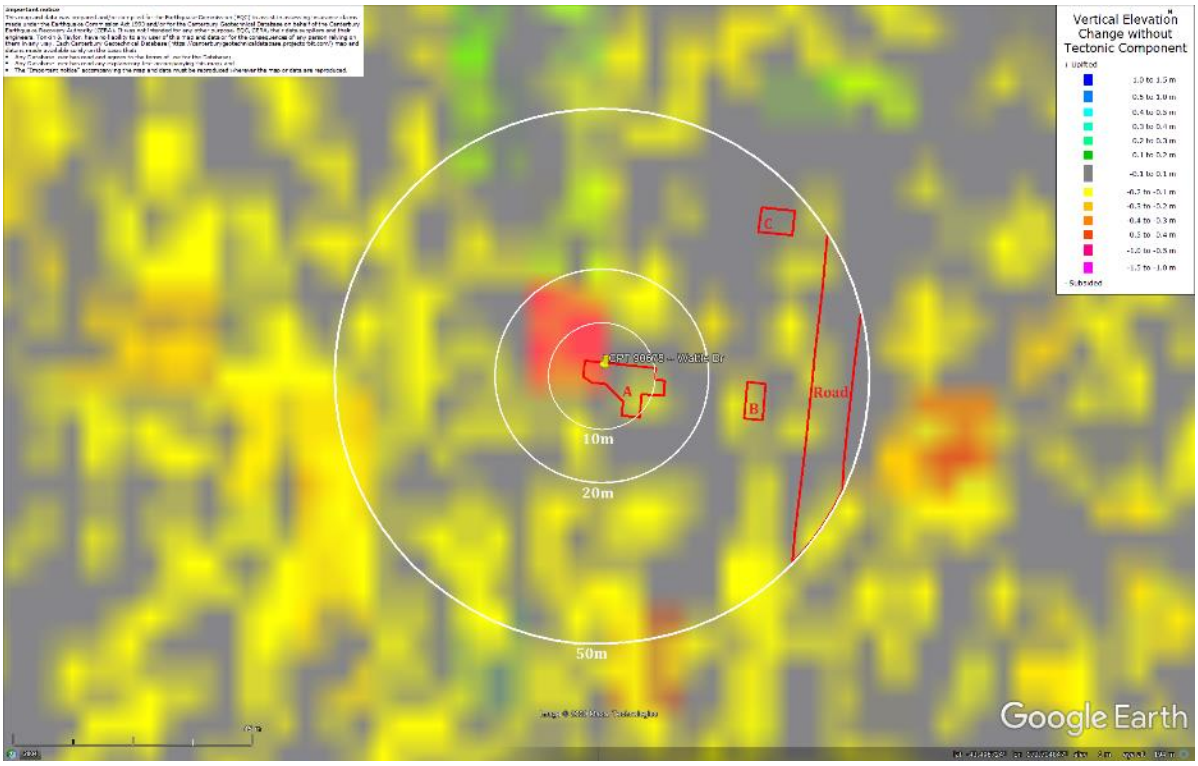

Figure 28: Ground surface subsidence without tectonic component for Sep 2010 Earthquake according to the LiDAR DEM.

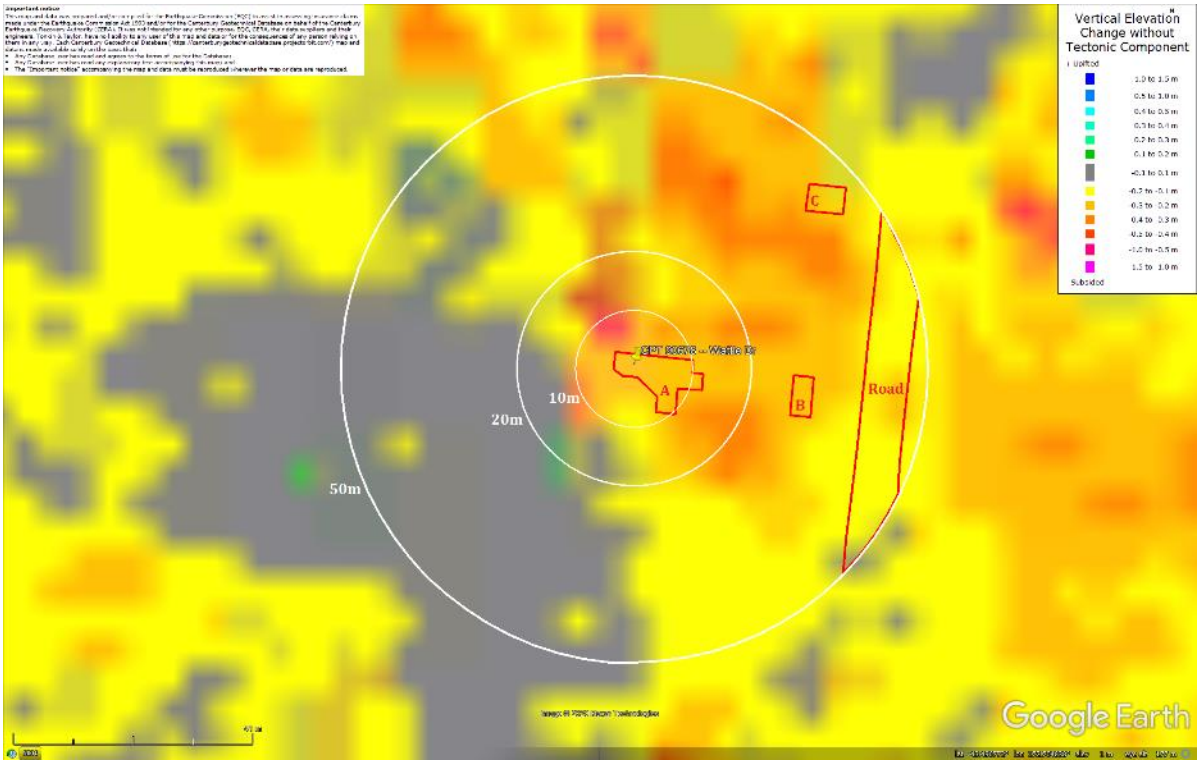

Figure 29: Ground surface subsidence without tectonic component for Feb 2011 Earthquake according to the LiDAR DEM.

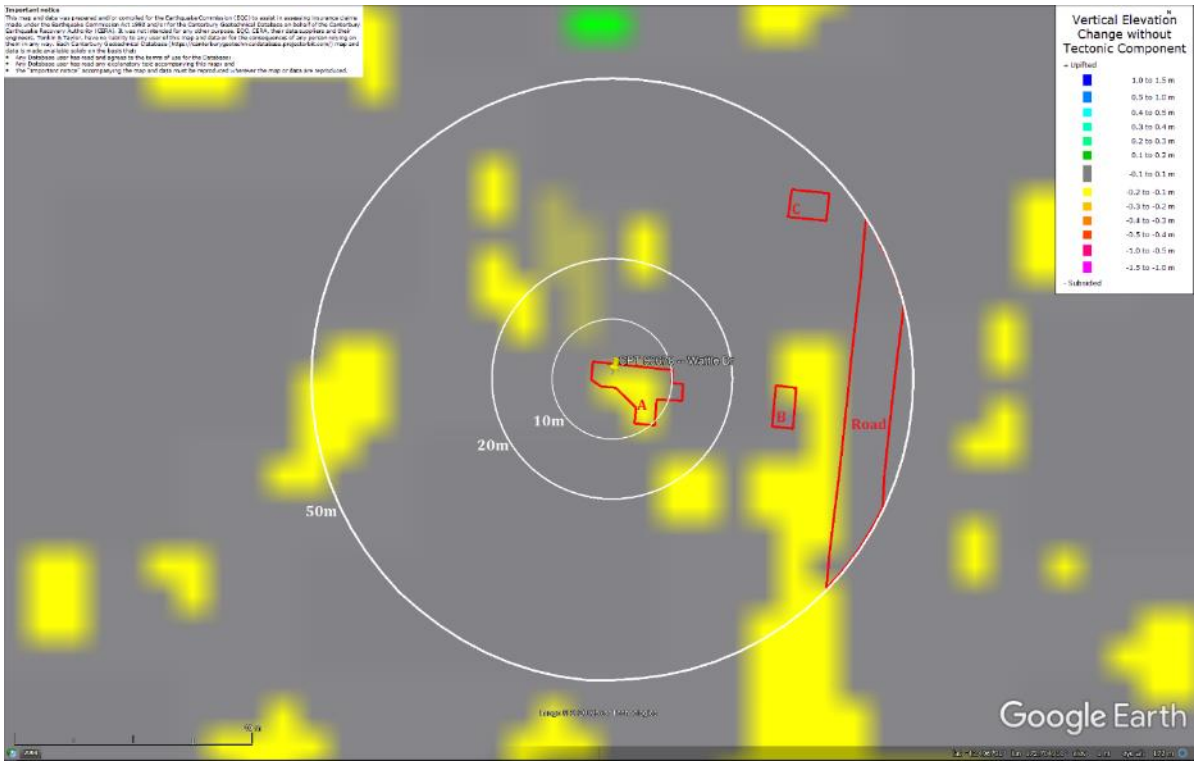

Figure 30: Ground surface subsidence without tectonic component for June 2011 Earthquake according to the LiDAR DEM.

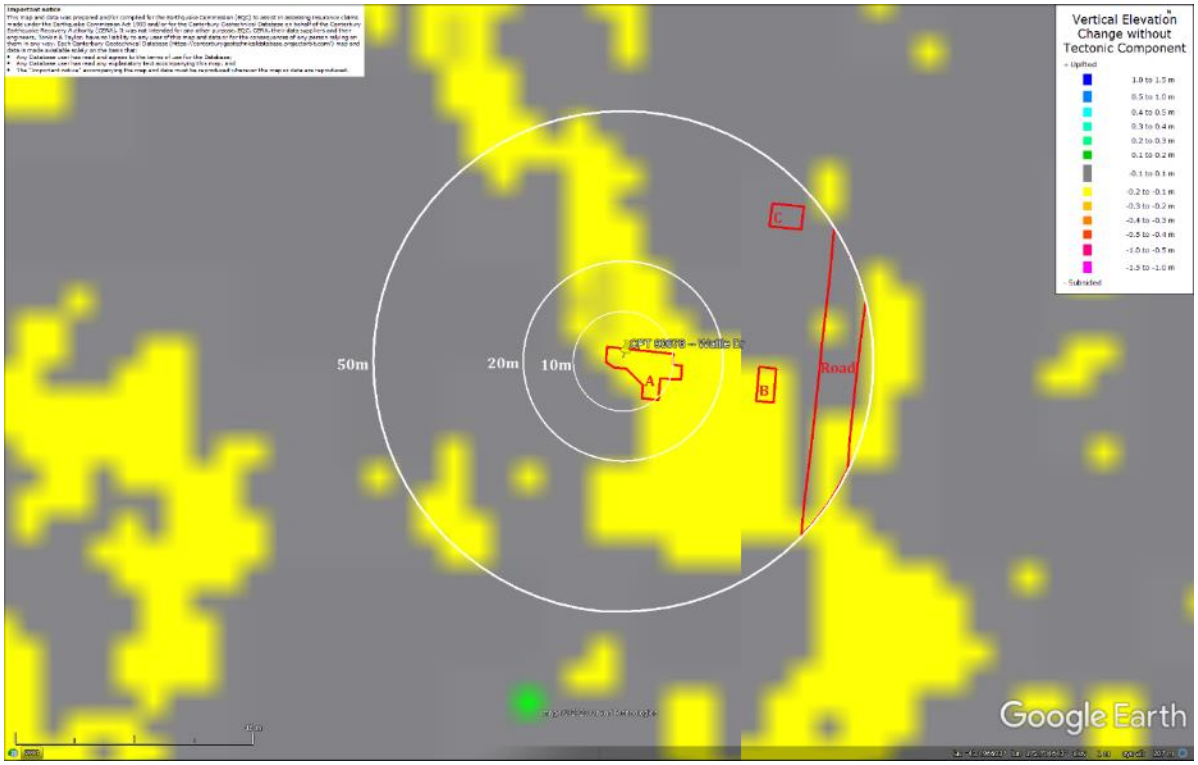

Figure 31: Ground surface subsidence without tectonic component for Dec 2011 Earthquake according to the LiDAR DEM.

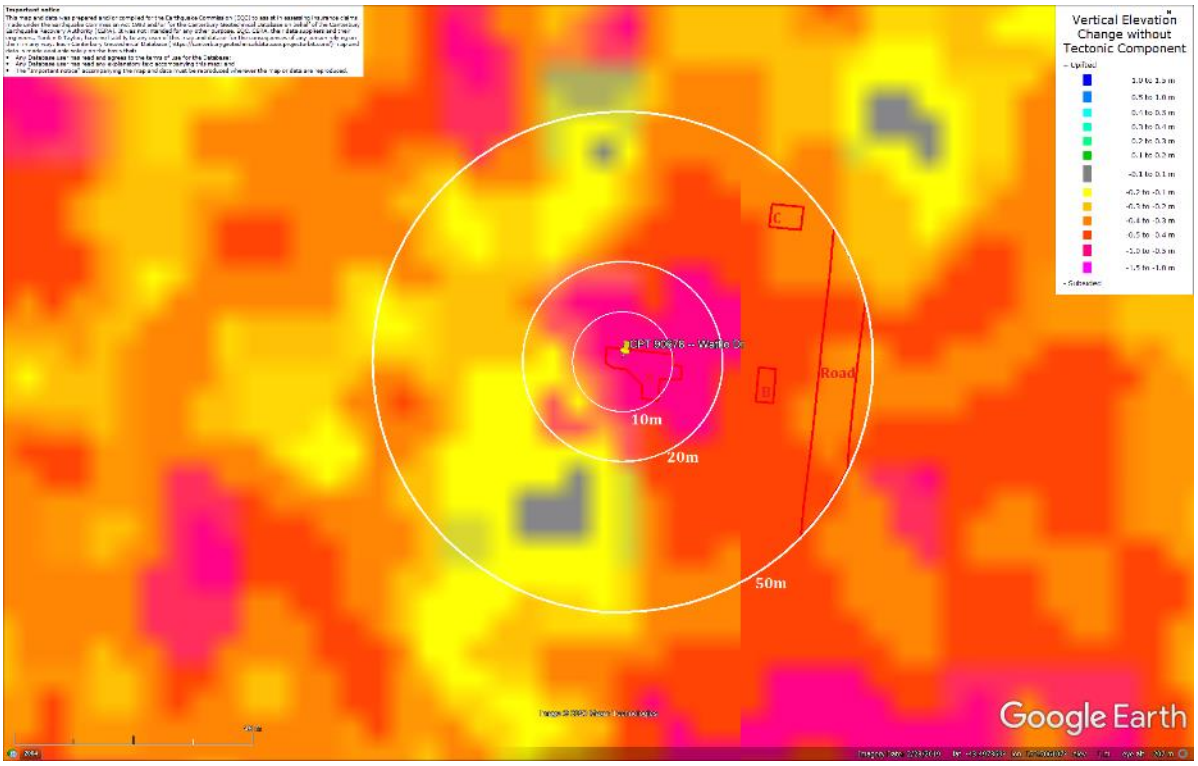

Figure 32: Ground surface subsidence without tectonic component for Canterbury Earthquake Sequence according to the LiDAR DEM.

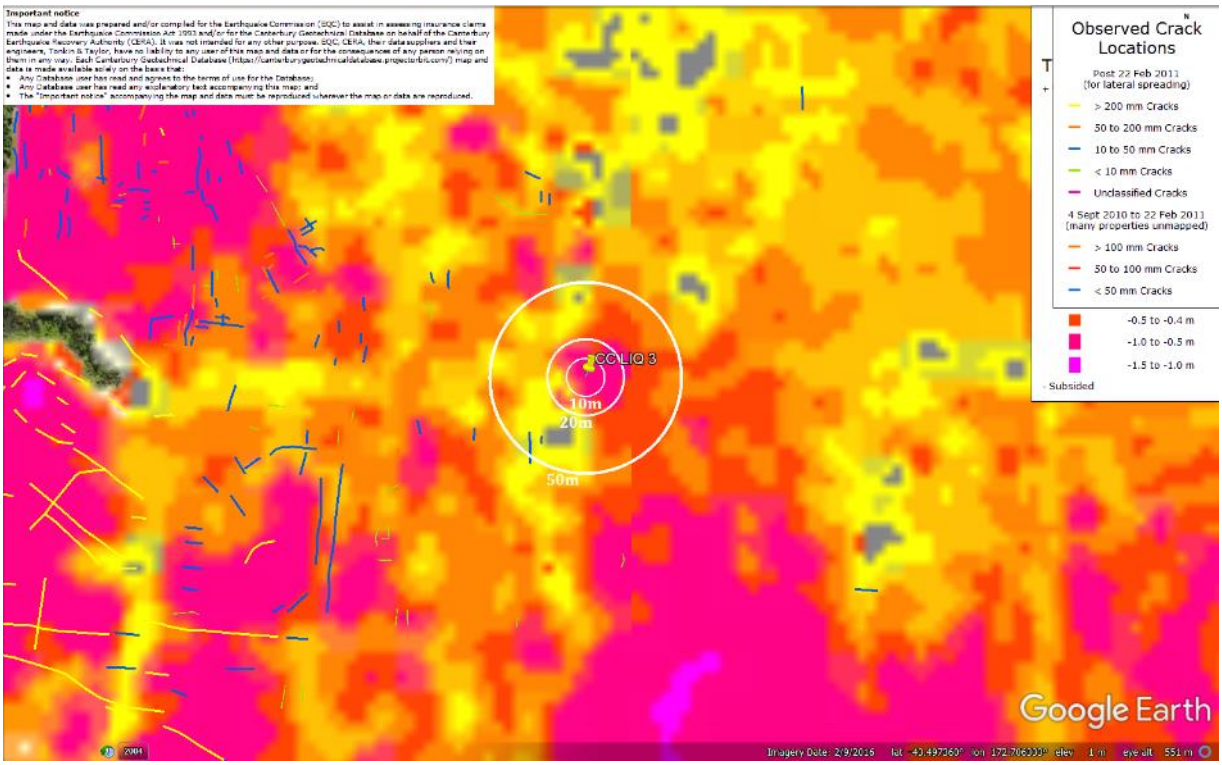

Figure 33: No lateral spreading for Canterbury Earthquake Sequence.

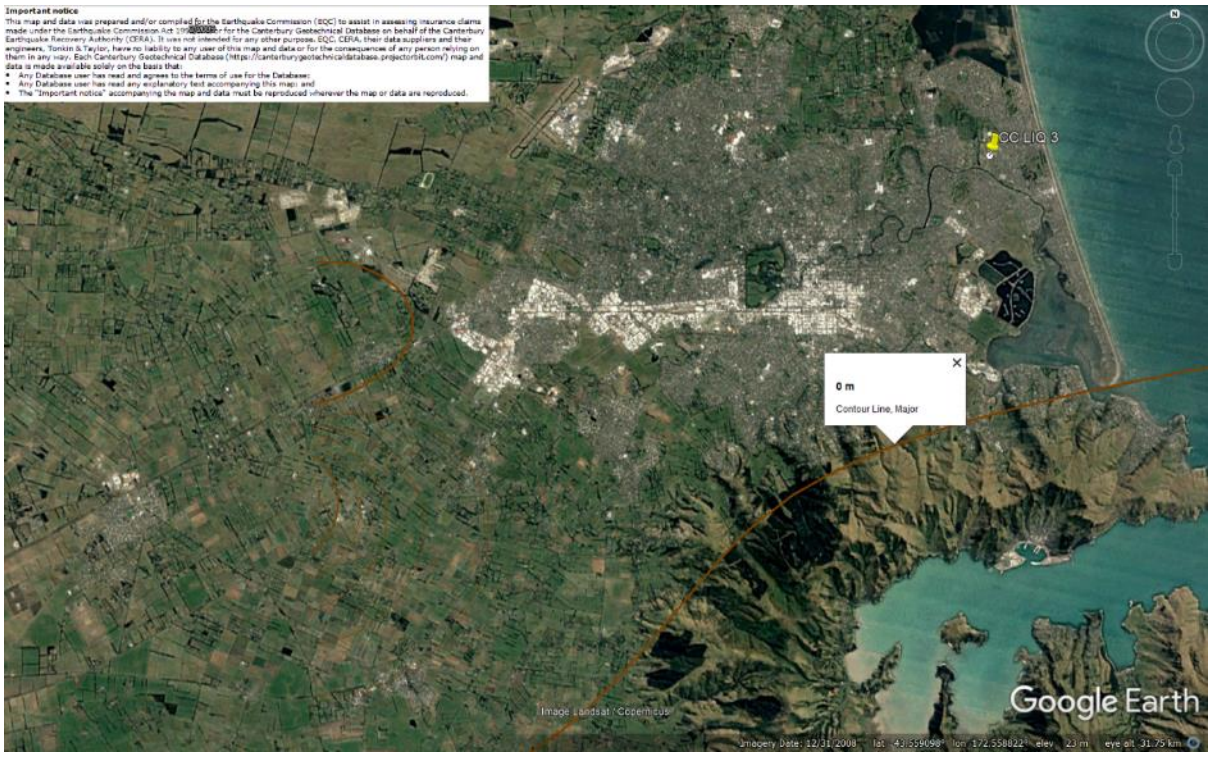

Figure 34: Vertical tectonic movements for Sep 2010 Earthquake.

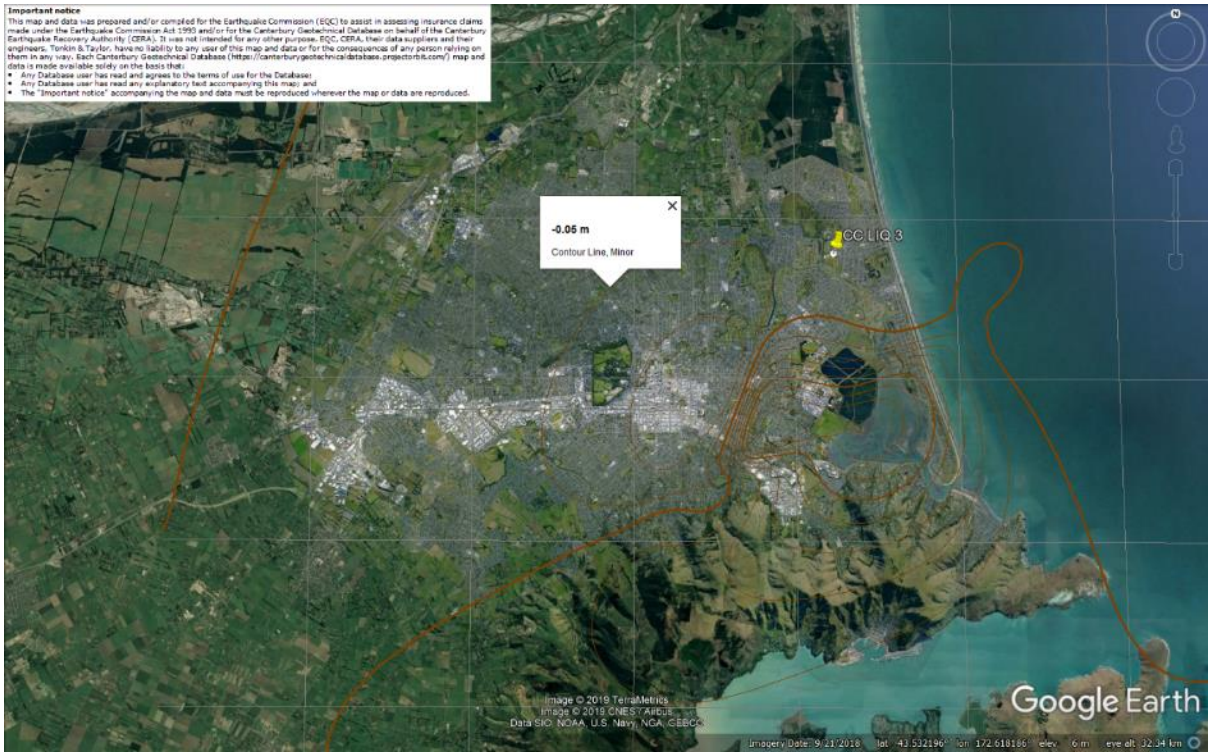

Figure 35: Vertical tectonic movements for Feb 2011 Earthquake.

Figure 36: Vertical tectonic movements for June 2011 Earthquake.

Figure 37: Vertical tectonic movements for Dec 2011 Earthquake.

Figure 38: Vertical tectonic movements for Canterbury Earthquake Sequence.

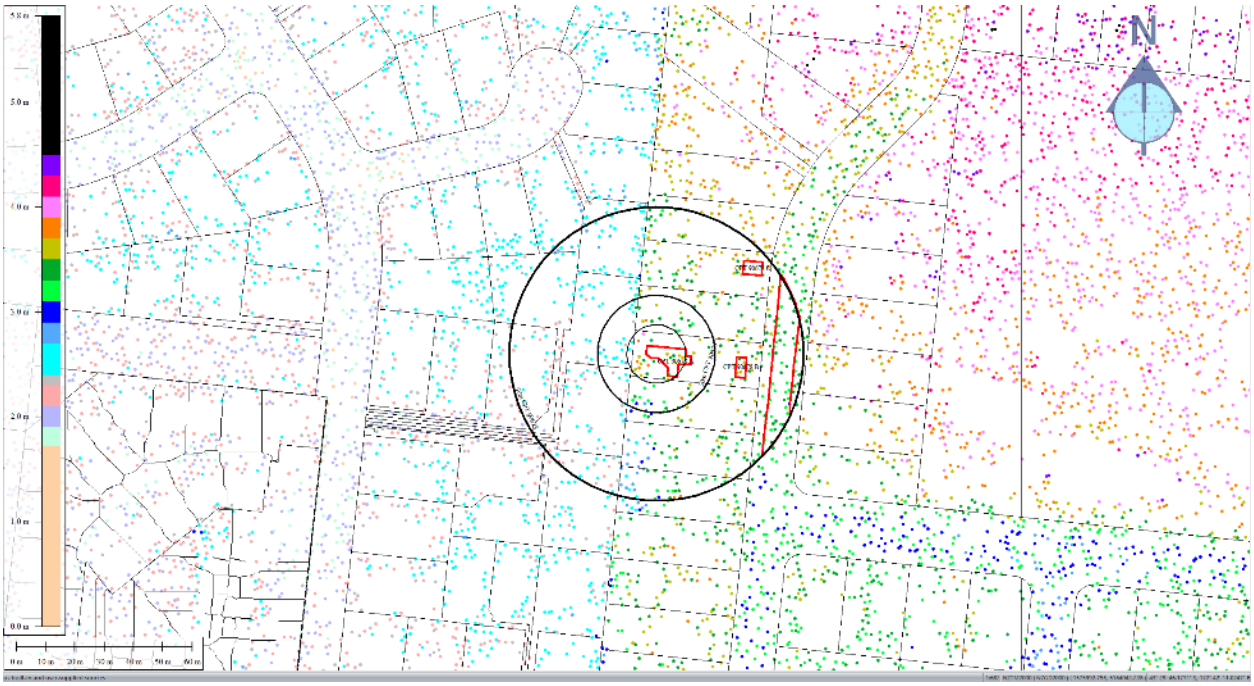

Figure 39: Jul 2003 LiDAR survey.

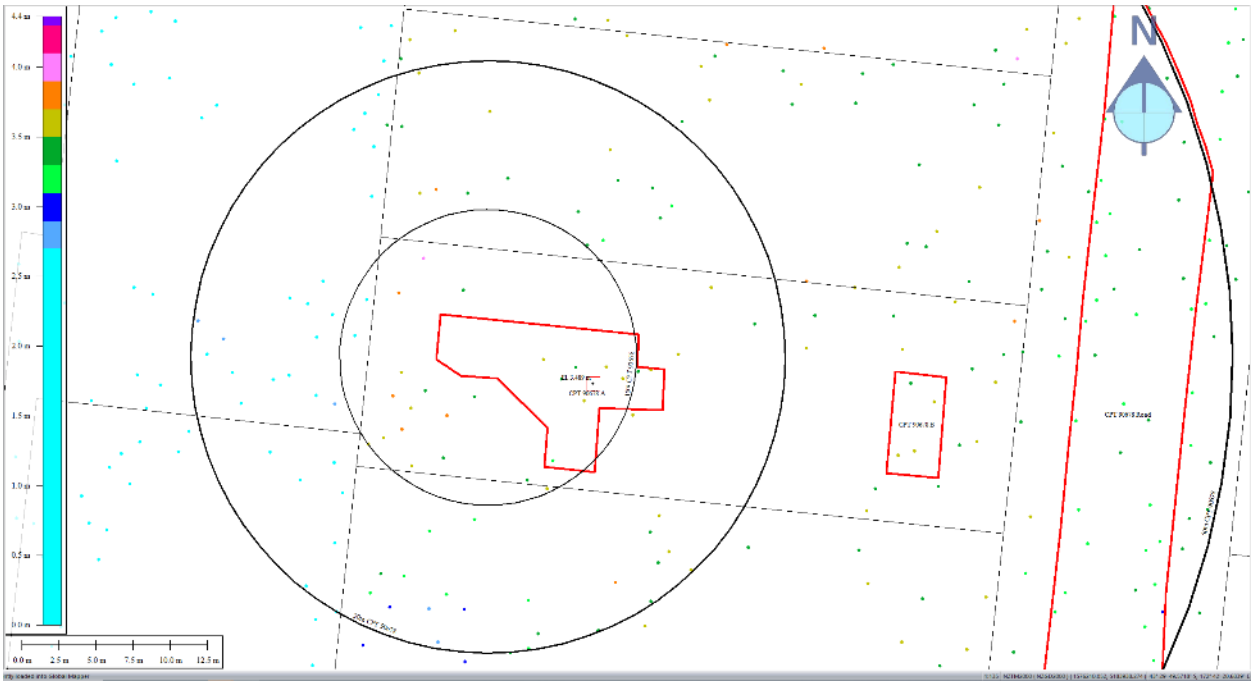

Figure 40: Ground surface elevation averaged over 10-m 20-m, and 50-m buffers for Patch A for Jul 2003 LiDAR survey.

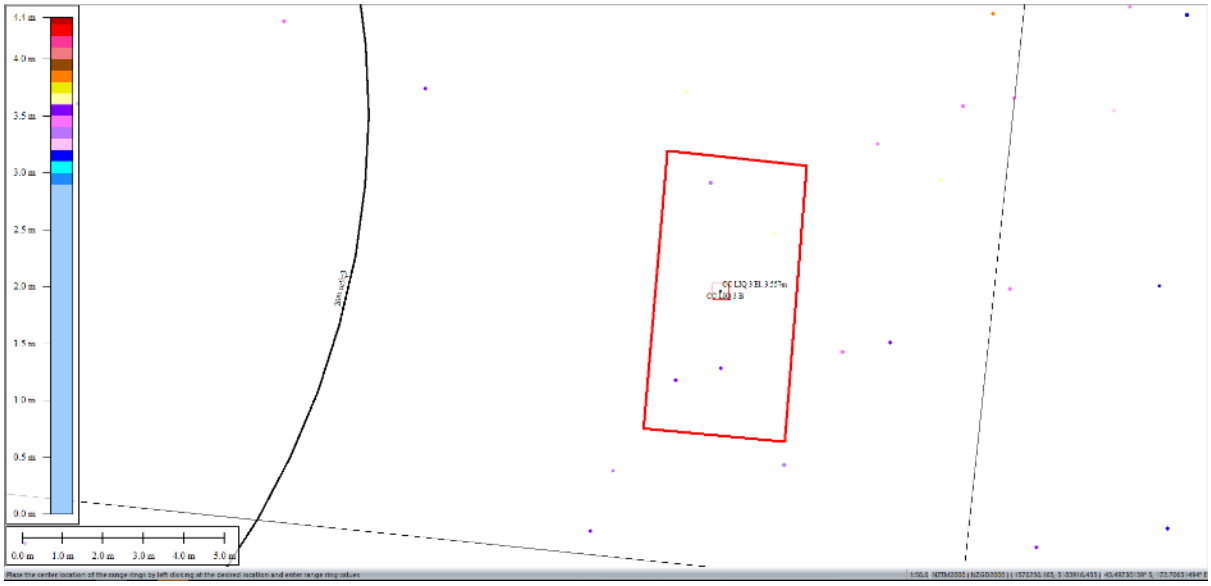

Figure 41: Ground surface elevation averaged over 50-m buffer for Patch B for Jul 2003 LiDAR survey.

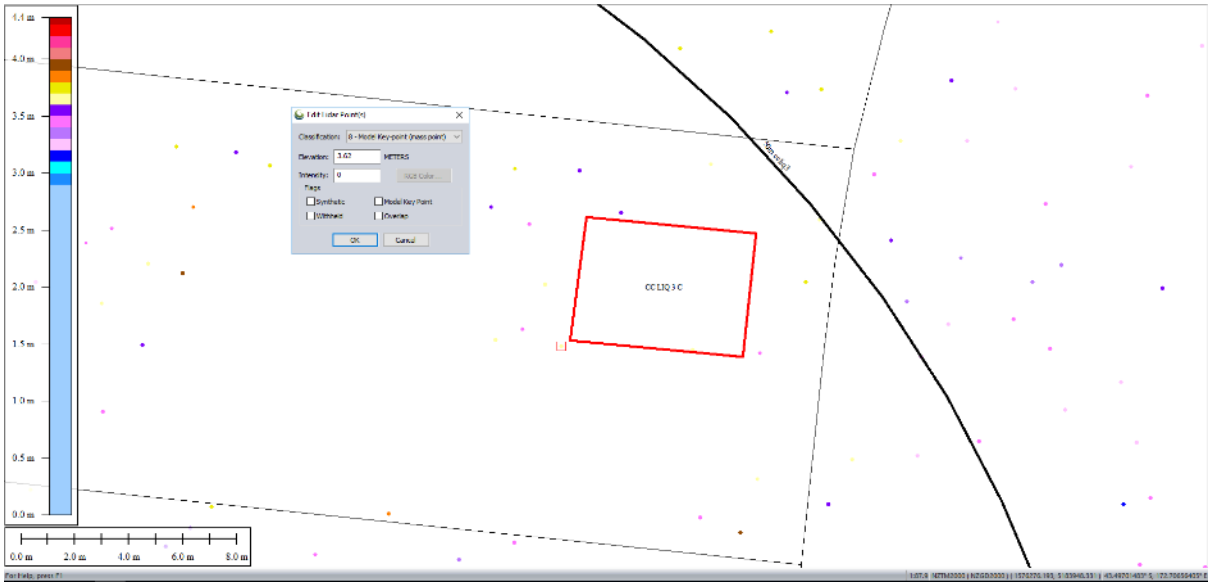

Figure 42: Ground surface elevation averaged over 50-m buffer for Patch C for Jul 2003 LiDAR survey.

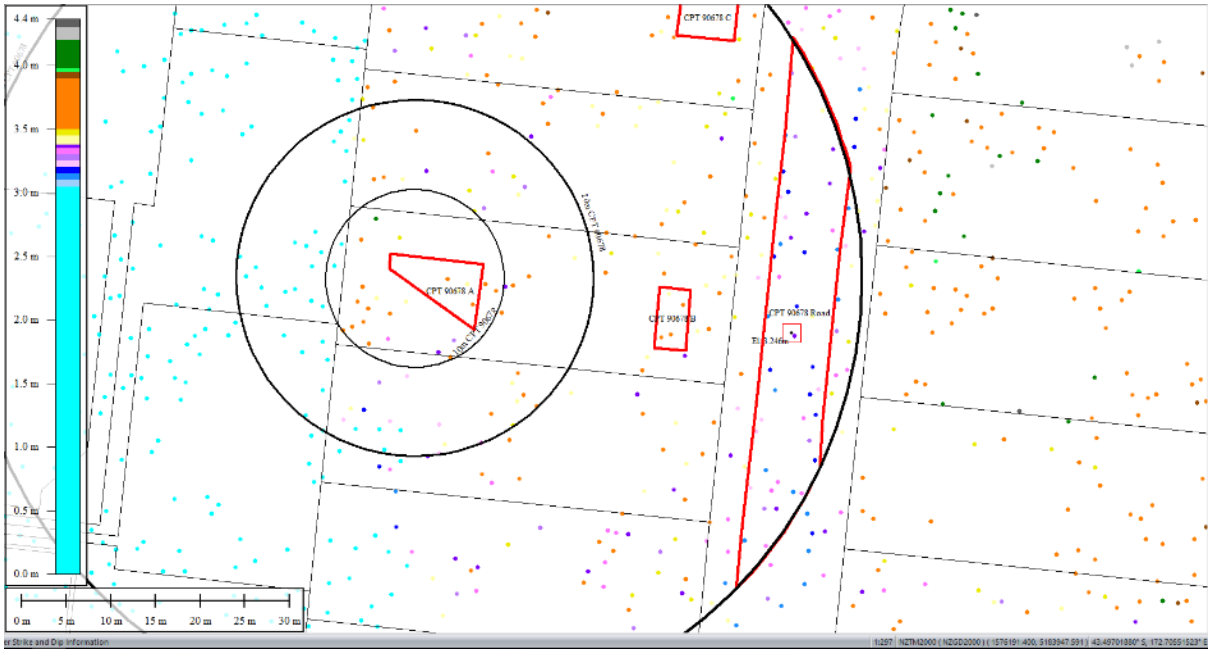

Figure 43: Ground surface elevation averaged over 50-m buffer for Road for Jul 2003 LiDAR survey.

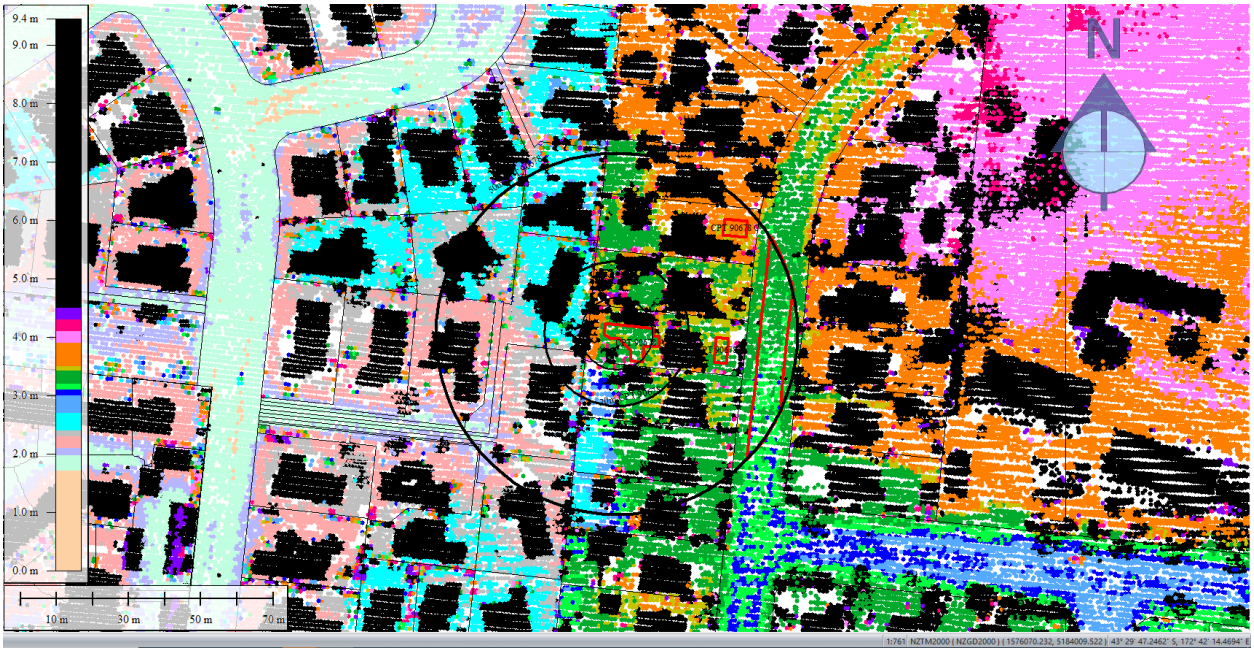

Figure 44: Sep 5, 2010 LiDAR survey.

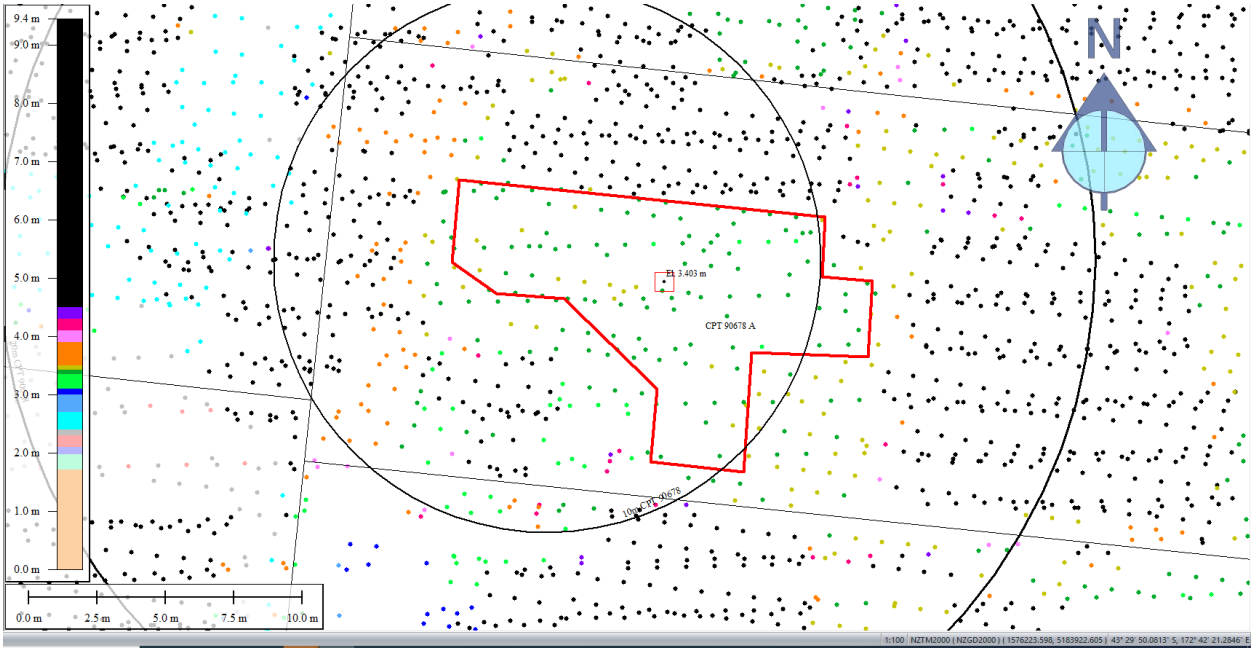

Figure 45: Ground surface elevation averaged over 10-m, 20-m, and 50-m buffers for Patch A for Sep 5, 2010 LiDAR survey.

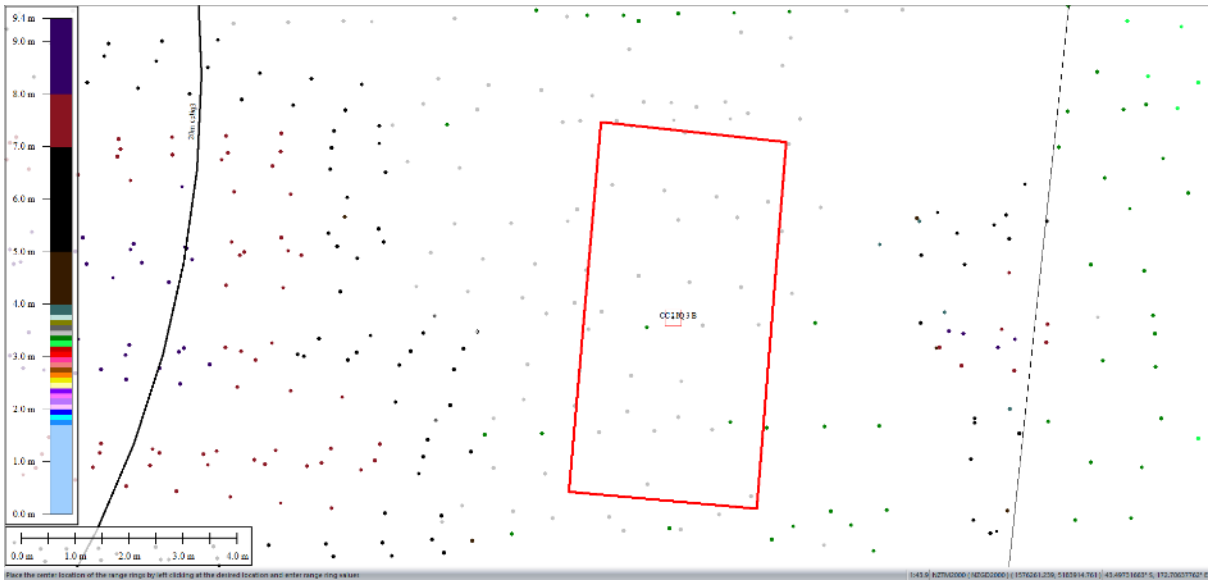

Figure 46: Ground surface elevation averaged over 50-m buffer for Patch B for Sep 5, 2010 LiDAR survey.

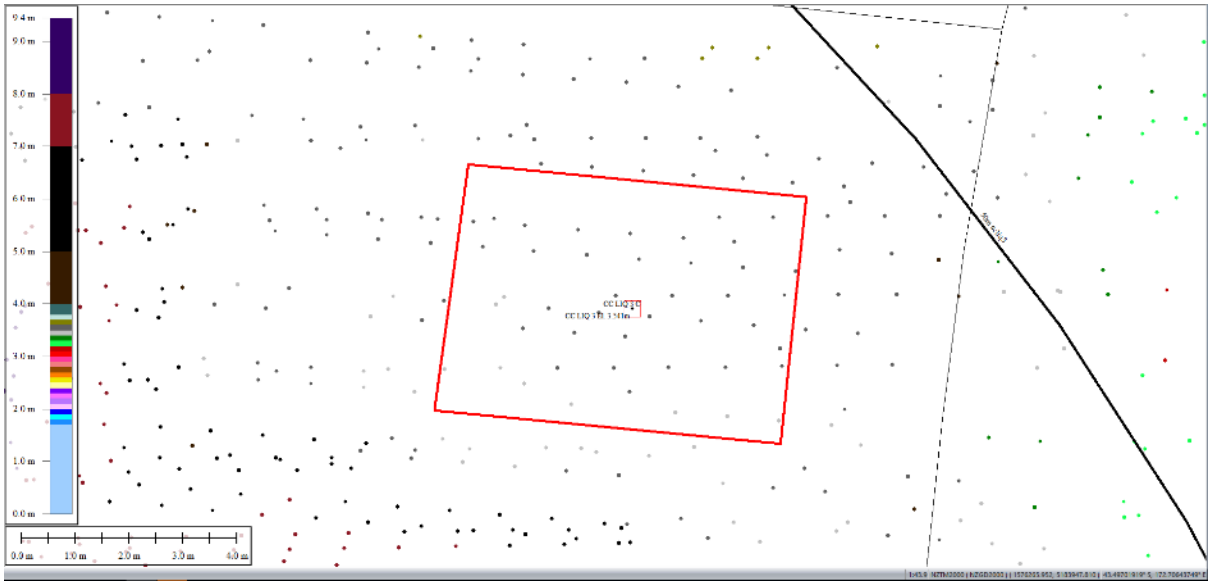

Figure 47: Ground surface elevation averaged over 50-m buffer for Patch C for Sep 5, 2010 LiDAR survey.

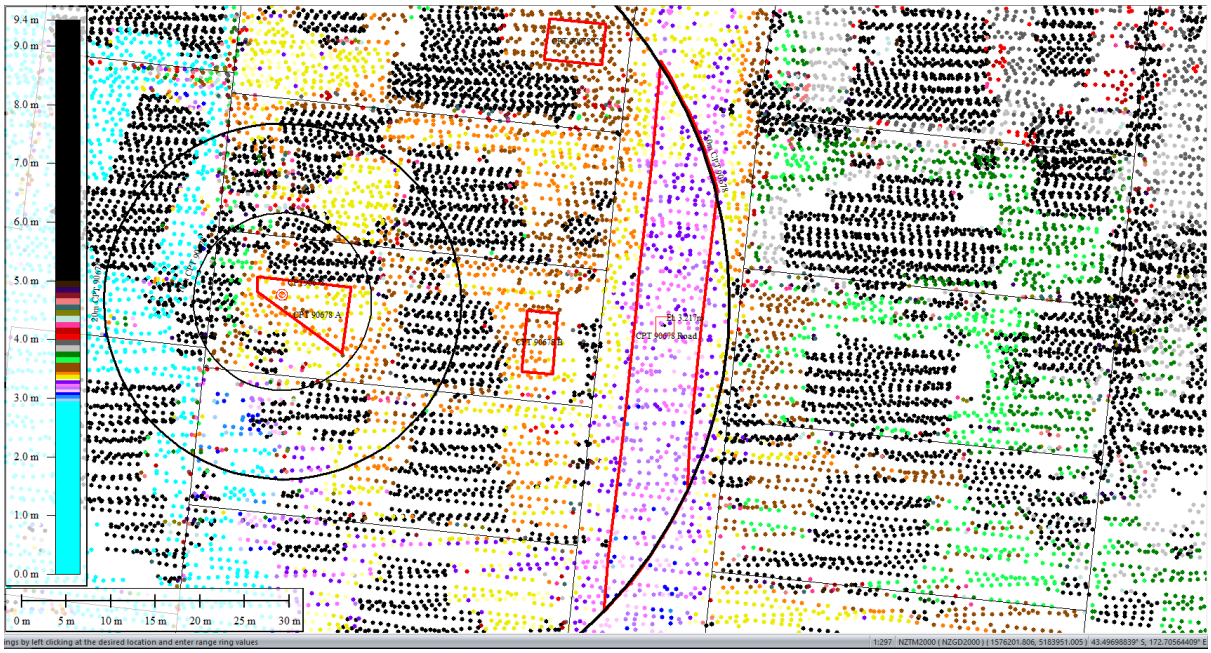

Figure 48: Ground surface elevation averaged over 50-m buffer for Road for Sep 5, 2010 LiDAR survey.

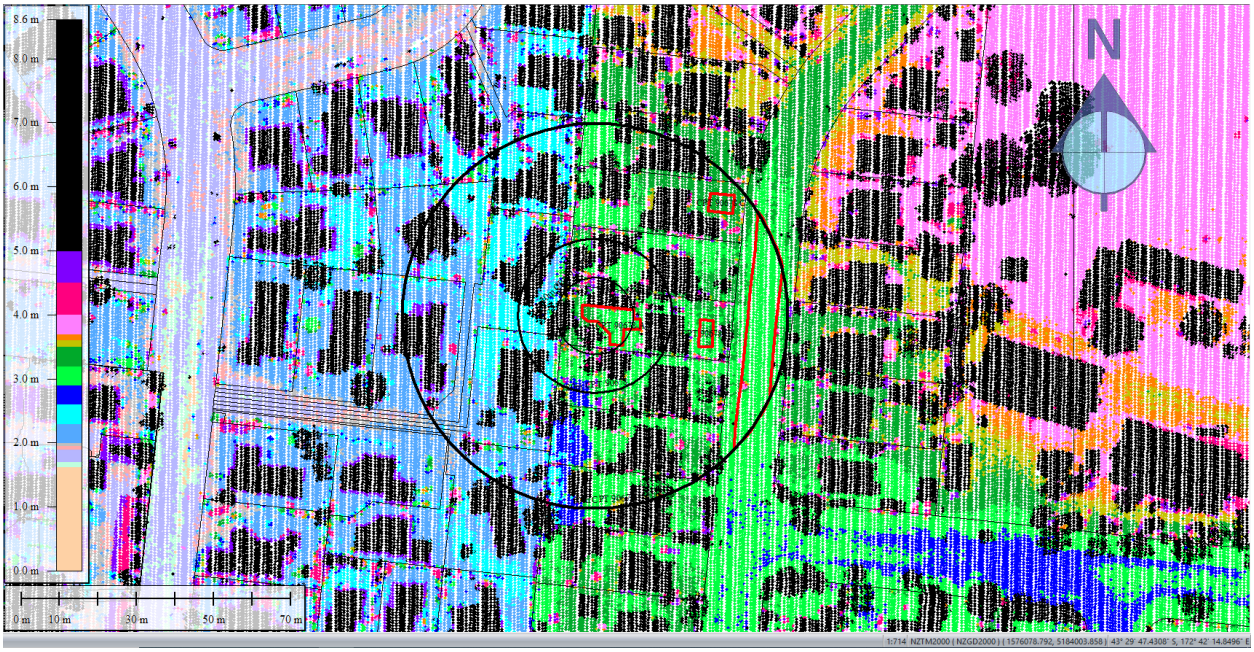

Figure 49: Mar 2011 LiDAR survey.

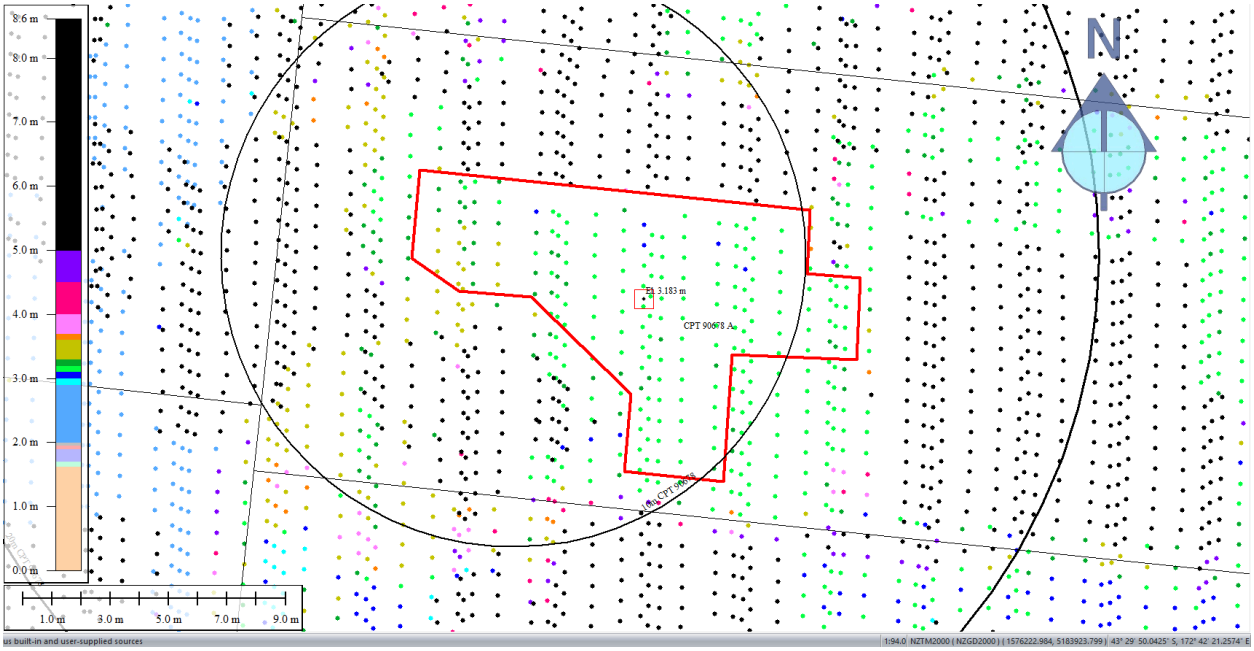

Figure 50: Ground surface elevation averaged over 10-m, 20-m, and 50-m buffers for Patch A for Mar 2011 LiDAR survey.

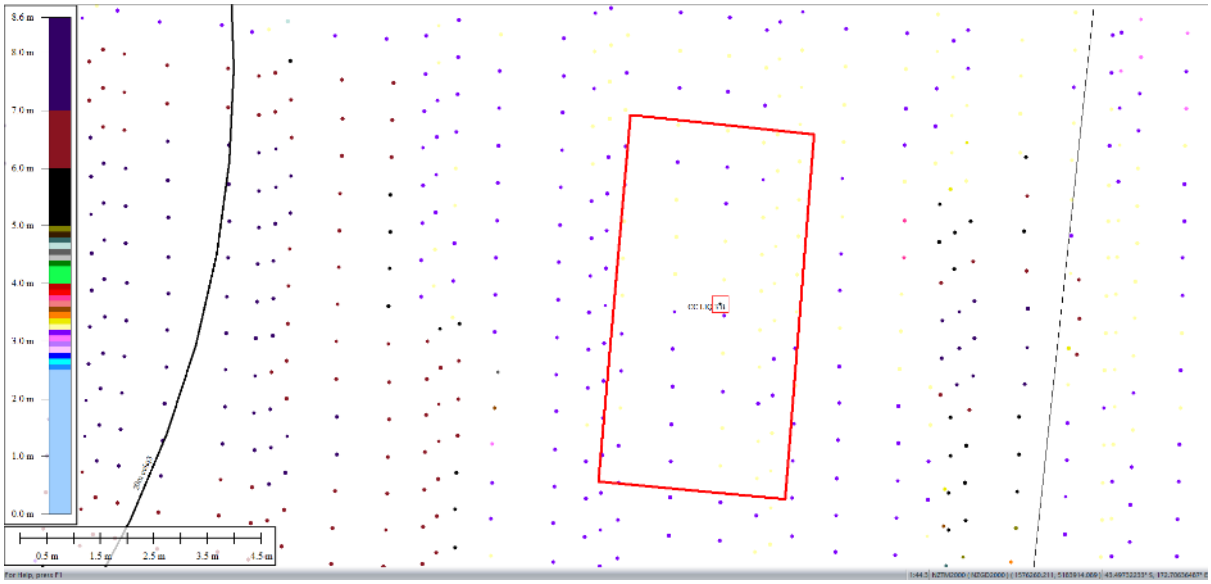

Figure 51: Ground surface elevation averaged over 50-m buffer for Patch B for Mar 2011 LiDAR survey.

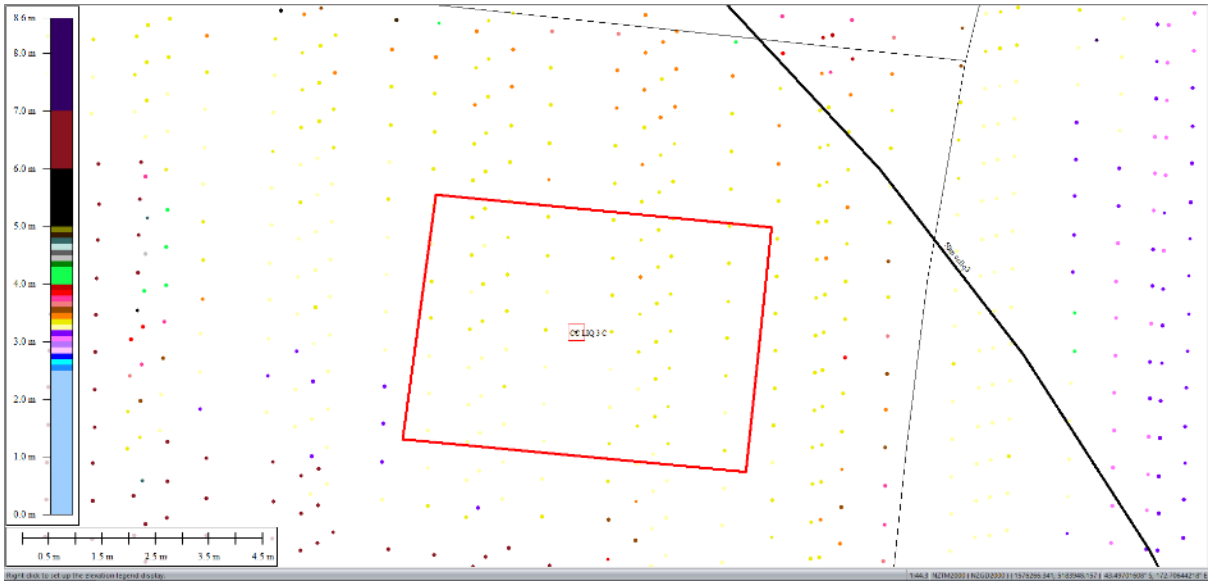

Figure 52: Ground surface elevation averaged over 50-m buffer for Patch C for Mar 2011 LiDAR survey.

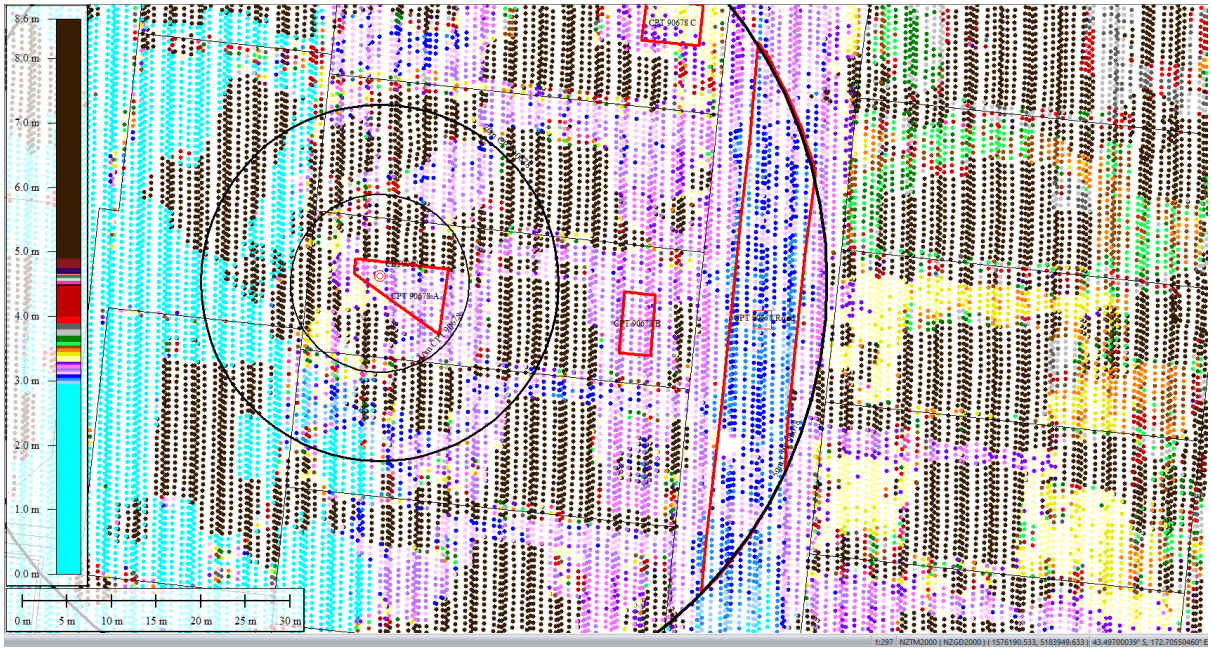

Figure 53: Ground surface elevation averaged over 50-m buffer for Road for Mar 2011 LiDAR survey.

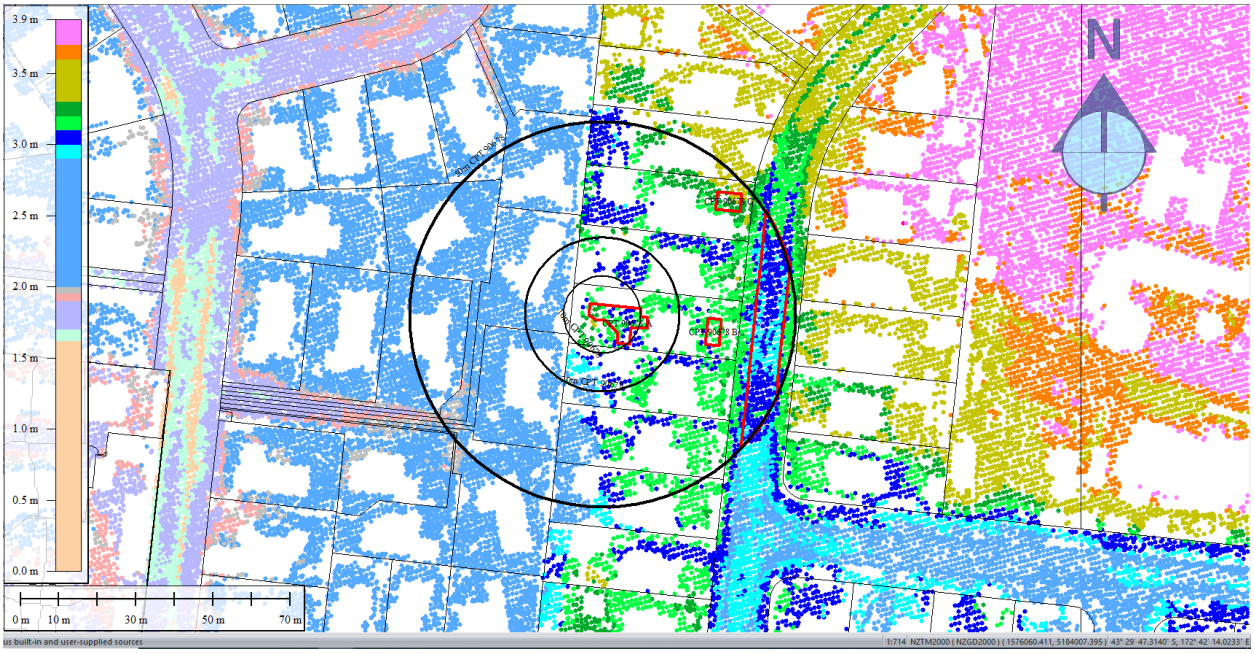

Figure 54: May 2011 LiDAR survey.

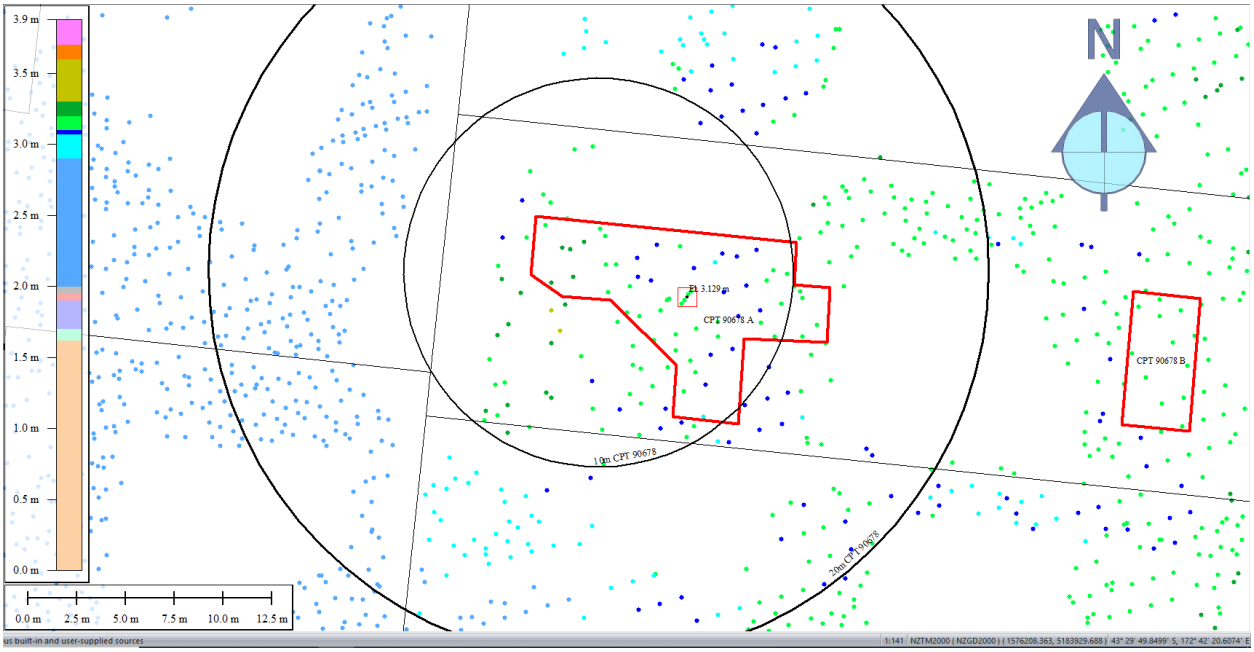

Figure 55: Ground surface elevation averaged over 10-m, 20-m, and 50-m buffers for Patch A for May 2011 LiDAR survey.

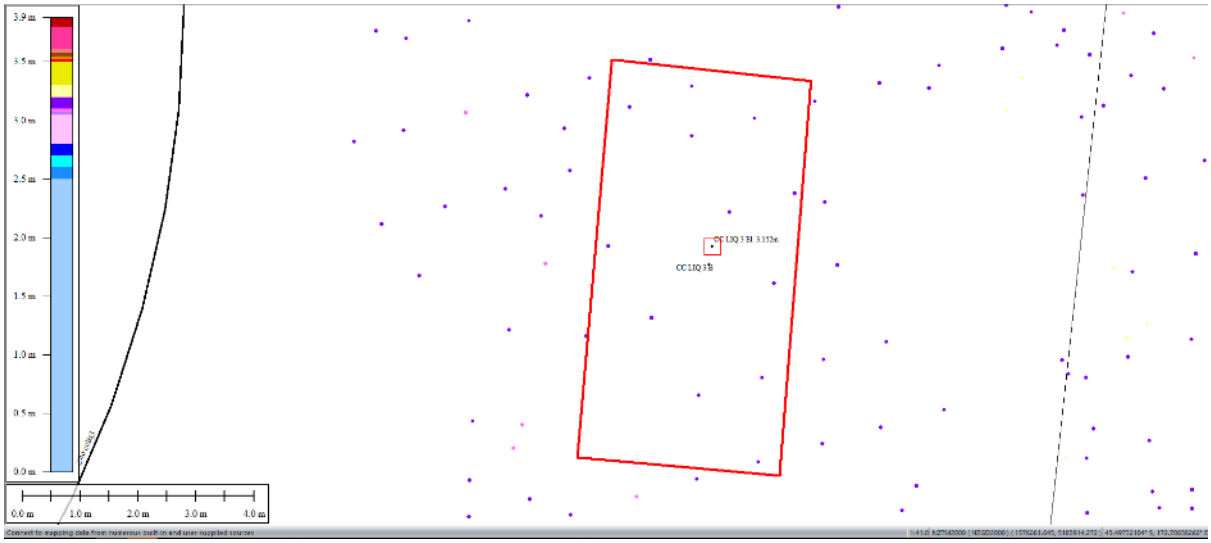

Figure 56: Ground surface elevation averaged over 50-m buffer for Patch B for May 2011 LiDAR survey.

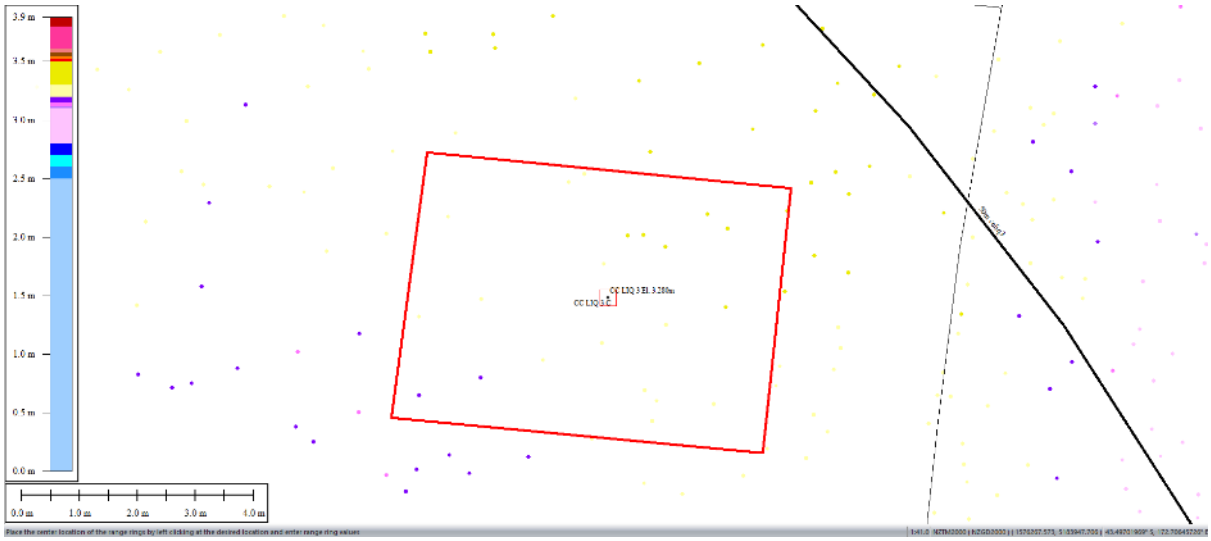

Figure 57: Ground surface elevation averaged over 50-m buffer for Patch C for May 2011 LiDAR survey.

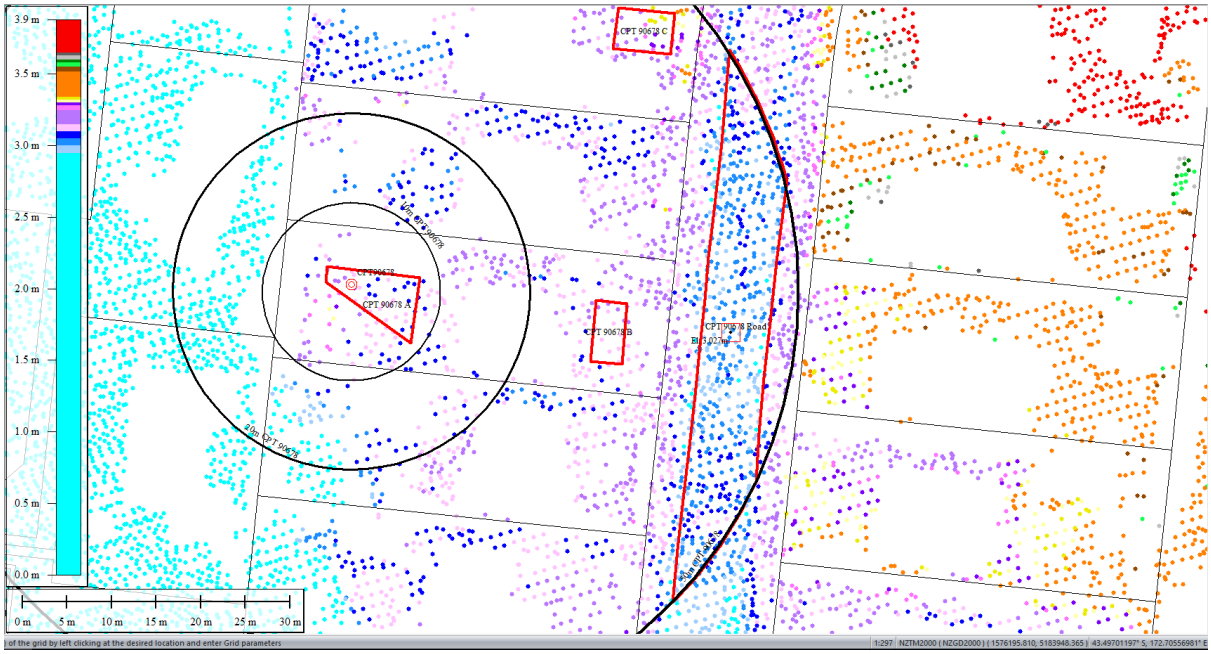

Figure 58: Ground surface elevation averaged over 50-m buffer for Road for May 2011 LiDAR survey.

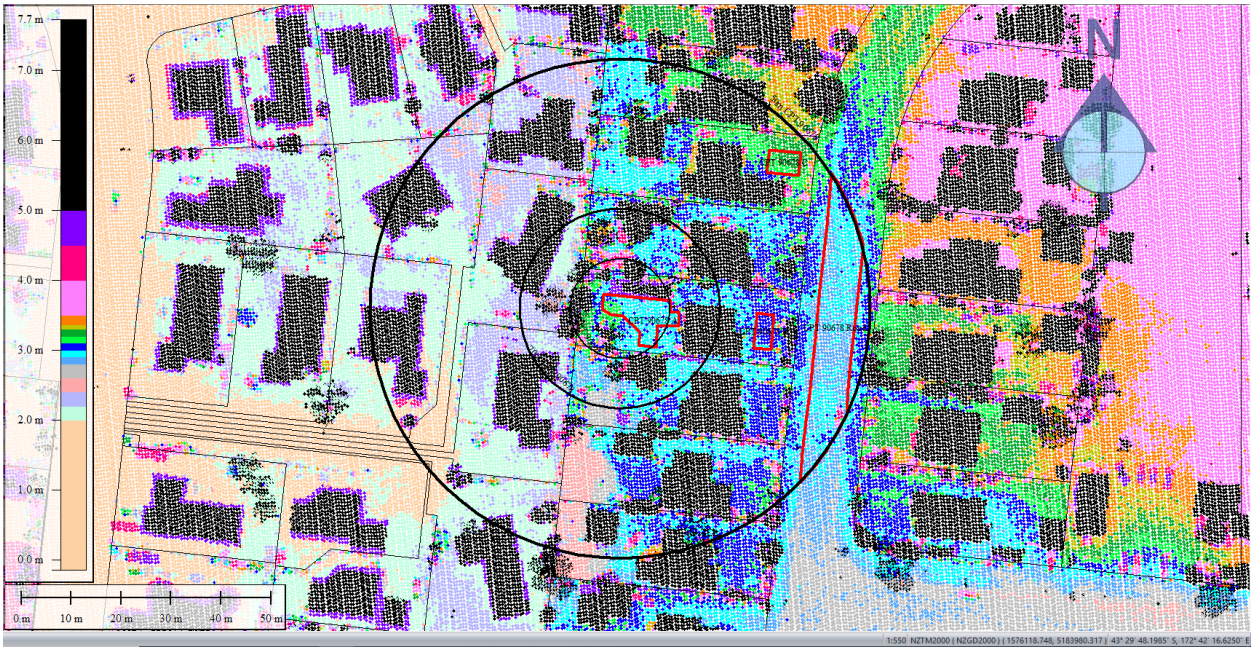

Figure 59: Sep 2011 LiDAR survey.

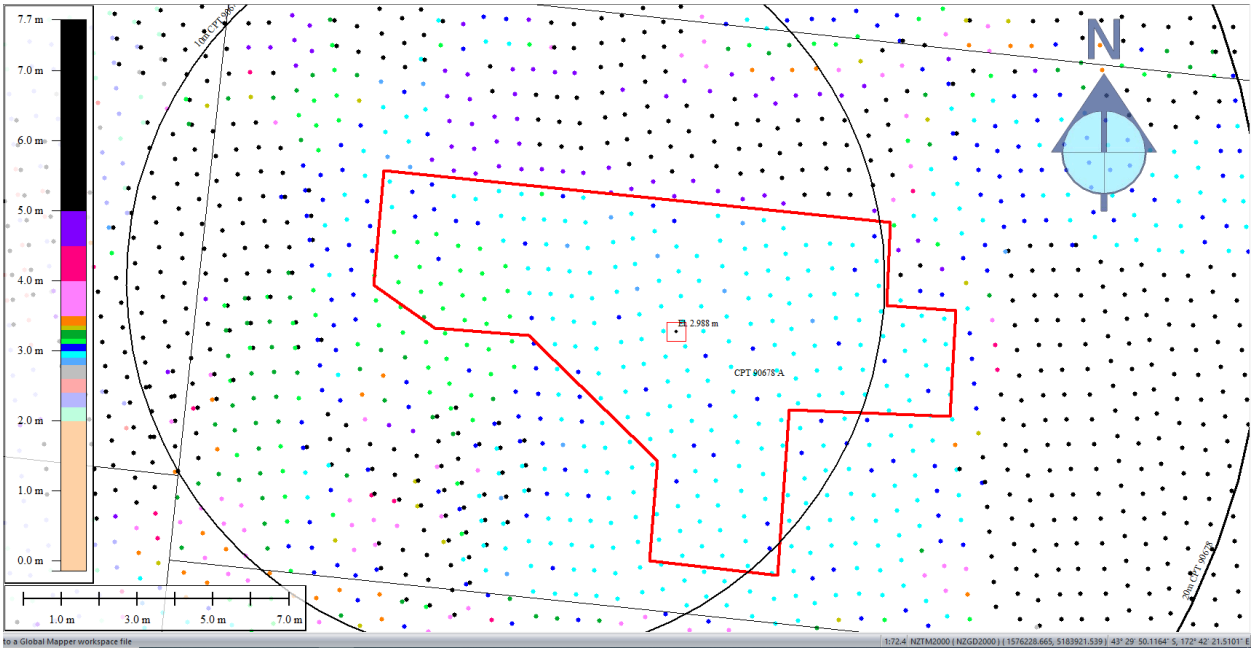

Figure 60: Ground surface elevation averaged over 10-m, 20-m, and 50-m buffers for Patch A for Sep 2011 LiDAR survey.

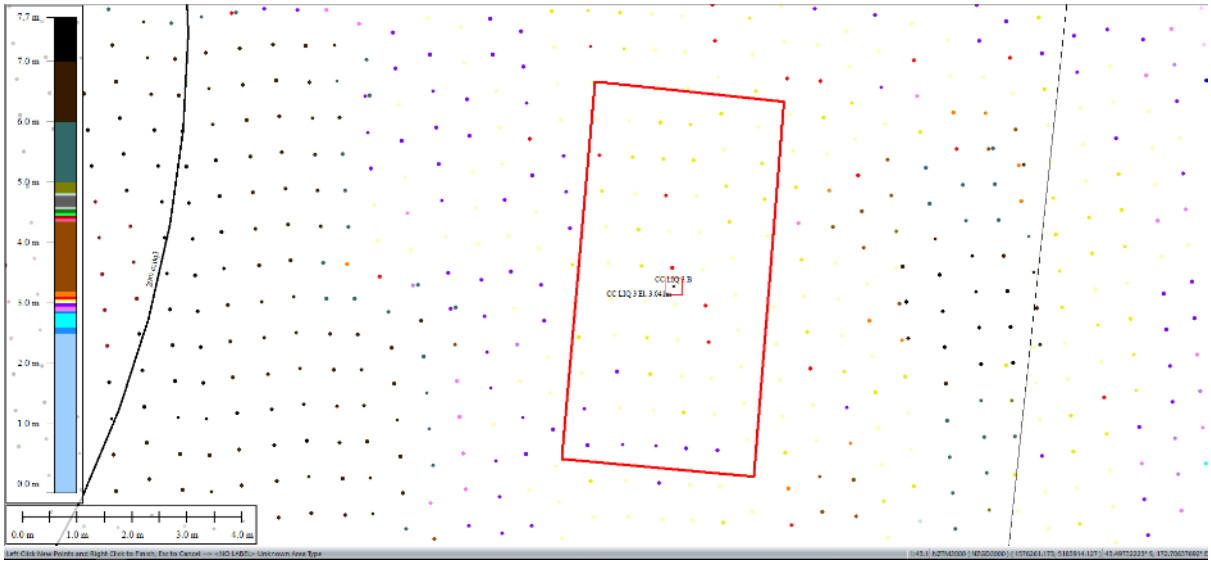

Figure 61: Ground surface elevation averaged over 50-m buffer for Patch B for Sep 2011 LiDAR survey.

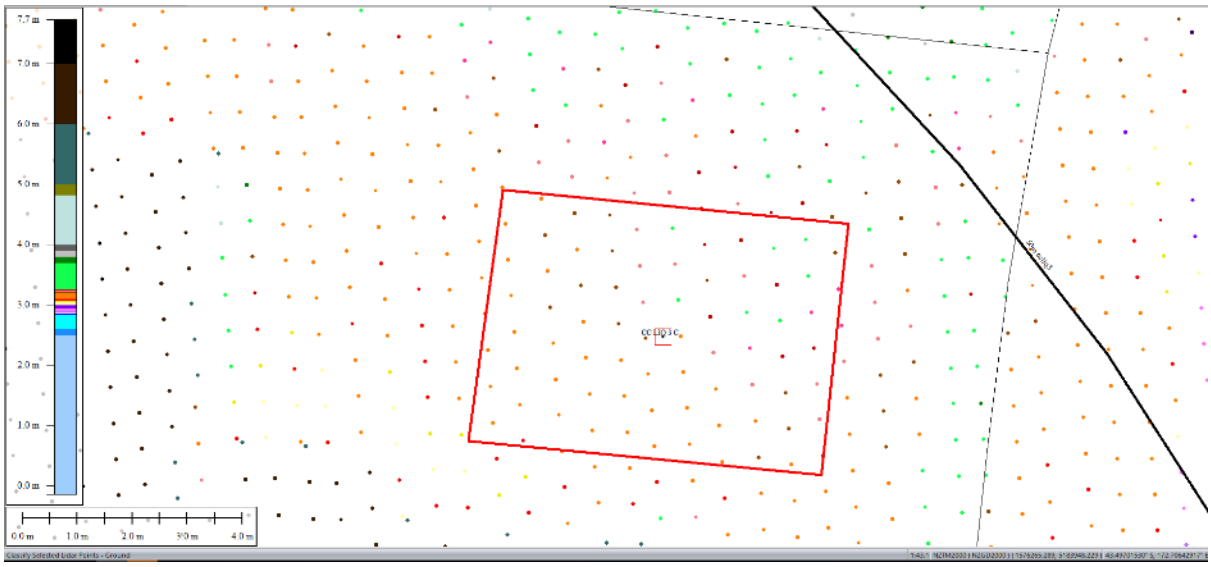

Figure 62: Ground surface elevation averaged over 50-m buffer for Patch C for Sep 2011 LiDAR survey.

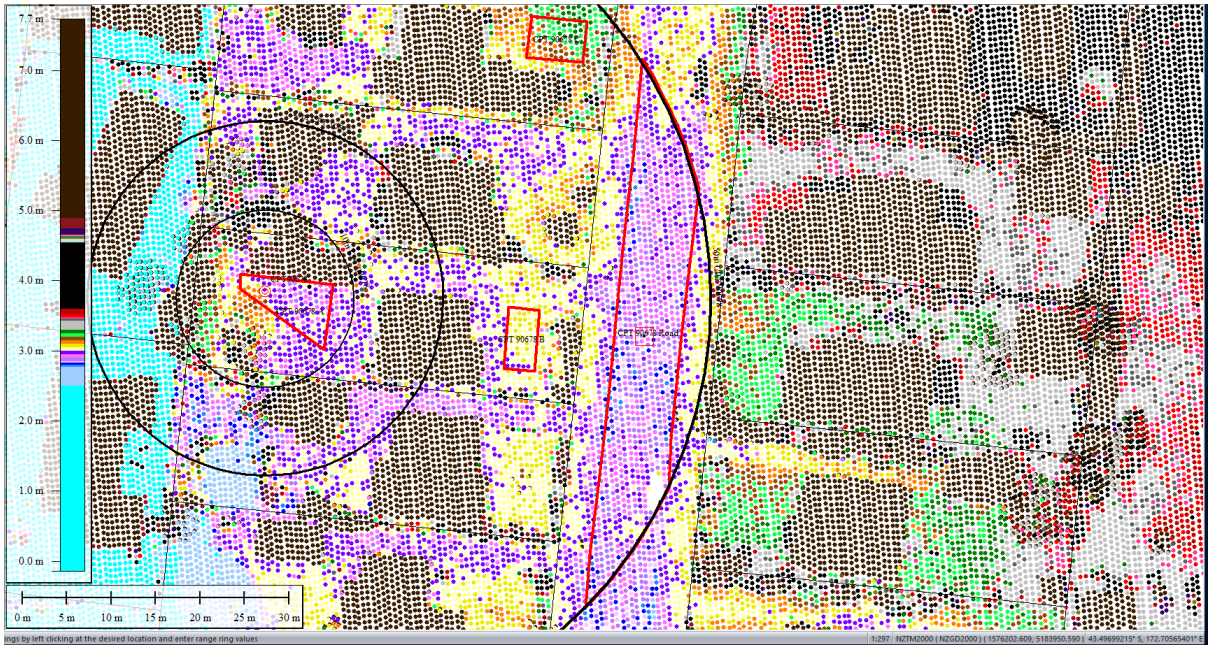

Figure 63: Ground surface elevation averaged over 50-m buffer for Road for Sep 2011 LiDAR survey.

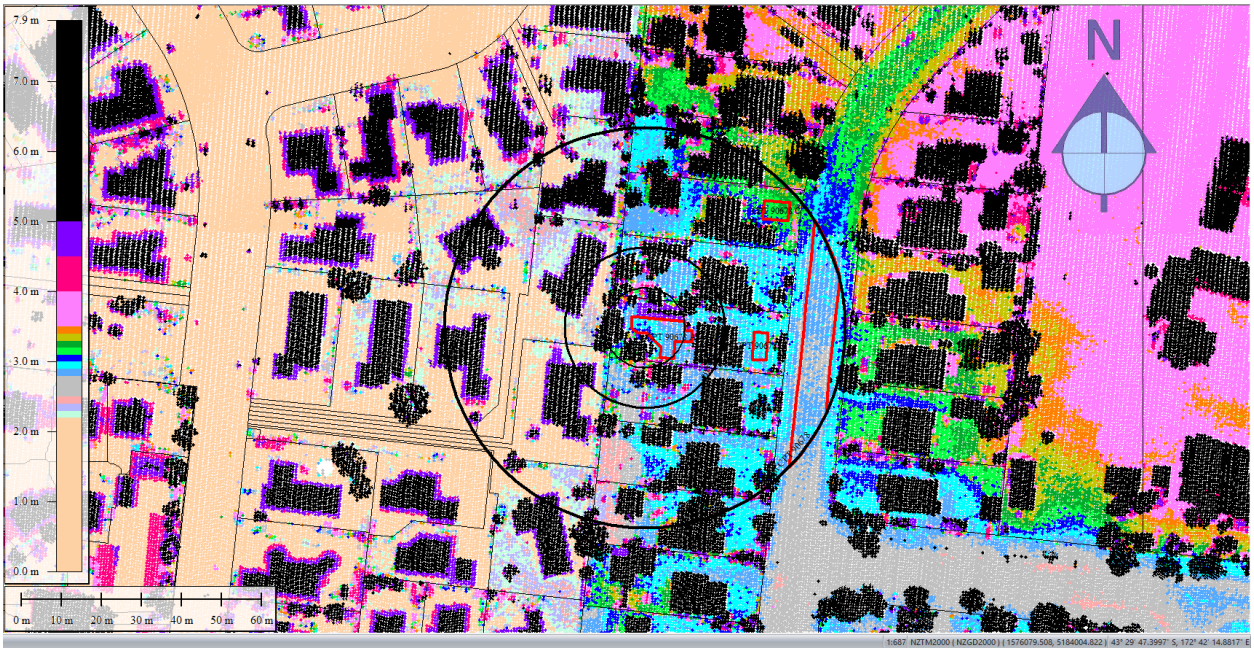

Figure 64: Feb 2012 LiDAR survey.

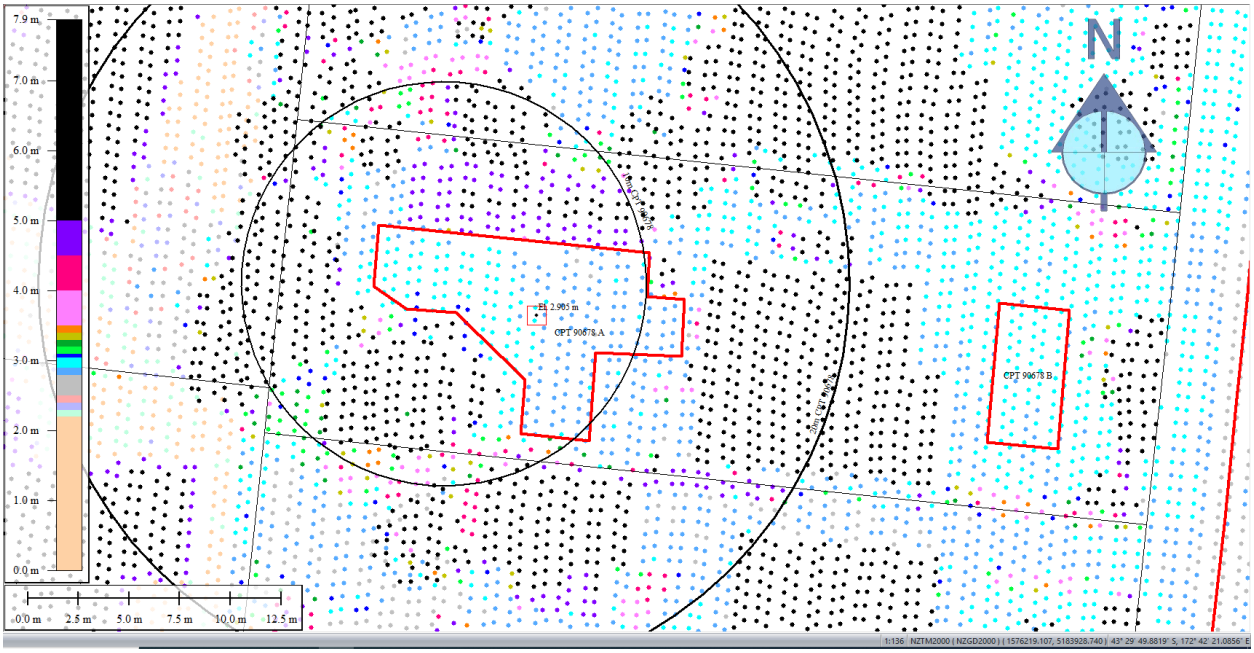

Figure 65: Ground surface elevation averaged over 10-m, 20-m, and 50-m buffers for Patch A for Feb 2012 LiDAR survey.

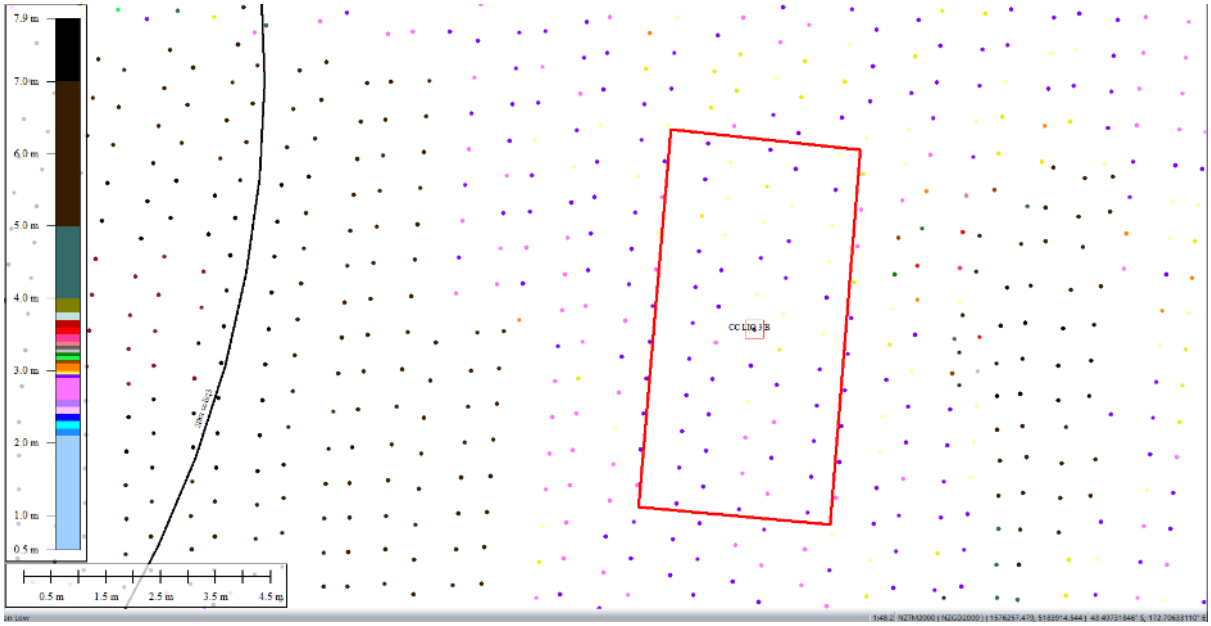

Figure 66: Ground surface elevation averaged over 50-m buffer for Patch B for Feb 2012 LiDAR survey.

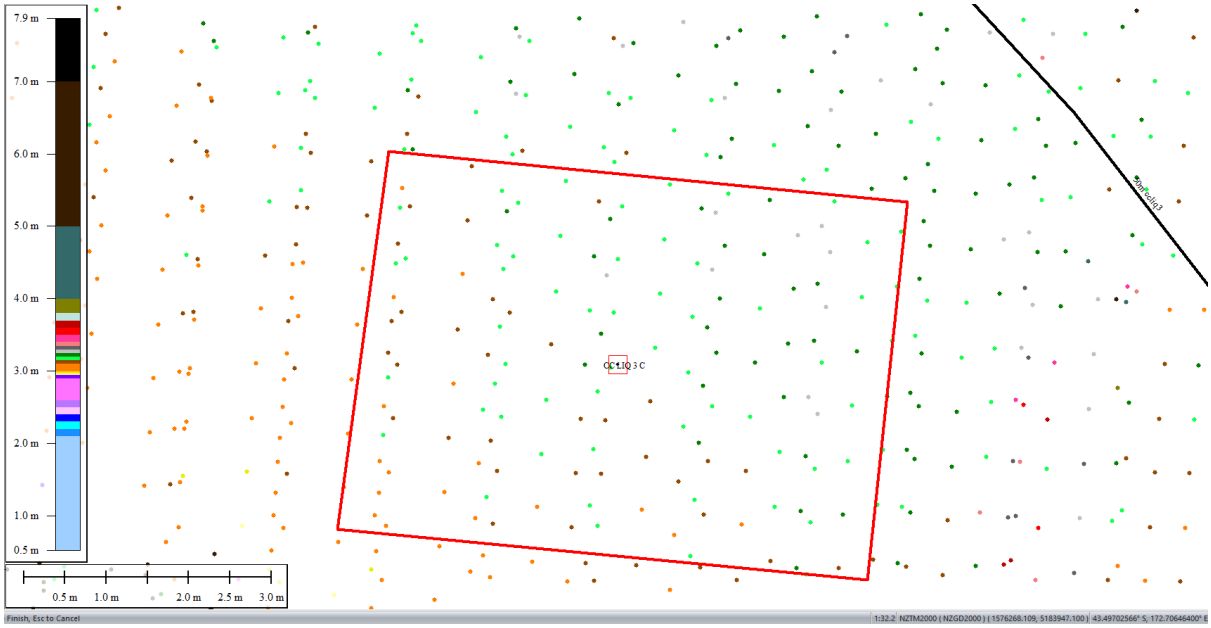

Figure 67: Ground surface elevation averaged over 50-m buffer for Patch C for Feb 2012 LiDAR survey.

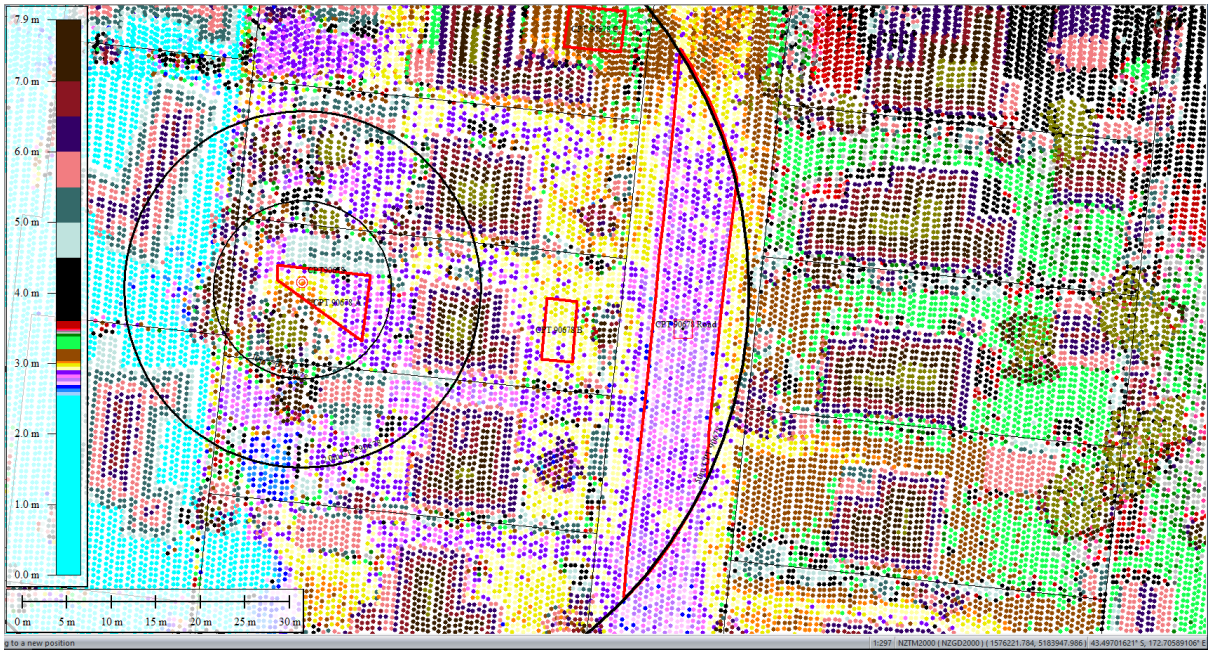

Figure 68: Ground surface elevation averaged over 50-m buffer for Road for Feb 2012 LiDAR survey.

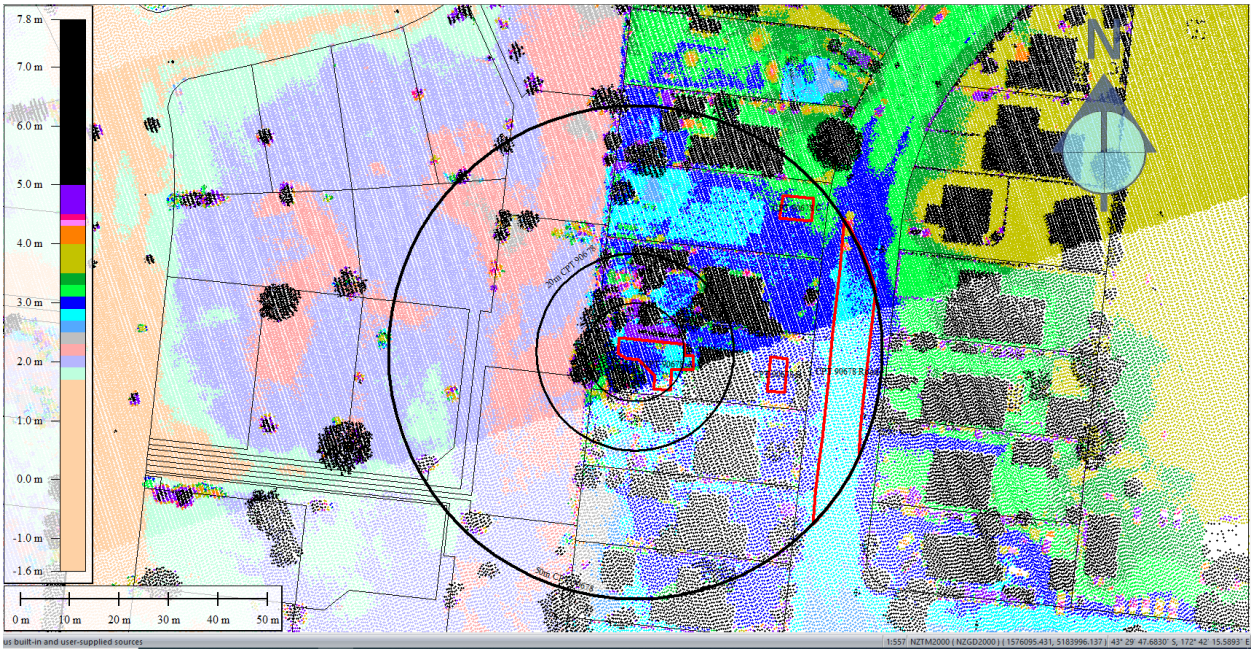

Figure 69: Oct 2015 LiDAR survey.

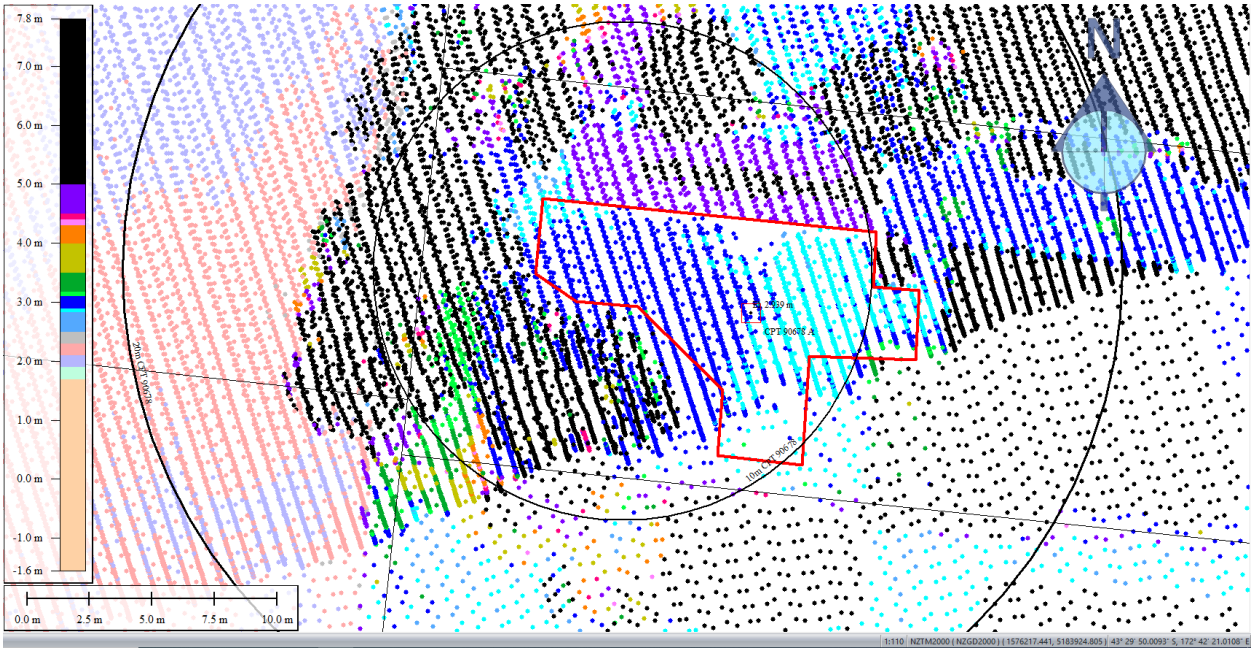

Figure 70: Ground surface elevation averaged over 10-m, 20-m, and 50-m buffers for Patch A for Oct 2015 LiDAR survey.

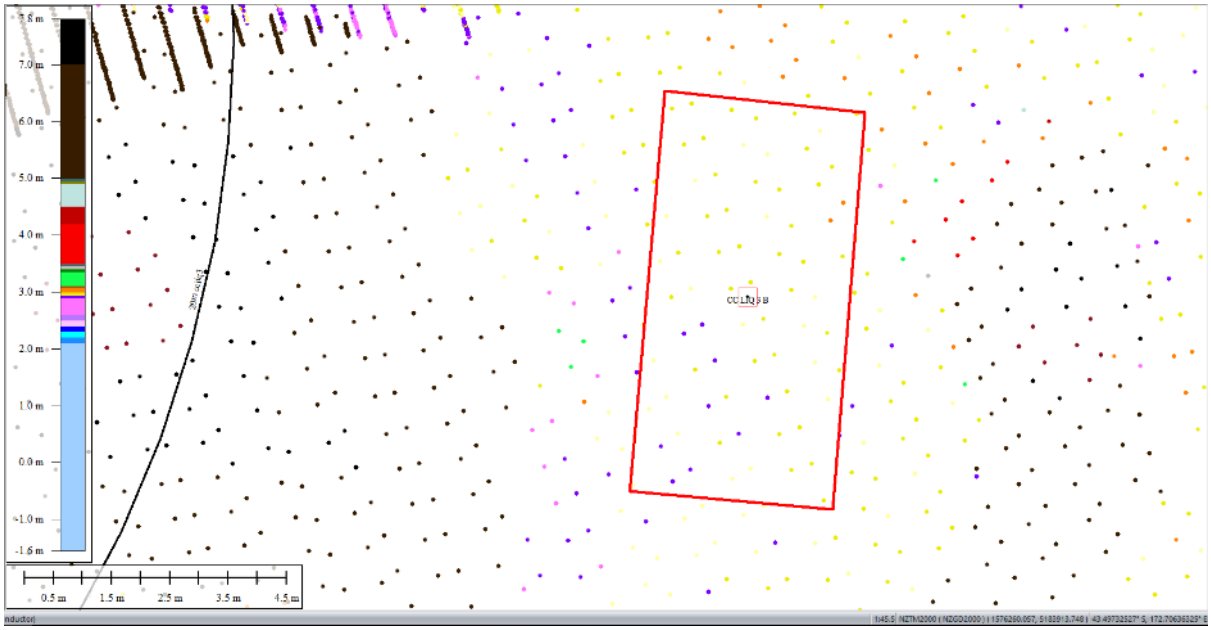

Figure 71: Ground surface elevation averaged over 50-m buffer for Patch B for Oct 2015 LiDAR survey.

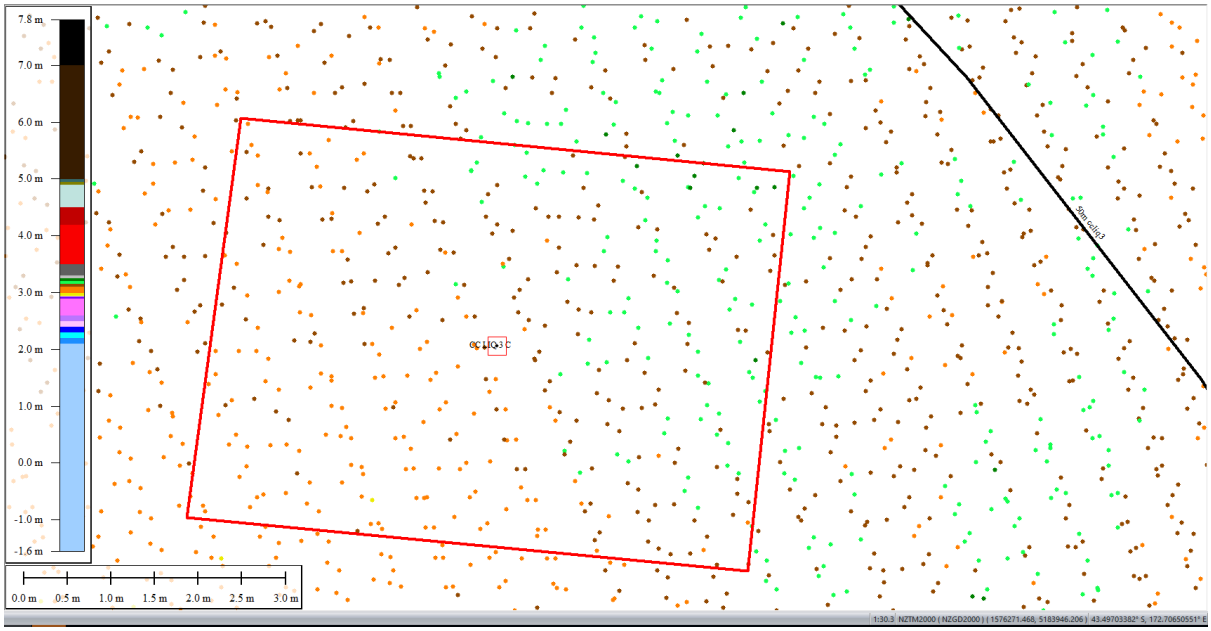

Figure 72: Ground surface elevation averaged over 50-m buffer for Patch C for Oct 2015 LiDAR survey.

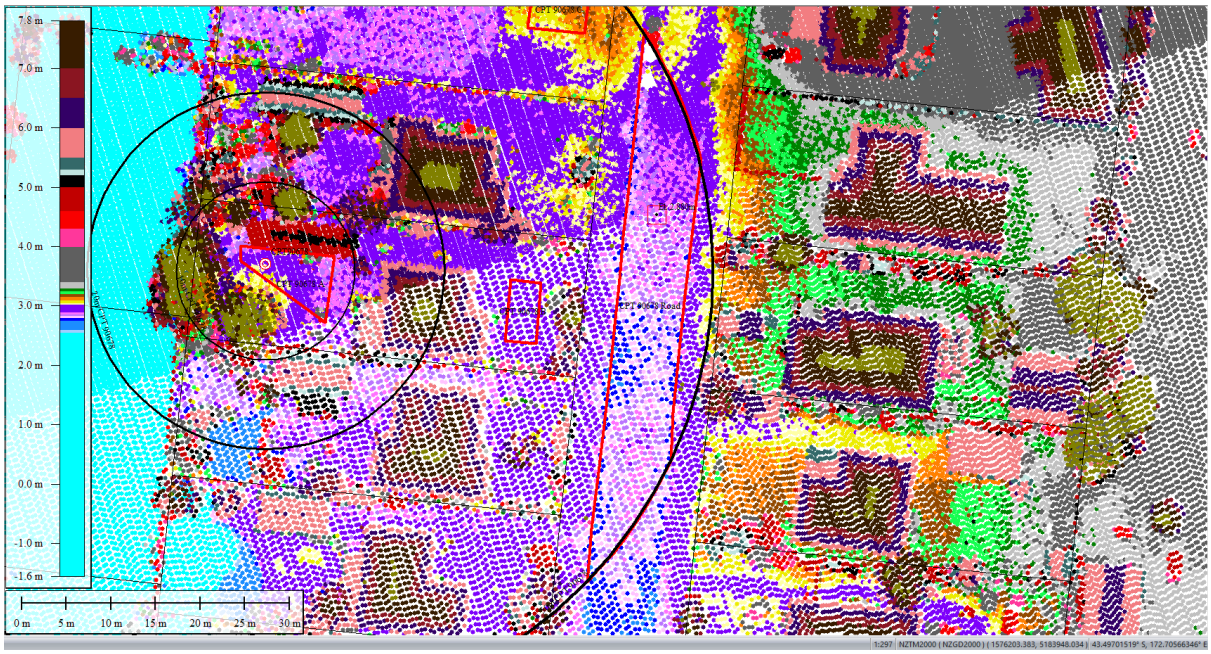

Figure 73: Ground surface elevation averaged over 50-m buffer for Road for Oct 2015 LiDAR survey.

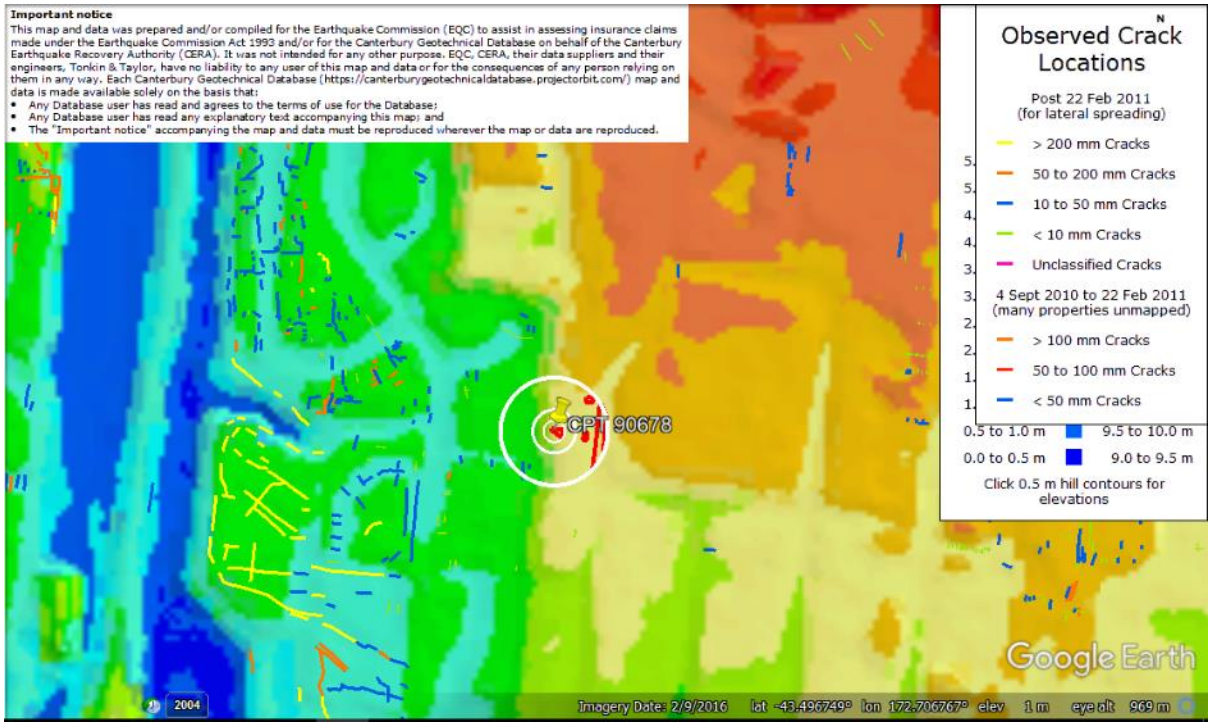

Figure 74: Ground surface elevation difference between the road and properties (LiDAR DEM Sep 2010).

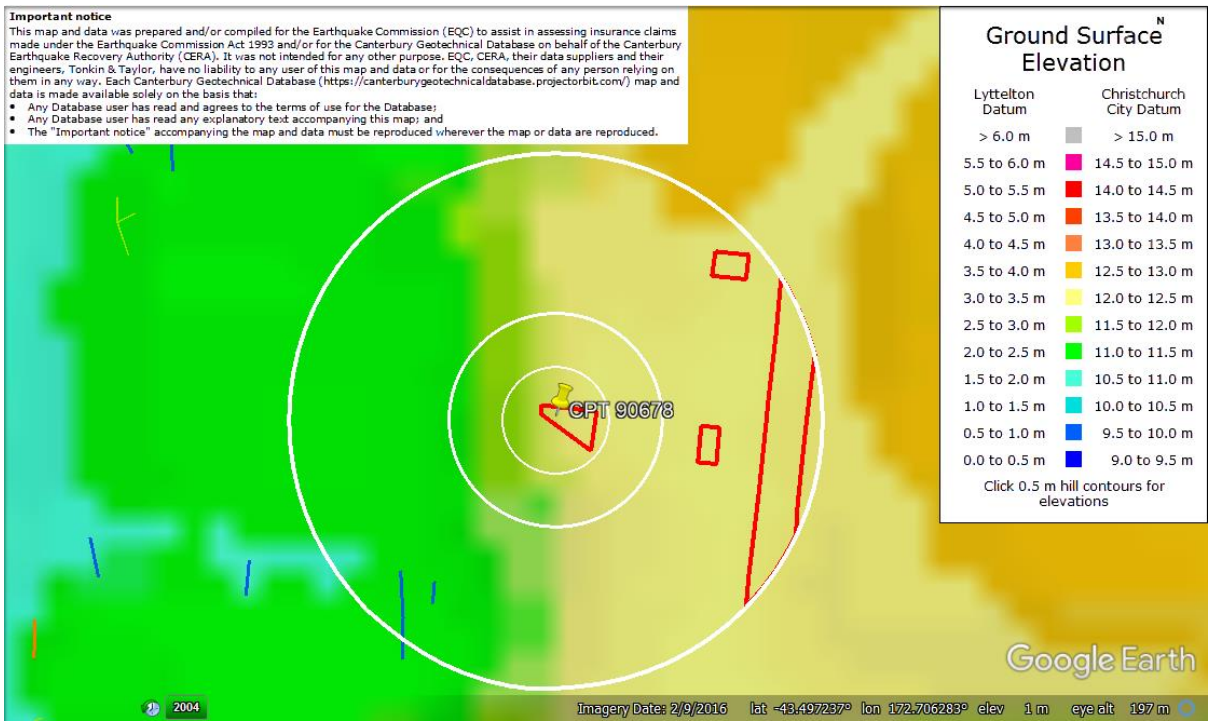

Figure 75: Enlarged view of ground surface elevation difference between the road and properties (LiDAR DEM Sep 2010).

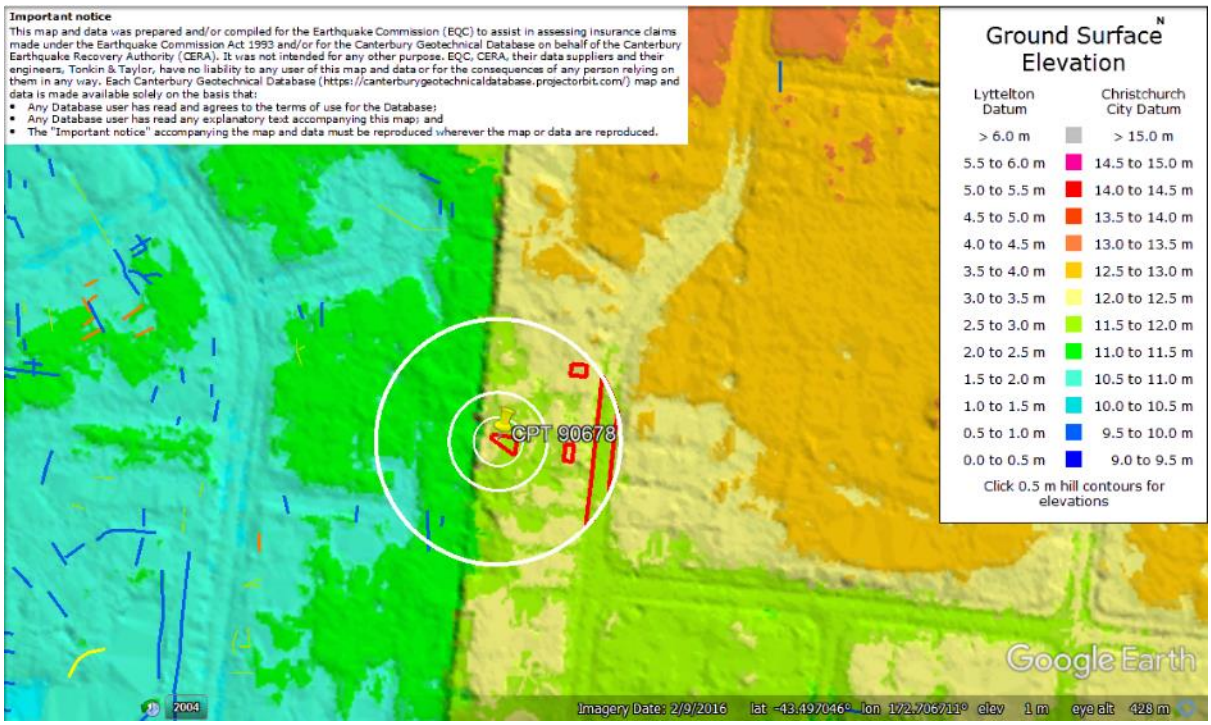

Figure 76: Ground surface elevation difference between the road and properties (LiDAR DEM Sep 2011).

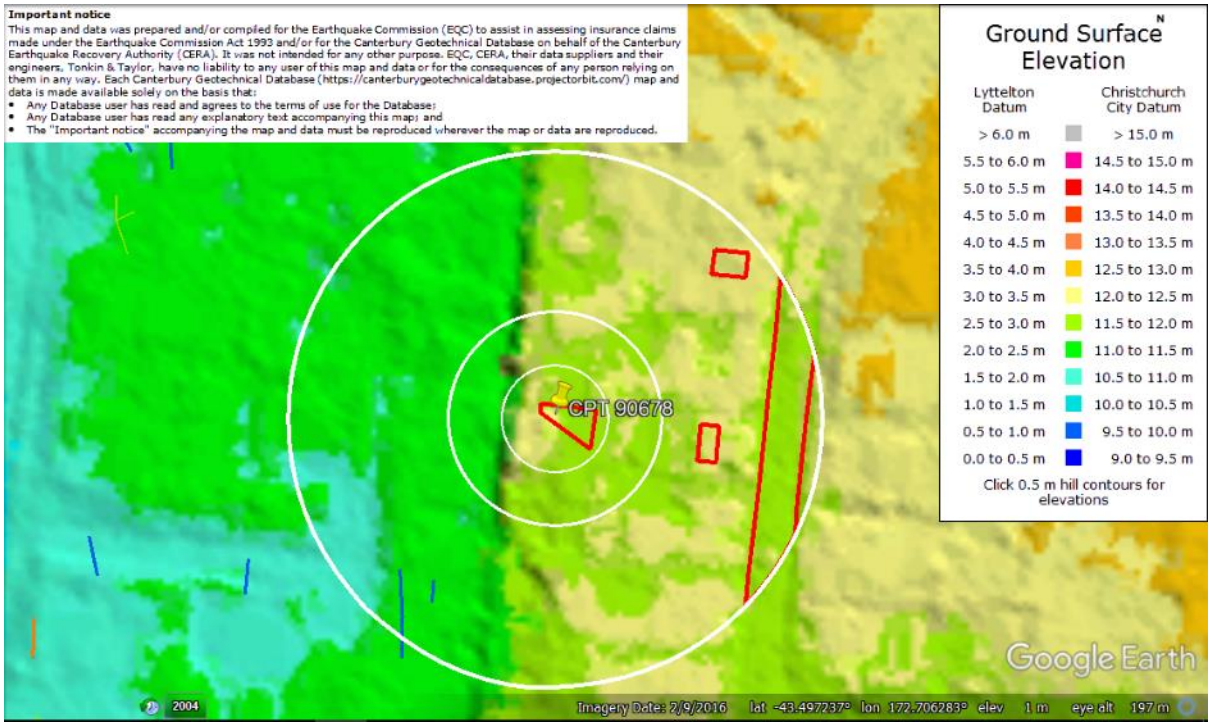

Figure 77: Enlarged view of ground surface elevation difference between the road and properties (LiDAR DEM Sep 2011).

Figure 78: Absence of ejecta for Sep-10 EQ.

Figure 79: Ejecta outline for Feb-11 EQ.

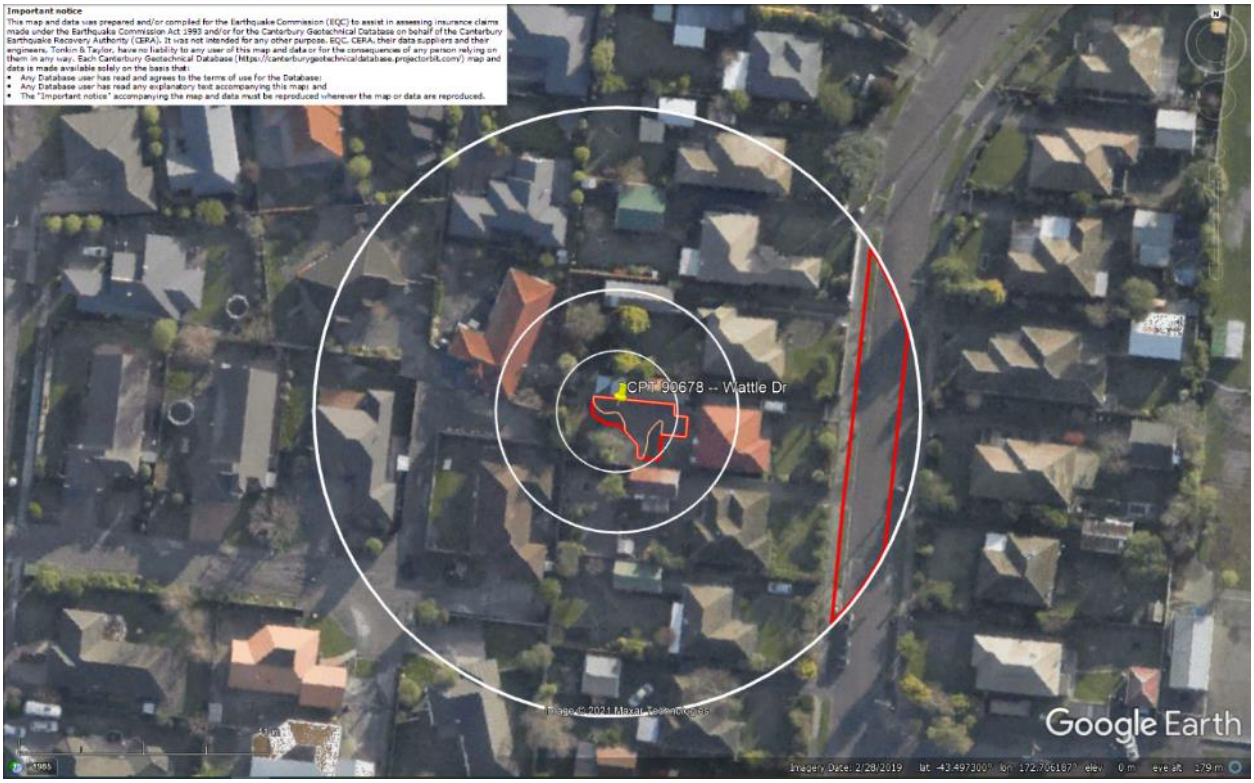

Figure 80: Aerial photograph acquired on 14-15 Jun 2011 showing ejecta at the site for Jun-11 EQ.

Figure 81: Ejecta outline for Jun-11 EQ.

Figure 82: Ejecta outline for Dec-11 EQ.

Figure 83: Ground photograph of Patch A taken on 31 May 2011. (The ejecta traces resulting from the cleaning are visible in the June aerial photograph.)

Figure 84: Ground photograph from 2 June 2011 of the 26 Atlantis St property in the SW quadrant of the 20-m and 50-m buffer, near Patch A.

Contents of this figure cannot be shared as doing so is restricted by a Non-Disclosure Agreement.

Figure 85: LDAT property inspection notes for Patches A and B.

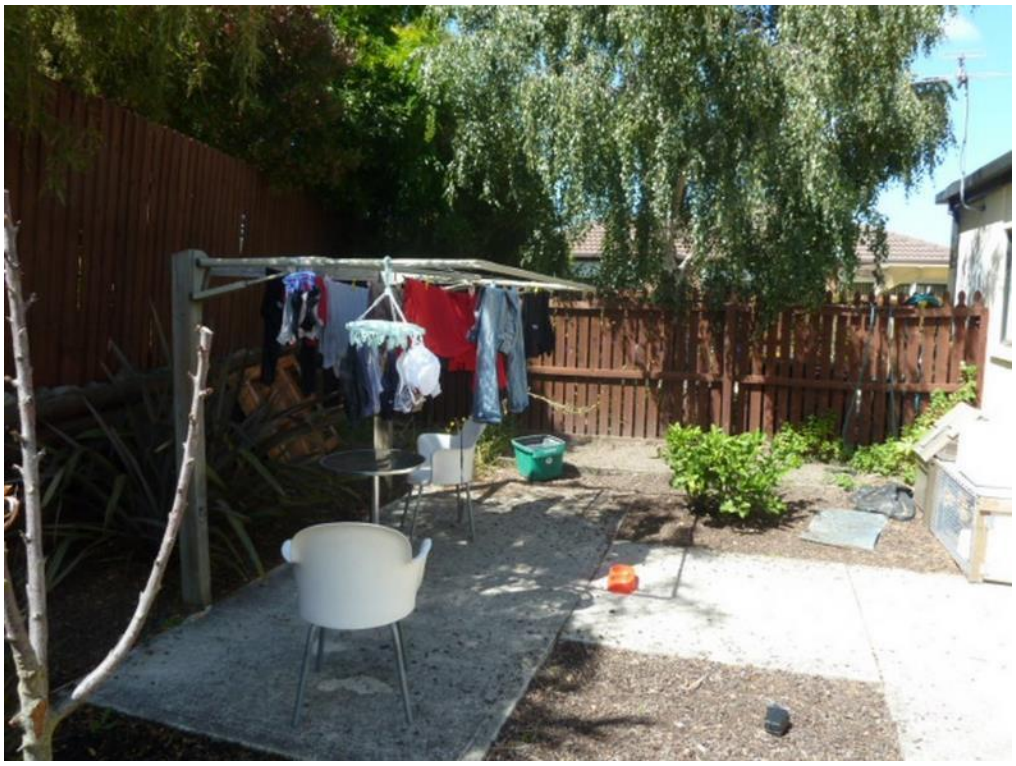

Figure 86: Retaining wall adjacent to the property with Patch A, as seen from 28 Atlantis St.

Contents of this figure cannot be shared as doing so is restricted by a Non-Disclosure Agreement.

Figure 87: LDAT property inspection report for Patch C.

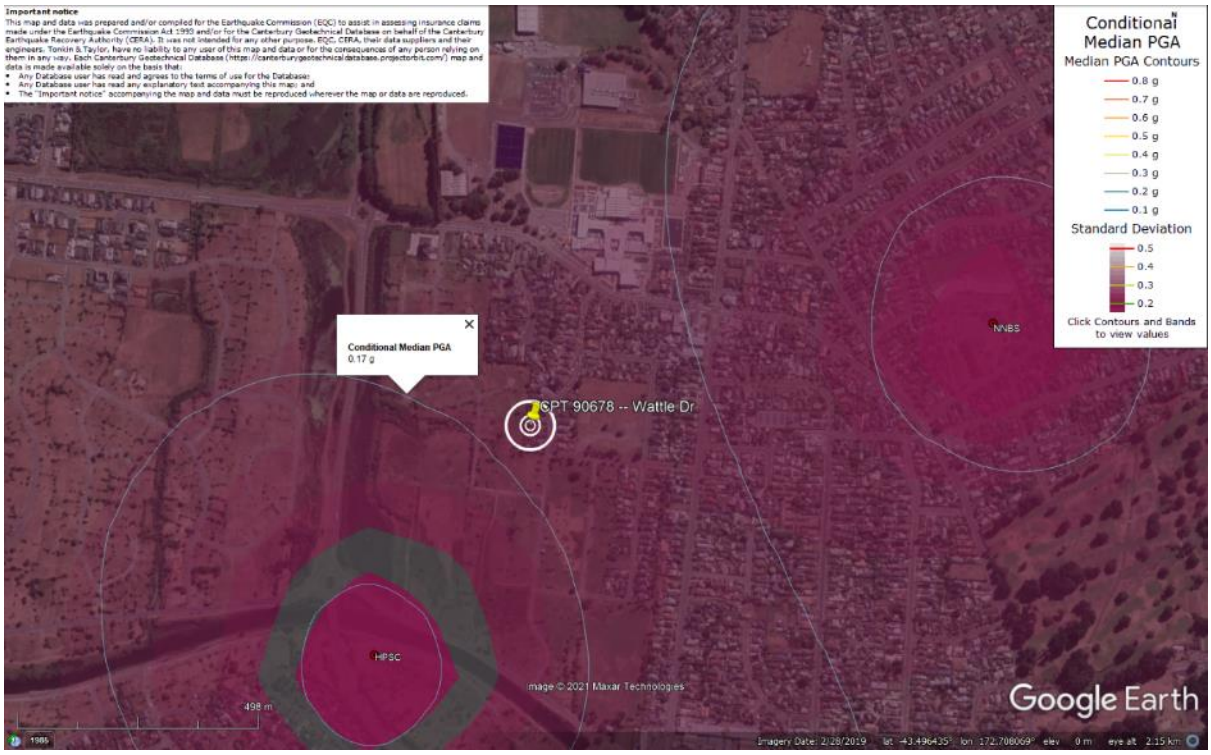

Figure 88: PGA for Sep-10 EQ (st. dev. = 0.225-0.275 ln units).

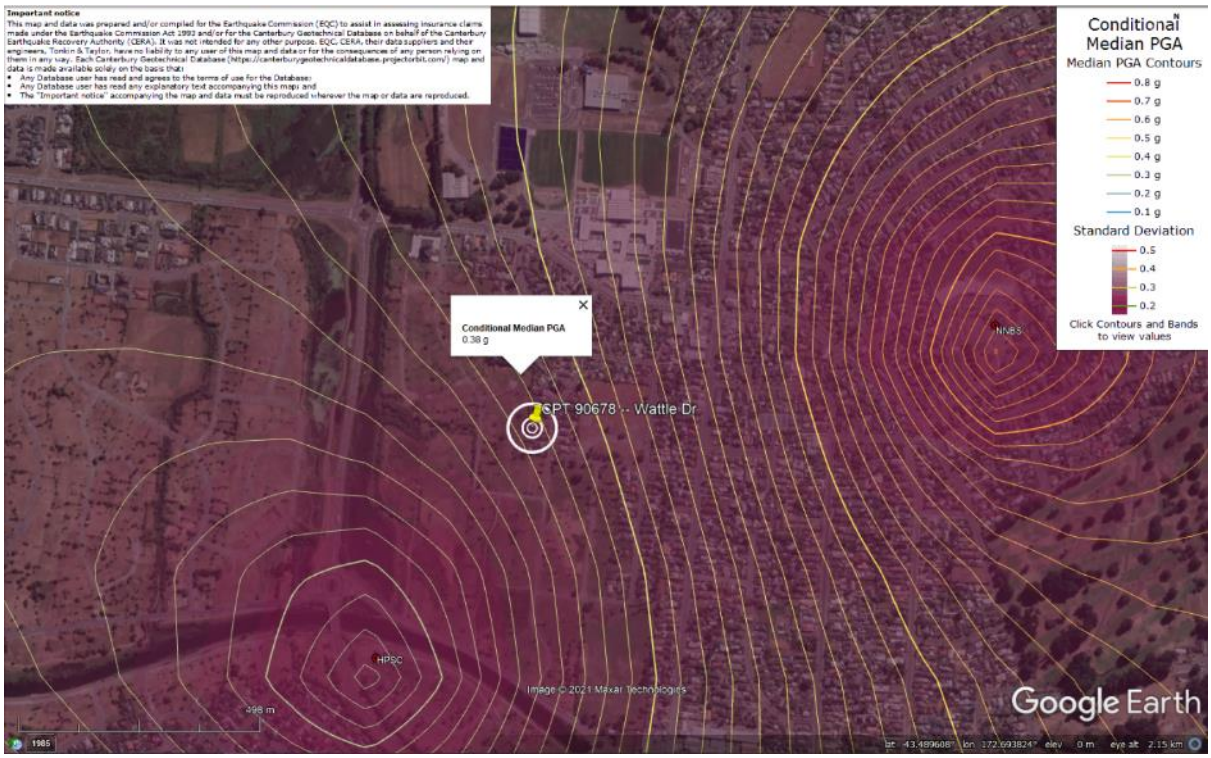

Figure 89: PGA for Feb-11 EQ (st. dev. = 0.250-0.275 ln units).

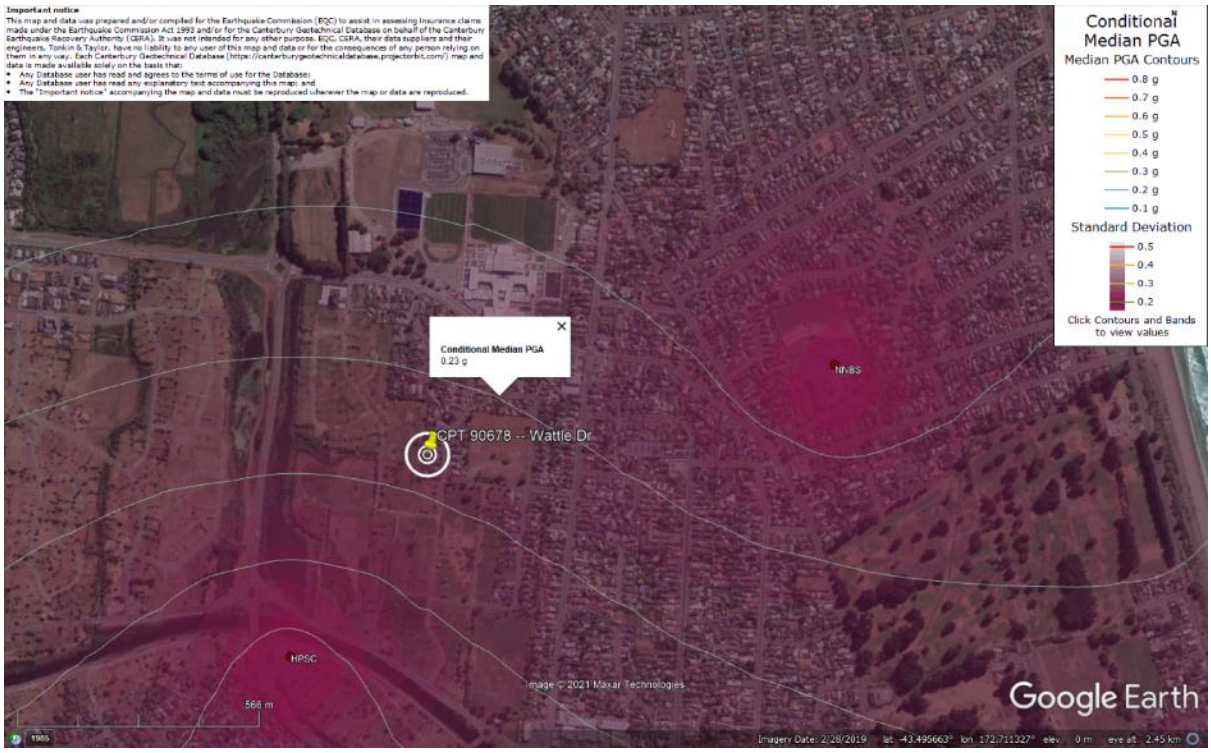

Figure 90: PGA for Jun-11 EQ (st. dev. = 0.275-0.300 ln units).

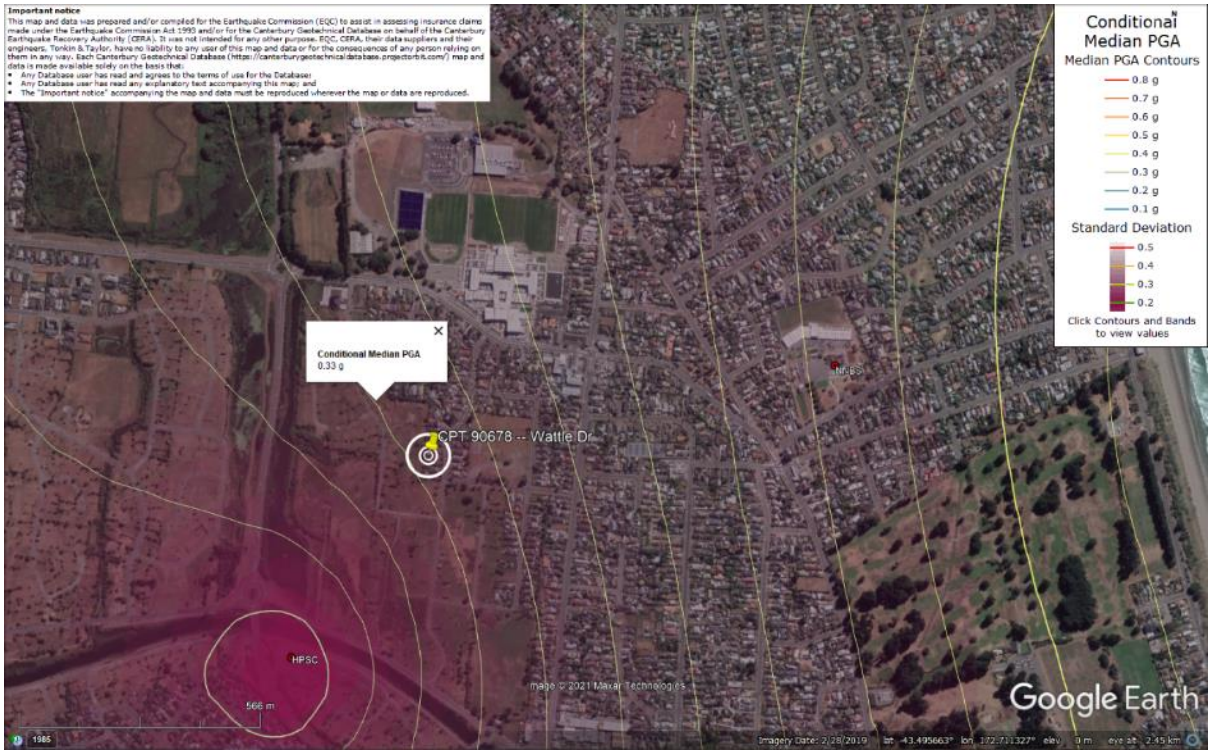

Figure 91: PGA for Dec-11 EQ (st. dev. = 0.300-0.325 ln units).

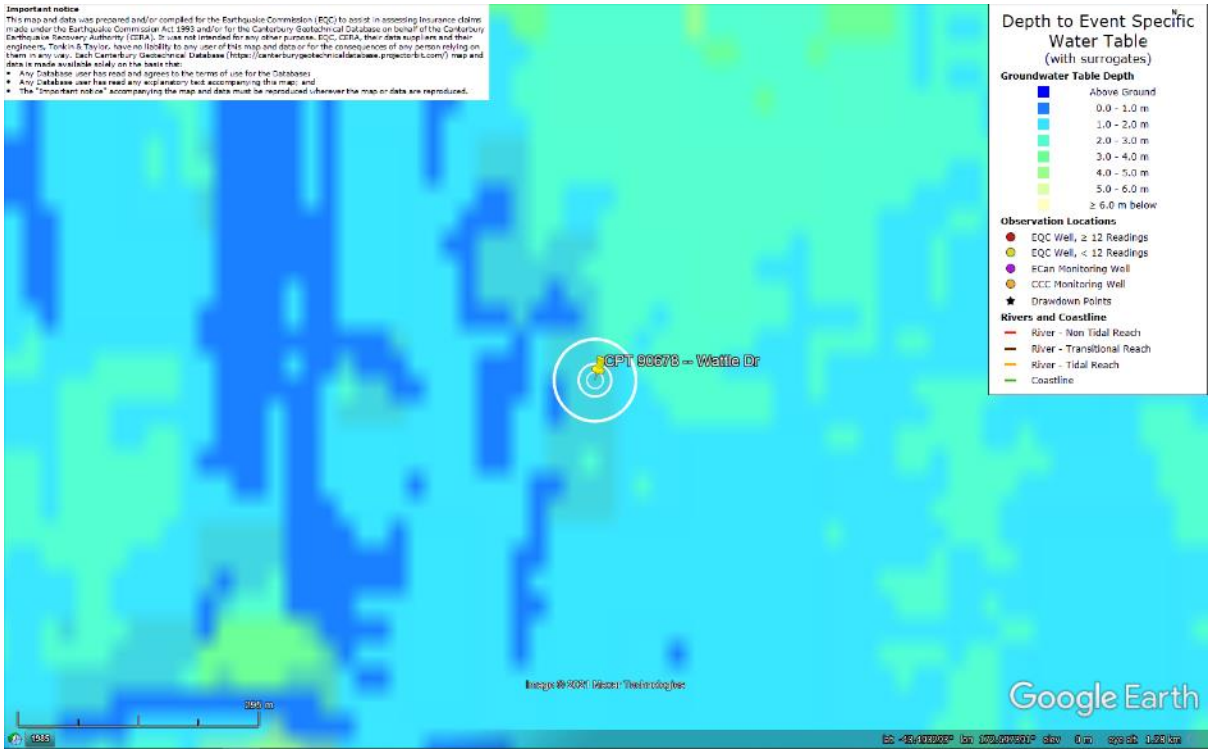

Figure 92: Depth to groundwater table for Sep-10 EQ.

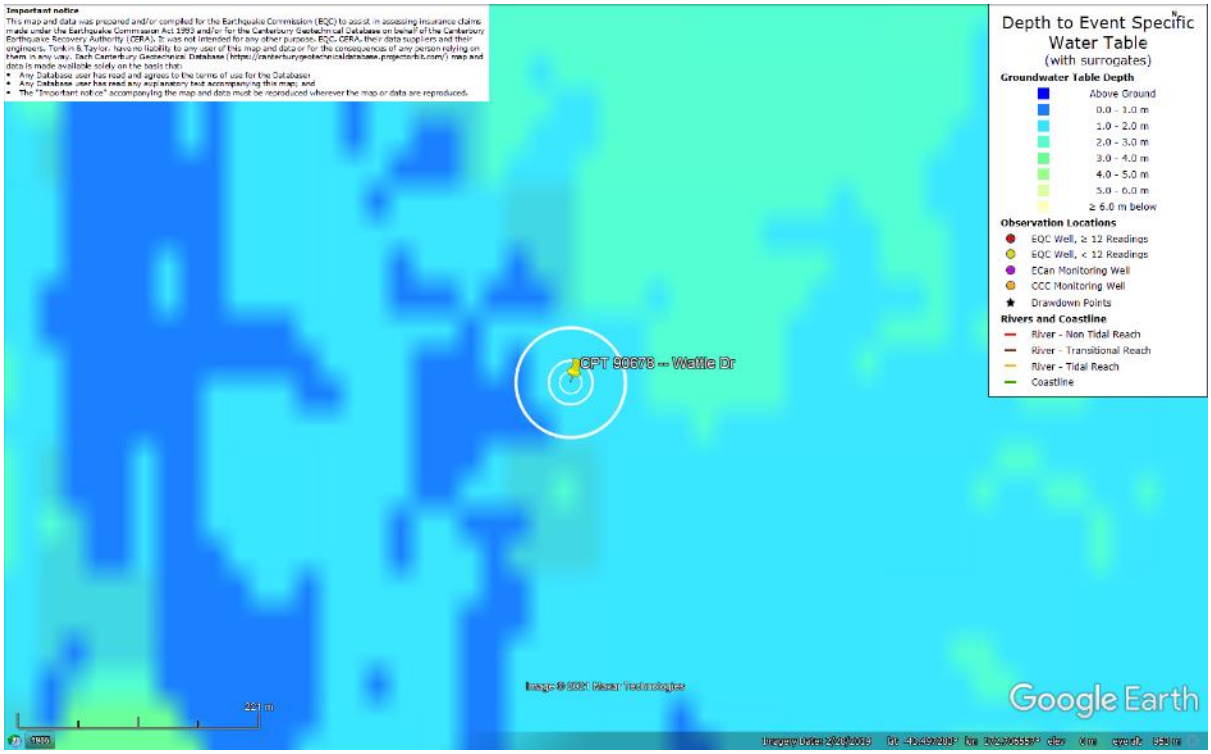

Figure 93: Depth to groundwater table for Feb-11 EQ.

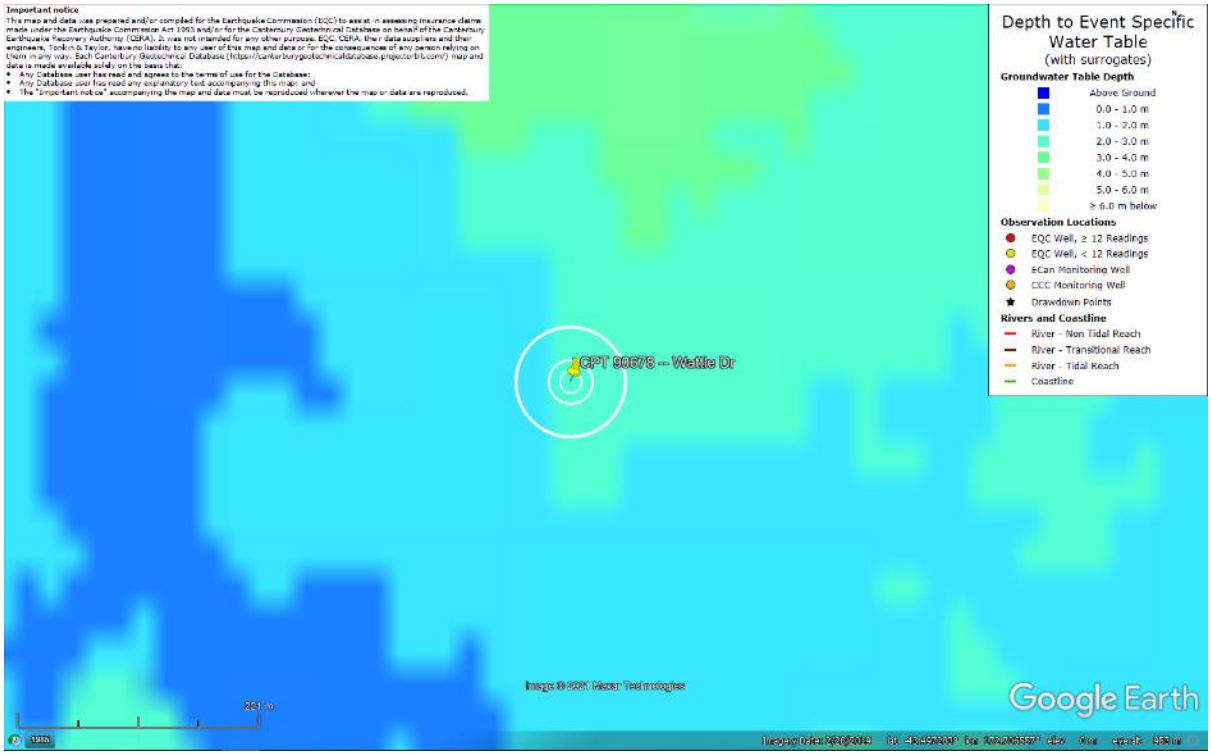

Figure 94: Depth to groundwater table for Jun-11 EQ.

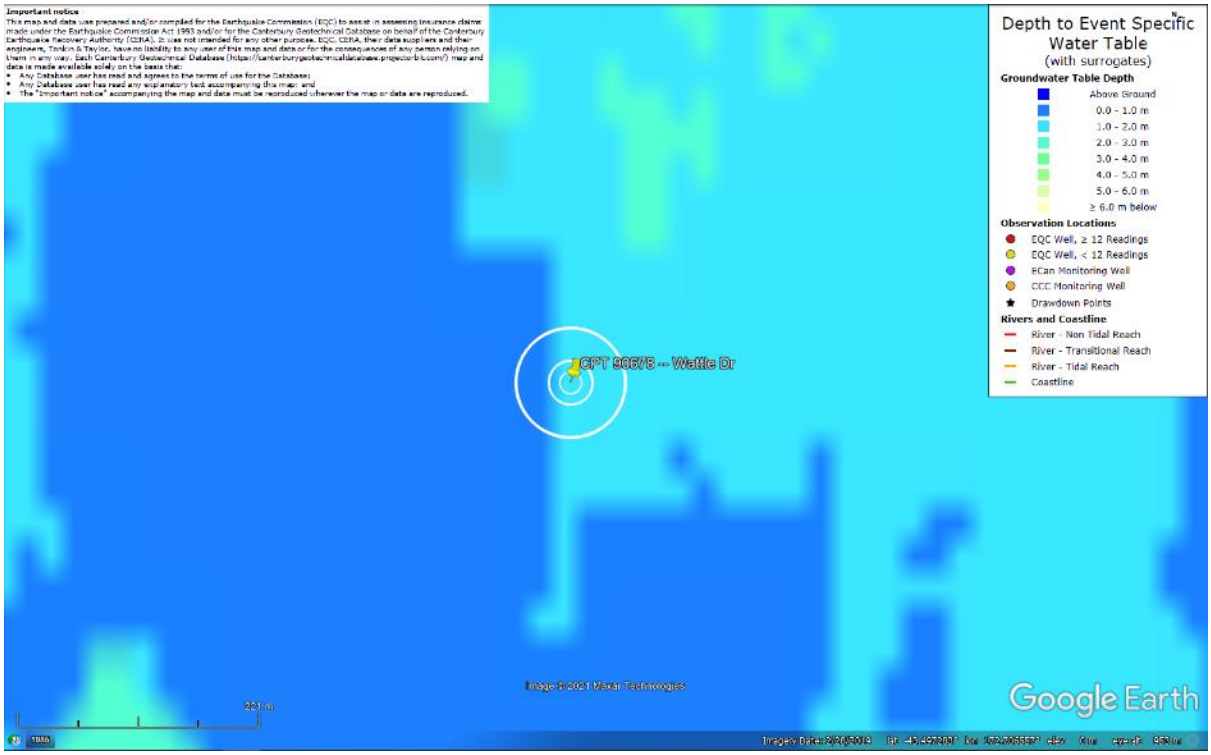

Figure 95: Depth to groundwater table for Dec-11 EQ.

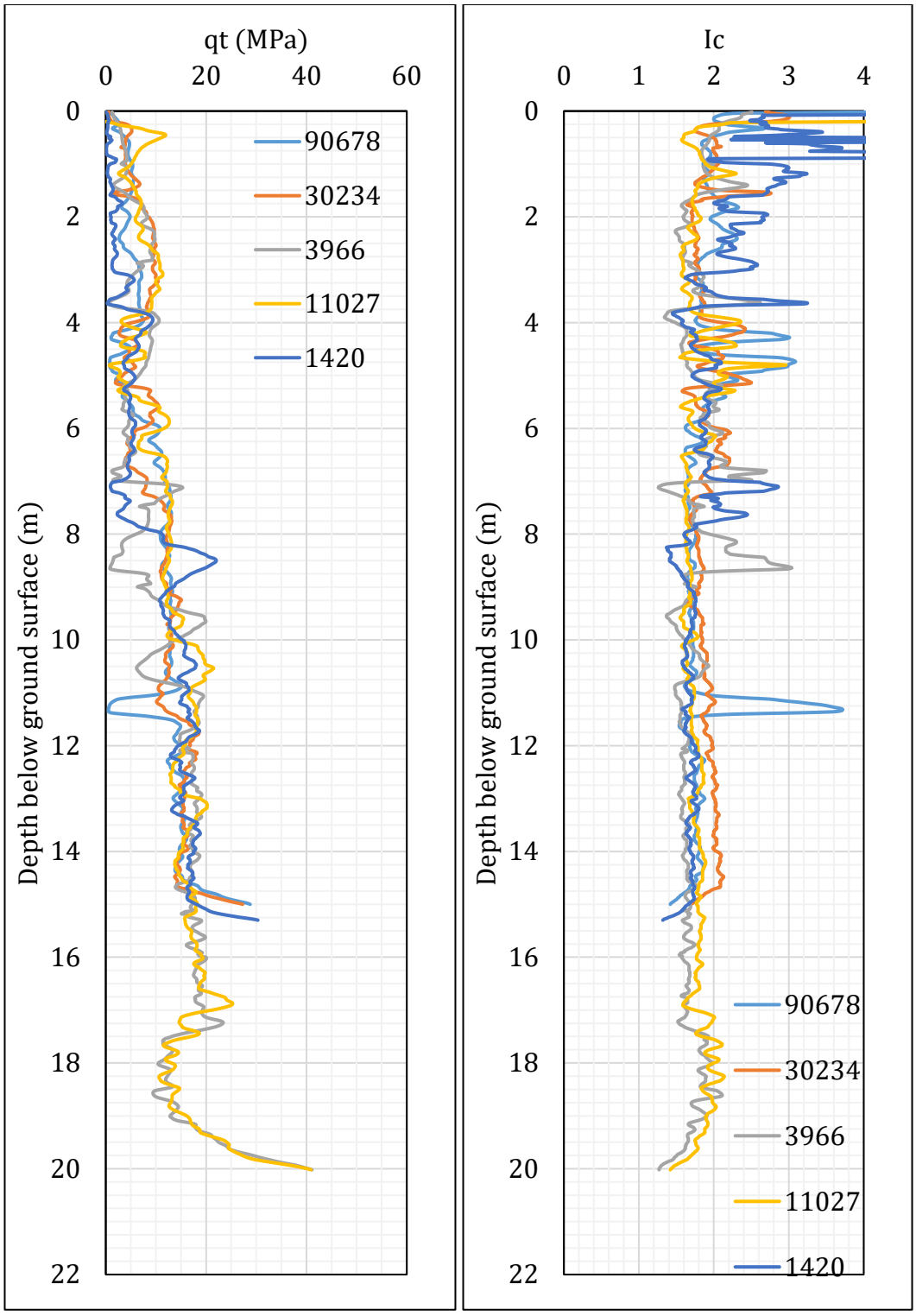

Figure 96: q_t and I_c profiles.

Note 8: The selection of CPTs for the area considered for settlement assessment (Figure 1) is based on the proximity of the CPTs to the considered areas. In accordance with that, the following table shows CPTs that were used for the volumetric settlement analysis in *Cliq v.3.0.3.2*, a CPT soil liquefaction software developed by GeoLogismiki. (The average volumetric settlements were reported in Table 8.)

Table 12: CPT profiles used in volumetric settlement analysis for areas selected for settlement assessment.

CPT ID No.	Patch A	Patch B	Patch C	Road
90678	✓	✓		
3966*			✓	✓
30234		✓		✓
11027*				✓
1420				

Note: * indicates CPTs that were used to calculate the volumetric settlement between the 15-m and 20-m depth for CPTs 90678 and 30234 and between the 15.3-m and 20-m depth for CPT 1420.

Table 13: CPT-based results for the upper 20 m of the soil profile.

		CPT ID						
EQ Event	Parameter	90678	30234	3966	11027	1420	$\Delta_{15m-20m}$*	$\Delta_{15.3m-20m}$**
Sep-10	S_{V1D} (mm)	11	8	57	8	49	1	1
	LSN	2	2	9	2	10	0	0
	LPI	0	0	1	0	1	0	0
	LPI_{ish}	0	0	0	0	0	--	--
	$D_{FS<1}$ (m)	undet.	undet.	6.36	undet.	6.62	--	--
Feb-11	S_{V1D} (mm)	92	58	188	83	153	6	11
	LSN	19	12	38	18	37	1	1
	LPI	7	7	22	7	22	0	0
	LPI_{ish}	5	4	0	5	18	--	--
	$D_{FS<1}$ (m)	2.08	4.00	1.22	2.12	1.6	--	--
Jun-11	S_{V1D} (mm)	17	15	86	16	69	1	1
	LSN	3	3	14	3	14	0	0
	LPI	1	0	4	1	3	0	0
	LPI_{ish}	0	0	0	0	0	--	--
	$D_{FS<1}$ (m)	4.44	undet.	4.86	4.84	2.78	--	--
Dec-11	S_{V1D} (mm)	64	50	165	59	144	3	6
	LSN	13	10	33	12	35	0	0
	LPI	4	5	17	4	18	0	0
	LPI_{ish}	1	1	4	3	0	--	--
	$D_{FS<1}$ (m)	2.24	4.01	1.30	4.22	1.60	--	--

Notes: $D_{FS<1}$ = Depth to the first liquefiable layer ($FS_L<1$) that is at least 200-mm thick, as determined by the Boulanger and Idriss (2016) liquefaction-triggering procedure (P_L=50%, C_{FC}=0.13, and $I_{c,cutoff}$ =2.6), and exported from *Cliq v.3.0.3.2*; undet. = the specified soil layer was not detected; * and ** indicate the amount of S_{V1D}, LSN, and LPI to be added to CPTs 90678 and 30234 and CPT 1420, respectively, due to their penetration depths being shallower than 20 m.

Note 9: Based on the borehole log (BH 3936, Figure 1), the groundwater table is at a depth of 1.5 m below the ground surface. The ground subsurface profile consists of (1) fine sand, SP, of the Christchurch formation to a depth of 5.0 m, (2) silt, ML, of the Christchurch formation to a depth of 5.4 m, and (3) fine sand, SP, of the Christchurch formation to a depth of 20 m.

Note 10: The ejecta-induced free-field settlement provided in Table 11 is an areal average settlement due to ejecta, which is based on the total settlement assessment area, A_T (provided in Table 9 and repeated in Table 14). However, the considered area was not always covered completely with ejecta; thus, it is important to provide the localized ejecta-induced settlement, too. The localized settlement due to ejecta is estimated using photographic evidence only as

$$S_{E,P\_localized} = \frac{V_E}{A_E}$$

where V_E is the total volume of ejecta within A_T and A_E is the total coverage area of ejecta within A_T. Please note that the areal ejecta-induced settlement provided in Table 14 as S_{E,P_areal} is the same as $S_{E,P}$ in Table 11, which was estimated as

$$S_{E,P\_areal} = S_{E,P} = \frac{V_E}{A_T}$$

where V_E is the total volume of ejecta within A_T and A_T is the total settlement assessment area.

Table 14a: Areal and localized ejecta-induced settlement estimates for Patch A (10-, 20-, and 50-m buffers) based on photographic evidence.

Earthquake Event	A_T (m^2)	A_E (m^2)	V_E (m^3)	S_{E,P_areal} (mm)	$S_{E,P\_localized}$ (mm)
Sep-10	89.5	0	0	0	0
Feb-11	89.5	78.2	5.3-10.4	90±30	100±35
Jun-11	89.5	67.3	2.7-6.7	55±20	70±30
Dec-11	89.5	80.0	4.3-7.2	65±15	70±20

Notes: $S_{E,P\_areal} = S_{E,P}$ reported in Table 11 = areal ejecta-induced settlement; $S_{E,P\_localized}$ = localized ejecta-induced settlement; A_T = total settlement assessment area; V_E = total volume of ejecta within A_T; A_E = total area of ejecta within A_T; The estimates of both areal and localized ejecta-induced settlement are rounded to the nearest 5 mm; Final plus/minus values are also rounded to the nearest 5 mm.

Table 14b: Areal and localized ejecta-induced settlement estimates for Road (50-m buffer) based on photographic evidence.

Earthquake Event	A_T (m^2)	A_E (m^2)	V_E (m^3)	S_{E,P_areal} (mm)	$S_{E,P\_localized}$ (mm)
Sep-10	381	0	0	0	0
Feb-11	361	361	12.6-15.4	40±5	40±5
Jun-11	380	380	8.4-13.7	30±5	30±5
Dec-11	394	66.1	0.6-1.2	5±5	15±5

Notes: S_{E,P_areal} = $S_{E,P}$ reported in Table 11 = areal ejecta-induced settlement; $S_{E,P\_localized}$ = localized ejecta-induced settlement; A_T = total settlement assessment area; V_E = total volume of ejecta within A_T; A_E = total area of ejecta within A_T; The estimates of both areal and localized ejecta-induced settlement are rounded to the nearest 5 mm; Final plus/minus values are also rounded to the nearest 5 mm.

Summary 2:

- **The best estimate of the localized ejecta-induced free-field ground settlement at the Wattle Dr site for the SEP 2010, FEB 2011, JUN 2011, and DEC 2011 earthquake is 0 mm, 100±35 mm, 70±30 mm, and 70±20 mm, respectively.**
- **The best estimate of the localized ejecta-induced settlement of the road at the Wattle Dr site for the SEP 2010, FEB 2011, JUN 2011, and DEC 2011 earthquake is 0 mm, 40±5 mm, 30±5 mm, and 15±5 mm, respectively.**